# SHEARING BEHAVIOR OF CURVED INTERFACES

A Thesis
Presented to
The Academic Faculty

by

Mehmet Iscimen

In Partial Fulfillment
Of the Requirements for the Degree
Master of Science in Civil and Environmental Engineering

Georgia Institute of Technology
July 2004

SHEARING BEHAVIOR OF CURVED INTERFACES

Approved by:

Dr. J. David Frost, Chairman

Dr. Paul W. Mayne

Dr. Glenn J. Rix

Date Approved: July 9, 2004

# ACKNOWLEDGEMENTS

I would like to greatly thank my advisor Dr. J. David Frost for providing me the opportunity to study in Georgia Institute of Technology, and for supporting me with his knowledge, assistance, guidance and encouragement during my graduate studies. I would like to extend my sincere gratitude to my other dissertation committee members, Dr. Paul W. Mayne and Dr. Glenn J. Rix.

Xuan, Greg, Alfredo and Andrew; thank you all for your help, patience and friendship. You were always there whenever I needed help…

My mother Z. Nevin Iscimen, my father Behzat Iscimen and my brother Selcuk Iscimen, who continuously supported me during my studies and helped me to overcome all difficulties, are also gratefully acknowledged. You were far away but your love is always with me, always in my heart…

And finally, I would like to specially thank a special person: Aslim, everything would be much more difficult without you….

TABLE OF CONTENTS

LIST OF TABLES

LIST OF FIGURES

# SUMMARY

## Shearing Behavior Of Curved Interfaces

The frictional behavior of soil-construction material interfaces is of significant importance in geotechnical engineering applications such as retaining structures, pile foundations, geosynthetic liners, and trenchless technologies. Since most failures initiate and develop on the interfaces, special attention is required to predict the capacity of these "weak planes" in the particular application.

Pipe-jacking and microtunneling technologies are being more widely used over the past decade and there is significant interest to predict the jacking forces and jacking distances achievable in order to achieve more efficient design and construction. This study focuses on the evaluation of the frictional characteristics and factors affecting the shear strength of pipe-soil interfaces. Eight different pipes made from fiber reinforced polymer (FRP), polycrete, steel, concrete, and vitrified clay were tested in the experimental program.

For this purpose, a new apparatus was designed to conduct conventional interface direct shear testing on pipes of different curvature. This device allows coupons cut from actual conduits and pipes to be tested in the laboratory under controlled conditions. The apparatus includes a double-wall shear box, the inner wall of which is interchangeable to allow for testing against surfaces of different curvatures. By considering a narrow width section, the circular interface of pipes was approximated with a surface along the axial direction and the boundary is defined by the inner box.

Roughness tests were performed using a stylus profilometer to quantify the surface characteristics of the individual pipes and relate these to the interface shear behavior. The surface topography showed different degrees of variability for the different pipes. To extend the range of roughness values tested and force the failure to occur in the particulate media adjacent to the interface, two artificial pipe surfaces were created using rough sandpapers.

Interface shear tests were performed using the new apparatus with air-pluviated dense specimens of Ottawa 20/30 sand. Additional tests were performed using Atlanta blasting sand to evaluate the effect of particle angularity. The effect of normal stress and relative density were also examined. The interface strength was shown to increase with surface roughness and finally reach a constant value above a certain “critical roughness” value, which corresponded to the internal strength of the soil itself. This represented the failure location moving from the interface into the soil adjacent to the interface. Both the strength and the shearing mechanism were thus affected by the surface topography. It was also shown that the interface shear strength was affected by particle angularity, relative density and normal stress.

# CHAPTER 1

# INTRODUCTION

The interaction of a media with another one and the related contact mechanics is an important research area in various engineering fields. This interaction may be chemical, electrical, thermal, or mechanical among others. Examples of mechanical interaction, which is the mechanism of interest in this study, can be the contact of the tire and the road, contact of gears, or interaction of a fluid and a pipe.

In geotechnical engineering, the interaction between soil and artificial construction material plays an important role in many applications such as retaining structures, deep foundations, geosynthetic liners and reinforcements, trenchless technologies, field and laboratory tests, and tunneling. Regardless of the function, the material properties and their role in interface behavior should be determined in relative terms that capture how the properties of one material are affected by the properties of the second one. This interaction affects the performance and constructability as well as the cost of the construction.

The desired interaction may differ from application to application: A maximum load transfer is desired for an anchor-soil interface in a tie-back wall system to increase the load carrying capacity whereas a minimum interface friction is desired for a pipe-soil interface during micro-tunneling to increase the distance that the pipe can be jacked. In both systems, regardless of whether it is desired to maximize or minimize the unit interface friction, the ability to predict and control the interface behavior can result in

improved constructability and/or performance. Improved test and design methods that allow for more accurate prediction of the interface performance are needed as the number and the types of interface-strength-dependent geotechnical systems being used in practice continues to increase.

Because most “failures” occur at the interface of two media, studies regarding the performance of the interface yield insight into the ultimate capacity of the geotechnical system. Not only is the ultimate strength of importance but also insight into the mechanism and soil behavior related to the shearing process may have relevance in many applications. An example of this would the prediction of the volume change during pile driving in relation with the predominant mechanism on the pile-soil interface. This in turn can be used to employ a more efficient design and construction.

## 1.1 Motivation For Study

Pipe-jacking and microtunneling applications gained more relevance in the last decade with the improvement in its technology and applicability. “Trenchless technology broadly brings under one banner a variety of non-disruptive techniques for installing, replacing or renovating underground pipes without open-cut excavation” (Thompson, 1993). It is primarily used for sewer construction but also for gas and water mains, oil pipelines, electricity and telecommunication installations, culverts and subways. Hydraulic jacks are used to push pipes through the ground while a tunnel boring machine or shield at the leading edge of the tunnel excavates the ground. In order to install a pipeline using this technique, thrust and reception pits are constructed. Pipes in a diameter range of 150 mm to 3000 mm can be jacked for a distance of more than 300

meters (http://www.pipejacking.org). The advantages of this technique compared to conventional open-cut excavation can be summarized as following:

- Minimal reinstatement of the soil
- Less risk of settlement
- Minimal surface disruption
- Significant reduction in social costs when compared to open-cut trenching in urban areas
- Reduced environmental disturbance
- Inherent strength of lining

Drawings and pictures of pipe-jacking applications can be seen in Figure 1.1.

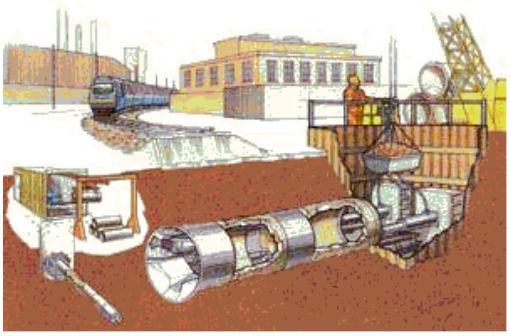

(a)

(b)

Figure 1.1 (a) Conceptual Drawing of a Pipe-jacking Application (http://www.pipejacking.org) (b) A Picture of the Thrust Pit http://cem.www.ecn.purdue.edu/CEM/Trench/micro.html)

(c) (d)

Figure 1.1 (continued) (c) A Picture of the Thrust Pit and the Hydraulic Rams (http://www.dsd.gov.hk/sewerage/technology_employed/pipe_jacking) (d) Picture of a Tunnel Boring Machine Attached to a Pipe (http://www.dsd.gov.hk/sewerage/technology_employed/pipe_jacking)

As a result of advances in trenchless technology over the past decade, there is significant interest in being able to predict the jacking distances and friction forces which act on circular conduits and pipes as they are jacked into the soil. This may be used in the design and construction of the pipeline as well as in feasibility and cost estimation.

## 1.2 Scope of Thesis

This thesis presents the results of a study focused on the shearing behavior of curved interfaces. The goals of this research were to: (1) develop a new apparatus design and test to measure the friction at a soil-pipe interface; (2) quantify the surface topography of a range of typical pipes used; (3) employ the new apparatus to measure the interface friction; and (4) correlate the surface topography with the interface shear strength.

Chapter 2 details and summarizes the previous research related in this area, while Chapter 3 describes the methodology used to measure the interface friction on pipes and

the new equipment design and fabrication. Chapter 4 quantifies the surface characteristics of pipes, and Chapter 5 evaluates the interface shear tests at various normal stresses and relative densities for two types of sand. Finally, Chapter 6 summarizes the findings of this research and provides recommendations for applications and future studies in this area.

# CHAPTER 2

# LITERATURE REVIEW

## 2.1 Introduction

To develop a new methodology for apparatus design and experimentation and to evaluate the experimental results in light of previous studies, different areas in the literature were reviewed.

The review was subdivided into five parts: Laws of friction and area of contact, surface topography characterization, specimen preparation techniques, interface shear device design, and previous research on interface strength.

## 2.2 Laws of Friction and Area of Contact

The two laws of friction were summarized by Bowden and Tabor (1956) as follows:

-The friction is independent of the area of contact between two surfaces,

-The friction is proportional to the load between the surfaces.

The real contact area of two plane surfaces touching each other is much smaller than the apparent area. Bowden and Tabor (1939) developed visual and electrical techniques to measure this area. The electrical technique was based on the measurement of the conductance of the surfaces after application of the load. It was observed that the conductance (real contact area) was independent of apparent area; it depends mainly on

the load applied. The load on the interface was supported by the irregularities or so called bridges. When the load was increased the number of the bridges also increased.

Temperature readings were taken on the sliding surfaces to analyze the contact area when the apparent area is changed 80 times. It was seen that, if the load and speed was kept constant, there was no considerable difference in temperature. This means that the area (the real contact area), which produced the heat, was the same.

According to Amonton's law, the shear force is just proportional to normal load. It was found in the study of Bowden and Tabor (1939) that the real area of contact is directly proportional to the load applied. That's why Amonton's law is true. Also the findings about the independence of the real contact area from the apparent area prove the validity of Amonton's law, which states that the friction is independent of the area.

The concept of real contact area has some implications: Even very light loads may cause plastic flow of the surface material. Larger surfaces do not necessarily mean that the pressure decreases but merely that the contact points are more distributed.

In summary, the real area of contact depends mainly on the load, not the shape, size and the roughness of the surface.

Archard (1957) stated that friction occurs due to the adhesion at the real contact points where the asperities touch each other. It is generally thought that the frictional force is proportional to the area of the real contact.

It follows from the Hertz's theory, where a single spherical particle is in contact with the counter face material, that the area A is related to the applied load W by

$$A = KW^{2/3} \tag{2.1}$$

if the deformation is truly elastic. K is a constant depending on the elastic properties the material and local radius of curvature. This contradicts Amonton's law where the friction is independent of area.

The above equation is modified with recent studies (Dove and Frost, 1999) as:

$$A = K'W^{n} \tag{2.2}$$

where n takes a value of between 0.67 and 1.0. The value of n becomes closer to 1.0 when the model is more similar to the real surface structure. For example, for one set of idealized protuberances, n may be 0.88. If complex models, which are closer to actual interface structure, are applied, n becomes approximately 1.0, which is consistent with Amonton's findings.

Change in area due to the change in load can be explained as follows: The load increase moves the surfaces together, the existing areas increase in size and new contact points develop (Archard, 1957). When the load is increased, the protuberances are pressed flat and the real contact area increases. The friction coefficient decreases if the deformation is elastic. For rougher surfaces, higher loads are required to press the asperities flat. At lighter loads, the asperities are not pressed flat, multiple contact conditions apply and Amonton's law is valid. At higher loads there is a single contact region and the friction behavior tends to deviate from Amonton's law due to the non-linear increase of the area in elastic behavior. Because the area does not increase as fast as the normal load, the coefficient of friction tends to decrease (Archard, 1957).

Amonton's law is correct when the normal load is less than about a fifth of the elastic limit.

## 2.3 Surface Roughness Characterization

Roughness plays a major role in interface shear mechanisms and behavior (DeJong, 2002). The interaction between the soil and various construction materials play a major role in geotechnical engineering, such as pile foundations, geosynthetic liners, earth retaining structures, and trenchless technologies (Frost et al., 2002). Various roughness parameters have been developed to characterize the surface topography, which is of vital importance for interface shear behavior. The most commonly used parameter to quantify the roughness is the average roughness $R_a$ parameter, which is given by:

$$R_a = \left(\int_0^L |z(x)| dx\right) / L \qquad (2.3)$$

L is the assessment length and z(x) is the height of the profile from the mean line (Ward, 1982).

The common parameters used in the literature to quantify roughness were summarized by DeJong and Frost (2002) in Table 2.1.

Uesugi and Kishida (1986) proposed a concept called "normalized roughness" to evaluate surface characteristics. For the same steel surface, the angle of interface $\theta$, changes greatly with changing particle size. To compensate this effect and get a higher correlation between coefficient of friction and roughness, they proposed a new parameter called "normalized roughness" ($R_n$), which accounts for the relative aspect of the

roughness. It is defined as the ratio of maximum roughness ($R_{max}$) to mean grain size of sand ($D_{50}$).

DeJong and Frost (2002) evaluated and showed the relevance of the relative aspect of surface roughness. Considering a simplified "rough" surface consisting of just a valley and a peak and a traveling spherical particle, it can be easily seen that the effect of peaks and valleys are not the same over the centroid trace of that individual particle. In addition, the vertical deviation from the centroid trace is different for different sizes of particles. This is demonstrated in Figures 2.1 and 2.2.

DeJong and Frost (2002) also studied different filters used in roughness measurements to remove the unwanted surface characteristics such as waviness and their effects on roughness parameters in the same study. They calculated roughness parameters on a simple theoretical profile consisting of one valley and one peak as well as on real construction materials. They found that the conventional filtering methods such as Gaussian filter and sharp cutoff filter may alter the original profile and result in misleading surface features.

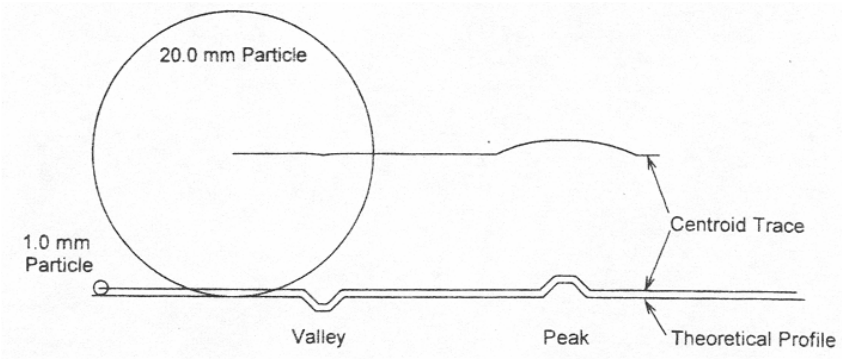


Figure 2.1 The Centroid Trace of an Individual Particle on a Simplified "Rough" Surface (DeJong and Frost, 2002)

Table 2.1 The Common Roughness Parameters (DeJong and Frost, 2002)

| Symbol | Name | Definition | Horizontal Distribution | Vertical Distribution | Relative Aspect |
|---|---|---|---|---|---|
| $R_a$ | Average Roughness [7] | $R_a = \frac{1}{L}\int_0^L \lvert Z(x) \rvert dx$ where $Z(x)$ is a profile height function and $L$ is the evaluation profile length | | X | |
| $R_q$ | Root Mean Square (RMS) Roughness [7] | $R_q = \left(\frac{1}{L}\int_0^L Z(x)^2 dx\right)^{\frac{1}{2}}$ | | X | |
| $R_{sk}$ | Skewness [7] | $R_{sk} = \frac{1}{R_q^3}\cdot\frac{1}{L}\int_0^L (Z(x))^3 dx$ | | X | |
| $R_{ku}$ | Kurtosis [7] | $R_{ku} = \frac{1}{R_q^4}\cdot\frac{1}{L}\int_0^L (Z(x))^4 dx$ | | X | |
| $\Delta_a$ | Average Slope [7] | $\Delta a = \frac{1}{L}\int_0^L \left\lvert \frac{dZ}{dx} \right\rvert dx$ | X | X | |
| $\Delta_q$ | Root Mean Square (RMS) Slope [7] | $\Delta q = \left[\frac{1}{L}\int_0^L \left(\frac{dZ}{dx}\right)^2 dx\right]^{\frac{1}{2}}$ | X | X | |
| $\lambda_a$ | Average Wavelength [8] | $\lambda a = 2\cdot\pi\cdot\frac{R_a}{\tan(\Delta a)}$ | X | X | |
| $\lambda_q$ | Root Mean Square (RMS) Wavelength [8] | $\lambda q = 2\cdot\pi\cdot\frac{R_q}{\tan(\Delta q)}$ | X | X | |
| $R_{max}$ | Maximum Peak to Valley Roughness [7] | Largest Single Peak to Valley Height | | X | |
| $R_n$ | Normalized Roughness Parameter [2] | $R_n = \frac{R_{max}\ L = D_{50}}{D_{50}}$ | | X | X |
| $R_L$ | Profile Roughness Parameter [9] | $R_L = \frac{\text{Actual Profile Length } (L_o)}{\text{Projected Profile Length } (L)}$ | X | X | |
| $S_m$ | Average Feature Spacing [7] | $S_m = \frac{1}{n}\cdot\sum_{i=1}^{n} S_{mi}$ where $S_{mi}$ is the mean spacing between profile irregularities | X | | |

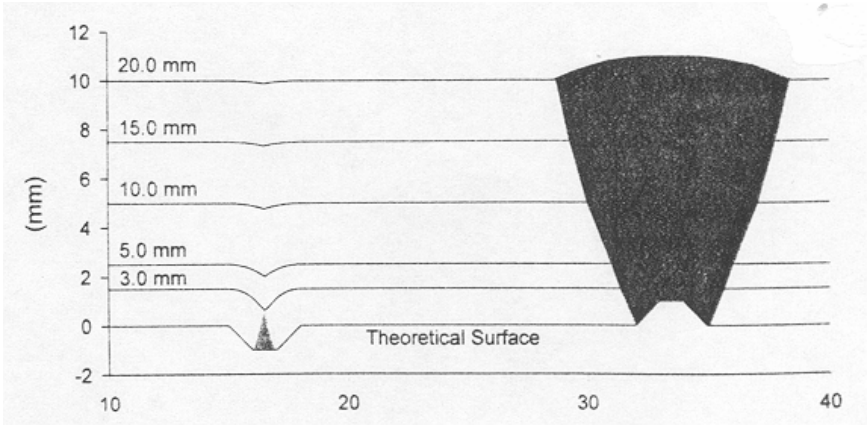


Figure 2.2 The Centroid Trace of Different Sizes of Particles on a Simplified "Rough" Surface (DeJong and Frost, 2002)

## 2.4 Specimen Preparation

Tests with granular soils are usually performed with laboratory-constituted specimens because it is not easy to use specimens from the field due to the lack of "cohesion". Different techniques that are developed to simulate specimens can be classified according to the moisture condition of the soil (dry, wet, moist), method of soil placement (e.g., pluviation, spooning) and the medium through which it is constituted (e.g., air, water). The specimens can be densified using different techniques such as vibration, tamping, rodding. (Frost and Park, 2003)

Differences in packing and orientation are the primary reasons for differences in dynamic strength of sands. Also, the liquefaction characteristics may vary significantly depending on the specimen preparation method (Ladd, 1974, Mulilis et al., 1977). Ladd (1977) found that the triaxial behavior of sands depends on specimen preparation because of the differences in grain and interparticle orientations, different variations in void ratio within the specimen and, segregation of particles.

Mulilis et al. (1977) found that pluviating the soil through air produced the weakest samples and vibrating the soil in moist condition produced the strongest ones. Also samples prepared in just one layer were stronger than the samples produced in more number of layers. Degregorio (1990) mentions about the increase in strength of the specimens prepared with the methods dry pluviation (lowest), moist tamping and moist vibration (highest).

In tamping method, the specimen is densified in layers where each layer has the same target density. Unfortunately the underlying layers become denser because they are impacted from the densification of the layers over them (Mulilis et al., 1977). This led to the concept called “undercompaction” (Ladd, 1978). In this concept, the target density decreases linearly from top to bottom layer to have a more uniform specimen in terms of relative density. The ratio of the densities of successive layers is called undercompaction ratio. Ladd (1978) showed that this method created more uniform samples and minimized particle segregation.

Frost and Park (2003) showed that specimens prepared with air pluviation or wet pluviation were more uniform than moist-tamped specimens. Moreover there were variations up to 15 % in relative density within the layer, and 10 % between the layers in moist-tamped specimens although they were prepared using the concept of undercompaction (Frost and Park, 2003). Similarly, Rad and Tumay (1987) concluded that pluvial compaction is the best reconstitution method for granular soils to simulate the formation of sand deposits.

The lower portions of the pluviated specimens are denser than the rest because the soil particles impact the rigid base at the beginning but later the energy dissipates through

soil particles. Also the upper portion of the specimen can be denser because of the effect of the top cap (Frost and Park, 2003).

Miura and Toki (1982) and, Rad and Tumay (1987) concluded that the smaller flask (sieve) opening and lower deposition intensity resulted in a higher relative density of the specimen. Also, the rotation of the flask and the height of fall affected the void ratio because of their influence on impact energy.

## 2.5 Interface Shear Device Design

Butterfield and Andrawes (1972) investigated possible sources of error at interface shear tests. These are:

- Boundary friction of soil with the sidewalls of the box
- Friction between the shear box and the interface

Another important consideration in the design of shear systems is the stiffness of the box. The box should be stiff enough to support all types of loading without a major deflection within itself. Stick slip motion might be observed within a loose and weak system (Butterfield and Andrawes, 1972).

Tatsuoka and Haibara (1985) studied the frictional resistance between the sand and sidewall surface of the shear box, which is considered as “non-frictional” in shear tests. They simulated nine different interfaces prepared with sand and various kinds of smooth and lubricated interfaces. They found that the choice of appropriate lubricant depended on the normal load applied. Moreover if no lubricant was used on the interface, the friction angle between sand and smooth counter material was 5 degrees or more, which was high for a “non-frictional” interface.

Desai et al. (1985) developed a “Cyclic Multi-Degree-Of-Freedom Shear Device” to test large size interfaces, which allows translational and torsional types of tests under cyclic and static loading conditions. They found that the distributions of the normal and shear load at the interface were not uniform. The effect of boundary walls and the rubber membrane tend to vanish the stresses near the edge. But for the most part of the interface, the distributions are quite acceptable. A test with an empty box pressurized with air was run to evaluate the effect of the membrane: It gave a friction value of 6% of the test with sand at same conditions.

Desai et al. (1985) also showed that the specimen thickness also affects the normal load transfer to the interface. The load decreased as the thickness was increased.

Ooi and Carter (1987) introduced a new device, which allows shear displacements to proceed under “constant normal stiffness conditions”, which is different than conventional constant stress or constant volume shear tests. Constant normal stiffness conditions are more representative of the actual behavior of the interface. If contraction/dilatation occurs in shear motion, the normal stresses are subject to change because of the confinement of the soil/rock. This probable change will be reflected on the shear strength of the interface (Ooi and Carter, 1987).

However if the ratio between shear stress and normal stress (friction angle) at peak and large displacement are considered, it can be seen that they depend on the normal load and horizontal displacement but not on the stiffness.

In case of dilatation (under constant stiffness conditions), large increases in normal load are observed which in turn result in large shear stresses across the interface. But in contrast, the normal stresses tend to decrease when contraction takes place.

Porcino et al. (2003) used a similar device called constant normal stiffness direct shear device (CNS), investigated the interface shear behavior and compared with the conventional constant normal load device (CNL). CNL test results showed that:

- The maximum shear stress increases with roughness as well as the corresponding peak horizontal displacements

- With increasing roughness, the softening behavior becomes more evident.

- With increasing roughness, the contractive/dilative behavior becomes more evident.

- Some dependence of friction angle on relative density and normal stress was observed.

- Friction coefficient versus normalized roughness shows a bilinear relationship.

CNS test results showed that:

- The surrounding soil resists “elastically” the dilative/contractive behavior and causes increase in normal stress and correspondingly in shear stresses. The increase was observed both at peak and residual (large displacement) values for rough and dense interfaces. Rough interfaces are predominantly dilative.

The vertical displacement, “u”, experiences the opposite - the higher the stiffness the lower is the u.

- In contrast, increasing the stiffness (K) decreases the shear stress at both peak and to a less extent at residual values for loose specimens with a smooth interface. The normal stresses tend to decrease during the test. The higher the stiffness the lower is the “u” (contractive).

- The difference in shear stresses in CNS and CNL tests are due to the differences in normal stresses and not due to a change in interface friction angle.

- The strength envelopes in residual range are linear no matter what the relative density is. The residual friction angle does not depend on the relative density but on the mineralogical and physical characteristics of sand particles and the roughness of the counter material.

- All $(\tau/\sigma_{n0})_{max}$ values are on the unique linear strength envelope that is same for CNL and CNS regardless of the value of the stiffness.

Hsieh and Hsieh (2003) studied various aspects in interface shear testing such as effect of the rigidity of the loading plate, the specimen width to thickness ratio, the specimen height, and the shear box dimension on interface strength among others. They used quartz sand, different types of geomembranes, and conventional shear boxes in their tests. The interface was instrumented with load cells to monitor the pressure distribution. Their conclusions can be summarized as follows:

- Conventional rigid loading plates employed in direct shear tests resulted in a concave pressure distribution along the interface. To compensate this effect, a minimum sample thickness of 5 cm was recommended. If a flexible membrane was employed for normal load application instead of a rigid plate, the required thickness decreased to 3 cm. The flexible load system ensured a more uniform and more reproducible pressure distribution at the interface but the measured shear strengths at both systems were very close to each other.

- The minimum specimen width to thickness ratio should be 2:1.

- The normal pressure was very low and unstable especially at corner locations when rigid load plates were used. The possible reason for this was the edge effect.

- If the box dimensions were increased, an increase in the shear strength was observed. This change does not contribute much when the dimensions are increased from 300 mm x 300 mm to 400 mm x 400 mm, proving that 300 x 300 mm is the ideal box dimension.

- A 3 mm gap was foreseen between the shear box and the geomembrane surface to prevent the contribution of the fiction at the boundary. To keep this gap open, a minimum sample thickness of 5 cm is required for a rigid loading plate systems and a sample thickness of 3 cm for flexible loading plate systems.

## 2.6 Previous Research on Interface Strength

Various researchers have studied soil-continuum interaction in the past fifty years. Potyondy (1961) investigated the skin friction between different types of soils (sands, silts, clays and an artificial mix of clay and sand) and construction materials (wood, concrete, steel) using stress and strain controlled boxes. He concluded that four factors determine the skin friction: the moisture content of the soil, roughness of the surface, composition of the soil, intensity of the normal load.

Similarly Butterfield and Andrawes (1972) concluded that the static and kinetic friction between particulate media and the continuum media is governed by the microscopic roughness of both surfaces and the relative aspect of the roughness, the angularity of particles, density and hardness of the particulate media with respect to the counter surface.

Brumund and Leonards (1973) used a “pullout” test apparatus consisting of a cylinder of sand encased in a rubber membrane and a rod located at its axis. Three different rods formed from steel, smooth mortar and rough mortar were used. Their surfaces were modified with graphite and Teflon cover at some tests to reduce the friction. This apparatus allowed taking “static” and “dynamic” shear tests. Angular and rounded sands were used within the tests.

The results showed that the dynamic friction is around 20% higher than static friction unless slippage occurs in the soil. The limiting value for friction, regardless whether static or dynamic, was the internal friction of the particulate media. Test results also showed that the surface roughness, angularity, size and surface texture of the particles play a major role in friction behavior.

Kulhawy and Peterson (1979) investigated the behavior of sand-concrete interfaces and concluded the following:

-For rough interfaces, the failure occurred in the soil rather than at the interface

-Relative roughness parameter ($R_R$) should be used to quantify the surface

Tatsuoka and Haibara (1985) studied the frictional resistance between the sand and sidewall surface of the shear box, which is considered as “non-frictional” in shear tests. They simulated nine different interfaces prepared with sand and various kinds of smooth and lubricated interfaces. These included teflon sheet, acryl plate, pyrex glass plate, normal sheet glass plate, latex membrane, polished stainless steel plate and dow high vacuum silicon grease and shin-etsu silicon grease as lubricants.

They found that the choice of appropriate lubricant depends on the normal load applied. The apparent friction angle decreases when the normal stress increases (consistent with

Archard, 1957; Dove and Frost, 1999). Moreover, the surfaces tested can not be called as "frictionless" because friction angles up to 10 degrees were observed for these lubricated or smooth surfaces.

Uesugi and Kishida (1986) used a modified shear apparatus capable taking tests at simple shear and direct shear mode and examined the effect of surface roughness, testing mode, $D_{50}$, angularity of the sand, uniformity coefficient, and normal load for dry sand-steel interfaces. They found that surface roughness, $D_{50}$, and sand angularity were the primary parameters controlling the shear characteristics. The type of test (simple versus direct), normal stress, and uniformity coefficient did not have a significant contribution on the shear behavior. Furthermore they proposed the "normalized roughness" concept to account for the relative aspect of the surface topography.

Tests with sands of different angularity allowed the authors to conclude that the friction decreases with the increase of particle roundness. They showed that the product of coefficient of friction and roundness ($\mu$ x R) was linearly correlated with relative roughness.

The plot of coefficient of friction versus normalized roughness gives a bilinear relationship for all types of sands. This is explained as follows: The coefficient of friction increases linearly with the increase in relative roughness until a critical roughness value is reached. At that critical point, the failure mechanism changes and the failure location moves from the interface into the soil. The coefficient of friction becomes constant and is equal to the internal strength of the soil itself. This is illustrated in Figure 2.3.

Paikowsky et al. (1995) developed a new dual interface shear apparatus (simple or direct) to evaluate the frictional behavior between granular materials and steel or

aluminum surfaces machined to desired roughness using sand blasting and other techniques. The apparatus consists of two shear boxes above and below the surfaces allowing independent measurements at each side. The surfaces consist of three independent instrumented plates to allow taking measurements at “front”, “center” and “rear” parts of the specimen. This design allows for measuring of the unrestricted soil/surface interaction at the central segment.

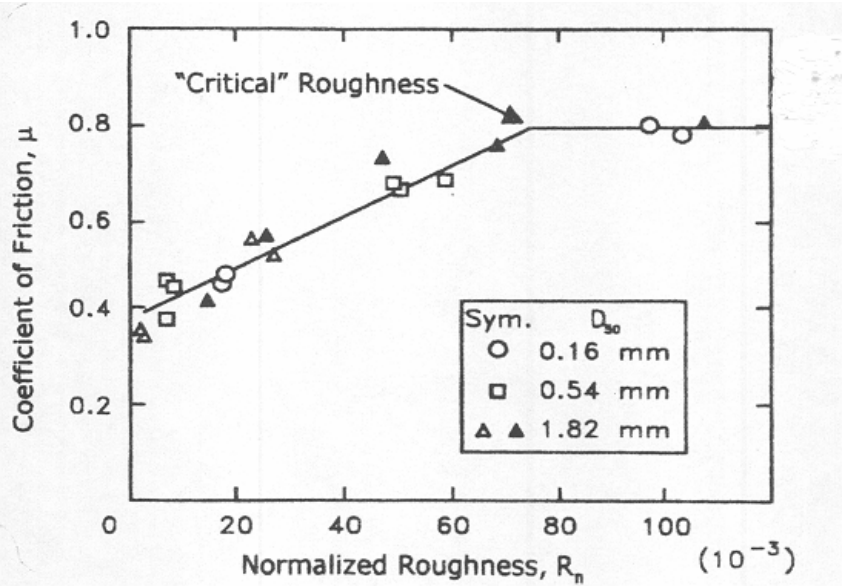


Figure 2.3 Coefficient of Friction versus Normalized Roughness For Mild Steel-Dry Sand Interfaces (Uesugi and Kishida, 1986)

Paikowsky et al. (1995) defined the surface roughness in three classes: A “smooth” interface (Zone I) with $R_n<0.02$, an “intermediate” interface (Zone II) with $0.02<R_n<0.5$ and a “rough” interface (Zone III) with $R_n>0.5$. Test results showed that the “smooth” interface results in constant coefficient of friction for all grain sizes. The friction increases with the increase in normalized roughness in “intermediate” interface,

and friction is constant and equal to the internal friction of the granular material in "rough" interface. This limit is a function of the soil's density. For "smooth" and "intermediate" surfaces, the failure occurs at the soil-surface contact. Test results showed that the relative surface roughness and the particle shape are the main parameters controlling the shearing behavior of interfaces.

Paikowsky et al. (1995) used Ottawa sand and glass beads of different size in their experiments. The quality-controlled glass beads enabled the measurement of the friction parameters of the same grain shape but different size. It was concluded that the particle size alone has no effect on the frictional resistance given that normalized roughness parameter is used to quantify the roughness.

They also compared the results of their apparatus with the results of the conventional 60mm x 60mm direct shear box and concluded that the interface is influenced by the boundary conditions in the conventional direct shear box and this led to higher values being obtained in the conventional device.

Dove and Frost (1999) studied the peak friction behavior of smooth geomembrane-particle interfaces and gave detailed insight on contact mechanics of particle-continuum media. The governing equation for the shear strength of the interface was defined by Amonton in the $17^{th}$ century as:

$$F = \mu N \tag{2.4}$$

Many materials do not obey this rule because the coefficient of friction changes with the normal load. Usually the failure envelope in interface shearing is reported to be

linear in the literature. Closer examination shows it to concave upward behavior (Dove and Frost, 1999). At higher normal stresses, the shear strength tends to increase faster than the normal load.

The friction force consists of two components: Adhesion and plowing. Adhesion occurs at the real contact points. Because the normal force is supported on this very small contact areas, the contact points “weld”. This force is defined as

$$F_{adhesion} = \tau_a A \tag{2.5}$$

where $\tau_a$ is material shear strength and A is the real contact area. Plowing is defined as the removal and abrasion of the softer material due to the friction of the harder material

$$F_{plowing} = \tau_p A \tag{2.6}$$

where $\tau_p$ is soft material bulk strength and A is the cross sectional area of the plowed track.

Dove and Frost (1999) conducted experiments to identify the contact area of a particle assemblage on geomembrane surfaces. Different normal loads were applied to 20/30 Ottawa sand and the contact area on the geomembrane interface was determined using image analysis techniques. The results were in good agreement with the results of the theoretical formulation of elastic contact. According to Archard (1957), if the number of contacts does not change when normal load is increased, single point contact dominates. This was the case in this experiment and the experimental n value of 0.69 is in good agreement with the theoretical value of 0.67.

The friction coefficient will decrease or remain constant depending on the n value between 0.67 and 1.0. In the multiple particle interface friction experiment, n was found to be 1.21, higher than the upper limit 1.0. The reason for this was the change of the friction mechanism from sliding to plowing. For angular particles, plowing occurs even at low normal stresses.

The friction coefficient decreases with increasing normal load, but then starts to increase due to the effect of plowing. This concept can be seen on Figure 2.4.

Plowing has little effect on harder surfaces. The particles are in sliding mode. If plowing is not occuring, the friction at higher stresses is less than the friction measured for softer counter face material.

In summary, if the contact behavior is elastic ($0.67<n<1.0$), the friction coefficient decreases with the increase in normal load. But for plastic and multi-asperity contact conditions, n becomes 1.0 and the friction coefficient is constant. At higher stresses, plowing is a major factor influencing the friction. It mainly depends on hardness, grain shape and grain roughness. In general, shear mechanism and friction coefficients depend on soil-counter material-normal load interactions.

Frost and Han (1999) studied the behavior of interfaces of fiber reinforced polymers and sands. They examined the behavior of different granular materials (Ottawa sand, glass beads, Valdosta blasting sand, and silica 120 powder) on FRP surfaces at varying testing conditions and parameters such as shear rate, surface roughness, and grain size.

They concluded that the frictional behavior between the FRP and the granular material was controlled by the relative surface roughness, normal stress level, relative

density of the granular material and angularity of the particles. The shearing rate, mean grain size, the specimen preparation method, and thickness of the specimen had little effect on the frictional behavior.

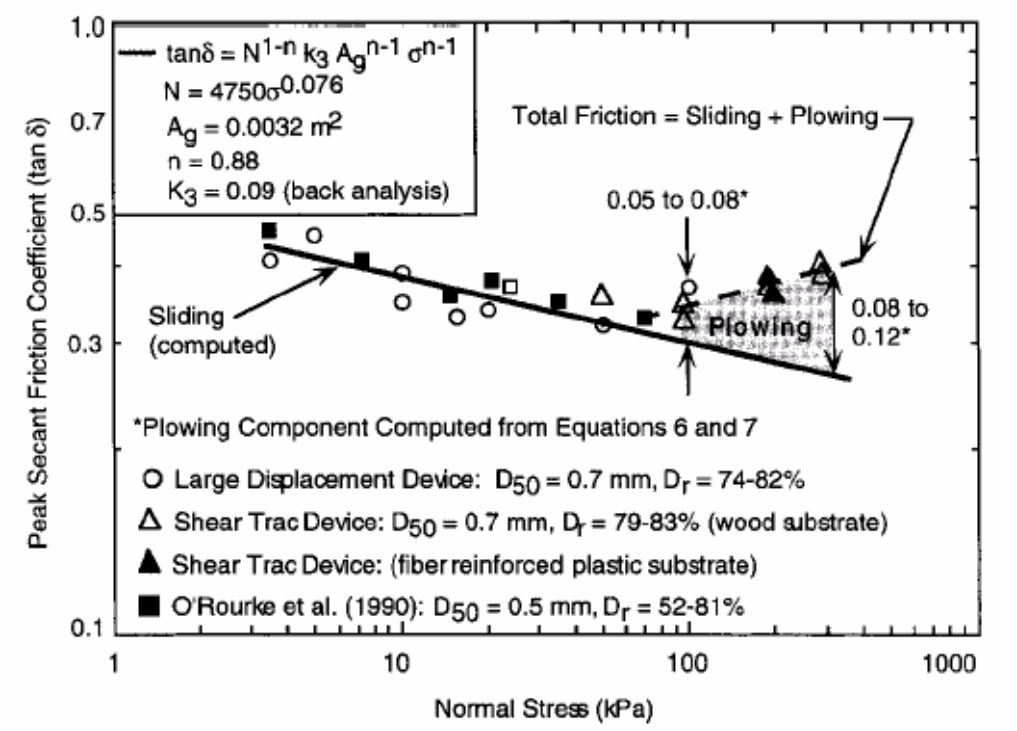


Figure 2.4 The Change of Peak Secant Coefficient of Friction with Normal Stress for Ottawa Sand-Geomembrane Interfaces (Dove and Frost, 1999)

Frost et al. (2002) conducted interface shear tests on a variety of materials (FRP, hardened steel, HDPE geomembrane, LDPE geomembrane, wood) using Ottawa sand and Valdosta blasting sand to evaluate the effect of surface roughness and hardness on interface behavior and strength.

Increasing surface roughness by approximately three orders of magnitude resulted in an increase of peak friction angle by 20°. The upper bound for interface shear strength

was set by the internal friction angle of the particular sand type regardless of which surface was used.

Also the effect of hardness was evident from the test results: Softer materials such as geomembrane experienced particle penetration and plowing during the shearing process. This process causes wear and decreases the durability but increases the friction. Related research showed that these two parameters, surface roughness and hardness, are not independent of each other; there is a coupling between them.

Frost et al. (2002) also performed discrete element modeling (DEM) of particulate-continuum interfaces using the program TRUBAL and similar outcomes were observed. DEM provided insight on the global specimen shear behavior as well as on the local particle behavior.

This concept, that the surface roughness and hardness are the main parameters determining the interface shear behavior, was investigated for cone penetration testing (DeJong et al., 2001, Frost and DeJong, 2001, DeJong et al., 2002).

The sleeve friction measurements are less understood among other parameters of CPT and are directly related to interface shear behavior. Previous research showed that $f_s$ readings were greatly affected by the sleeve roughness. DeJong et al. (2001) modified the cone penetrometer by adding sleeve surfaces with different roughness properties. Adding rougher sleeves resulted in an average increase of sleeve friction by 70%. This concept can also be used to measure the internal shear strength of the soil itself by using very rough sleeves and by forcing the failure to occur inside the soil. The multi-sleeve attachment may simulate many geotechnical systems such as pipe-jacking technologies or deep foundations, which are heavily dependent on the interface friction behavior.

DeJong and Frost (2002) studied the effect of machined friction sleeves for the cone penetrometer and concluded that for a smooth sleeve, no particle rearrangement has been observed whereas for rough diamond textured sleeve, there is distinct shear zone 5-7 particle diameters thick. This showed that for the smooth interface, the dominant mechanism is sliding along the interface but for the rough interface, the shearing occurs inside the soil and particles slip, roll and move vertically.

# CHAPTER 3

# INTERFACE SHEAR EQUIPMENT DESIGN

## 3.1 Introduction

Conventional direct shear testing is performed on planar surfaces. This is not applicable in this study, since the friction surface, which is the outer surface of the pipe, is curved. The pipes are cylindrical in shape, so the radius of curvature is constant along a pipe. On the other hand, the radii vary from pipe to pipe.

These differences required a new methodology to directly measure the interface shear characteristics. This chapter describes the development of a new apparatus that allows the measurement of interface behavior of curved surfaces.

## 3.2 Conceptual Design

The radii of the pipes typically used in pipe-jacking in practice and therefore considered in this study varied between 13 inch and 22 inch. This means that they would have a relatively small curvature across the interface surface to be tested if a narrow shear box were used. This concept led the author to design a shear box, which deviates from the more traditional “square” designs by having a rectangular shape. This allows the potential problem of the curvature of the shearing surface to be addressed by reducing the shear box dimension in this direction and get the need to maintain an adequate shearing surface area is accomplished by increasing the shear box dimension in the direction of shearing. This concept is illustrated in Figure 3.1.

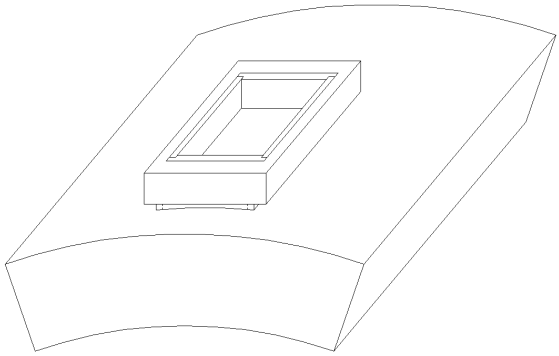

Figure 3.1 Shear Box on Top of a Coupon of a Pipe

This concept approximates the curved area of the interface by a planar one. This idealization requires the analysis of the following question: What is the range of error resulting from this approximation? To analyze this question, the curved area and its projection on the plane over the range of radii of typical pipes for different shear box widths were compared. The results were plotted in Figure 3.2:

As can be seen from the graph, the ratio of curved area to its projected area on a plane increases with the decrease of the pipe radius and increase of width of the shear box. If the magnitude of the error is evaluated more carefully, it can be seen that it is less than 1% for all pipes for shear boxes with a width less than 6 inches. This led to the conclusion that using a rectangular box has merit. Also the normal load can be assumed to be vertical at every point of the interface.

Another factor that requires careful evaluation is the effect of the boundary conditions. When designing the rectangular box, the boundary area should be carefully chosen in order to minimize its effect on the measured friction forces. Archard (1957) stated that the friction force is proportional to the area of the real contact. Accordingly,

the boundary area should be kept to a minimum in order to reflect the friction between the soil and the pipe and not between the box and the pipe.

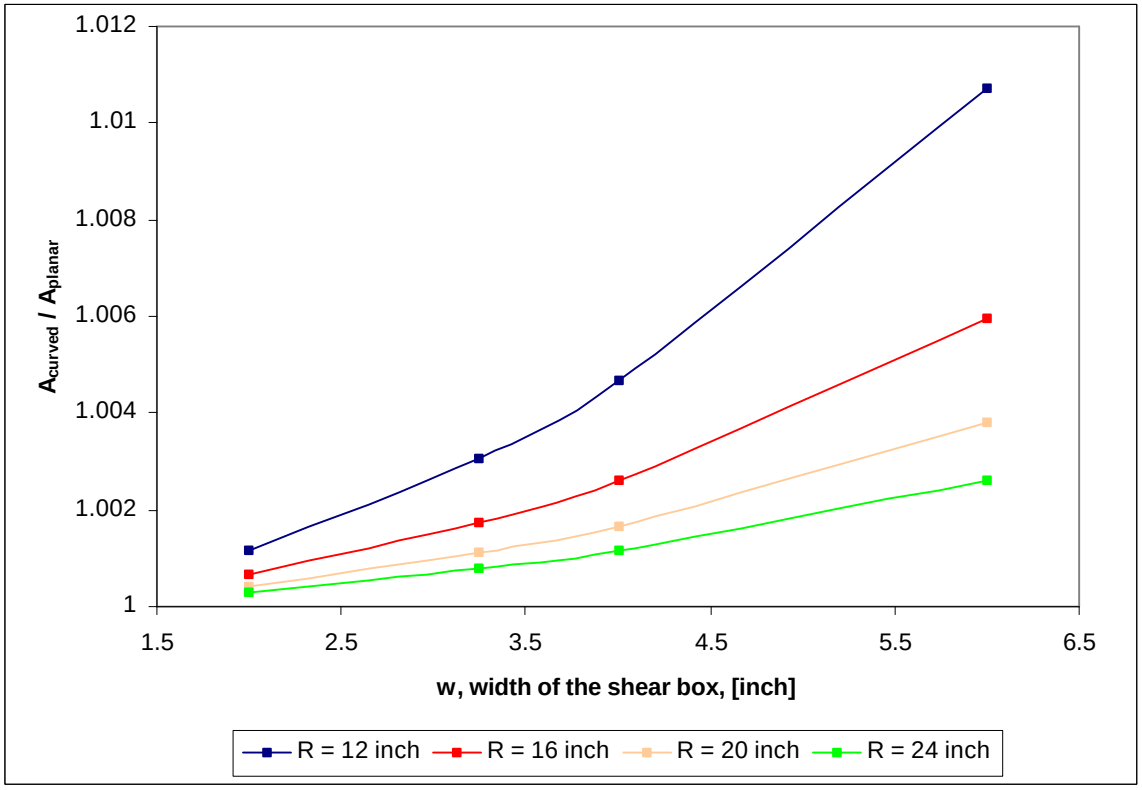


Figure 3.2 Ratio of the Curved Area To Its Projection on a Plane versus the Width of the Shear Box

On the other hand, the shear box has to be stiff and strong enough to support all the vertical and horizontal loads without allowing any compliance or deformation during shearing. These two constraints, “minimum boundary friction versus shear box stiffness”, played a major role in the final device design. A plan view of a shear box is simply illustrated in Figure 3.3. To analyze the effect of the boundary conditions, the plots in Figures 3.4 and 3.5 were developed:

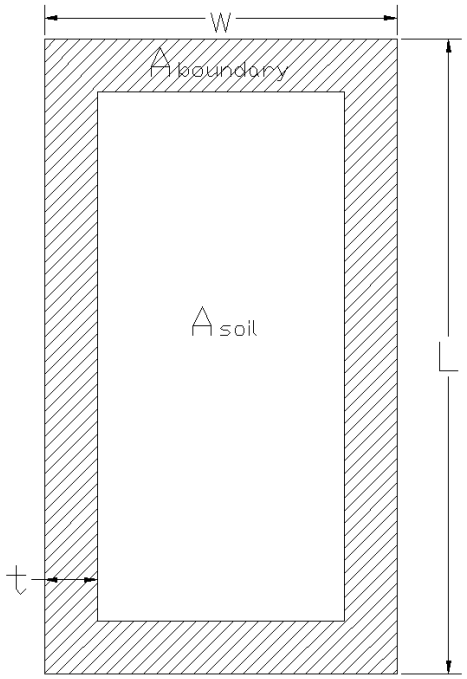


Figure 3.3 Simple Illustration of the Shear Box

These plots show that the ratio of the boundary area to the soil area decreases when the box length is increased but eventually tends to approach a constant value at higher L-values for a given box width. Accordingly, choosing a longer box does not continue to have the corresponding effect on the magnitude of the ratio of $A_{boundary}/A_{soil}$.

If the width of the box is increased, then the soil interface represents a larger area and the ratio decreases. Similarly, if the thickness of the walls is decreased, the ratio of $A_{boundary}/A_{soil}$ also decreases as seen in Figures 3.4 and 3.5 for wall thicknesses of 0.1875'' and 0.25'', respectively.

Considering all the aspects discussed above, the design box dimensions were chosen to be as w=4.25 inch, L=9 inch and t=0.1875 inch, which give a reasonable $A_{boundary}/A_{soil}$ ratio of 0.14. This value is comparable to or less than the commercially

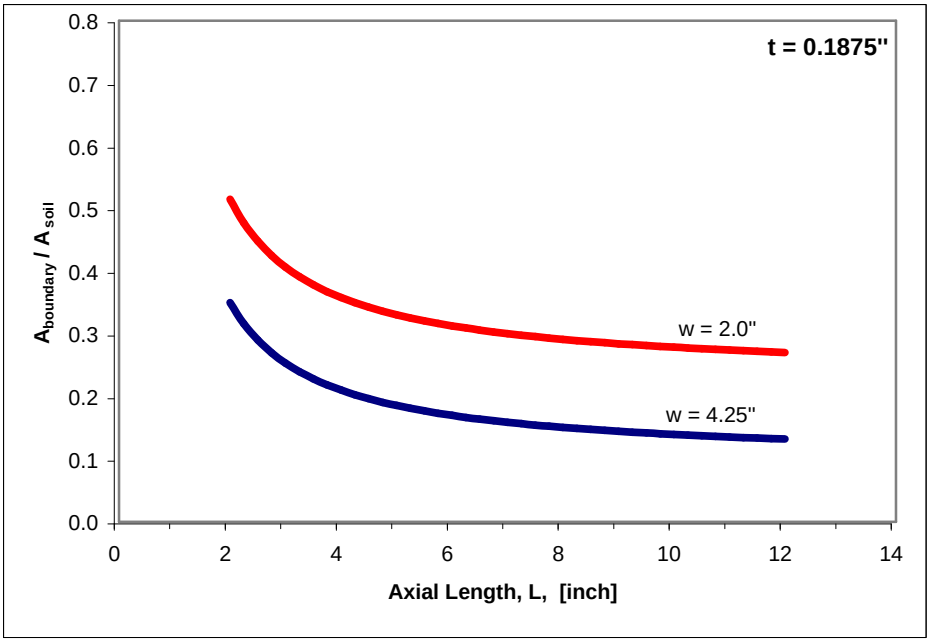


Figure 3.4 The Ratio of the Boundary Area to the Area of the Soil For Two Different Shear Box Widths and a Wall Thickness of 0.1875 inch

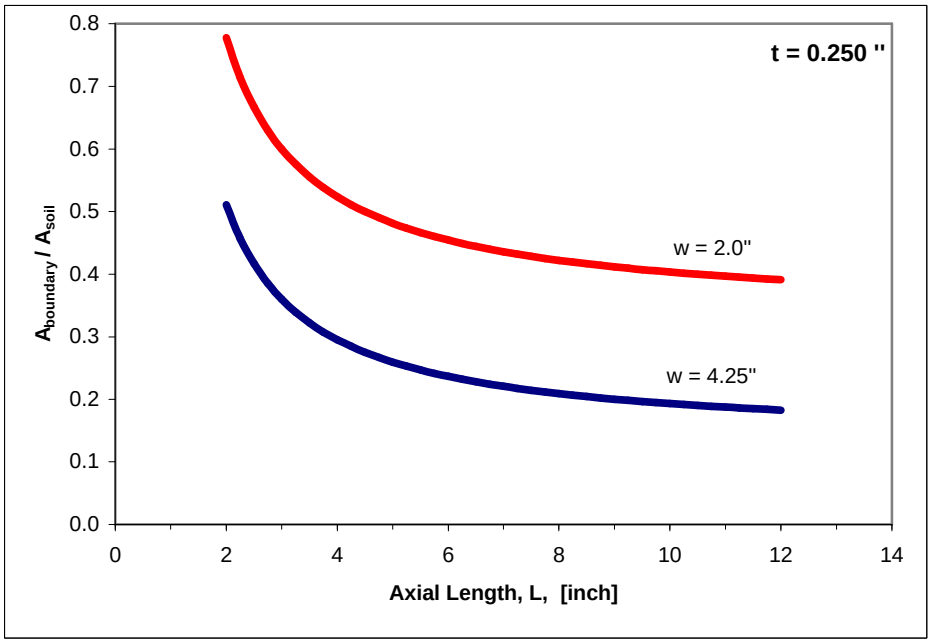


Figure 3.5 The Ratio of the Boundary Area to the Area of the Soil For Two Different Shear Box Widths and a Wall Thickness of 0.250 inch.

available devices. However, the proposed wall thickness, while satisfying boundary area constraints, is small for carrying imposed during shearing the loads without deformation. This problem was overcome by the design enhancement explained in the next section. The height of the box was proposed to be 2.125 inches at the center of the box.

## 3.3 The New Apparatus

As previously noted, the pipes to be tested were of different radius. In section 3.2, the validity of using a planar box on a curved surface was discussed in terms of normal stress. Besides this, the compatibility of the underside of the box with the surface to be tested was another major design consideration. In conventional direct interface shear testing, this is not critical because both the underside of the box with the surface to be tested are planar. In other words, they have both infinite radius of curvature, whereas in the case of curved surfaces, the radius of curvature changes from pipe to pipe. If the underside of the box does not “fit” the surface, particle leakage would be inevitable under the application of normal and horizontal loading.

This problem is solved in the new design. The new device includes a double-wall shear box, the inner wall of which is interchangeable to allow for testing against surfaces of different curvature. The outer wall serves as a frame, to which the inner walls are attached. This outer wall (frame) is not in contact with the interface, it is an element to increase the stiffness of the box. The ability of this apparatus to use different sets inner walls allows the user to test the interface behavior of any curved surface.

The pipes used in this study can be classified as having one of the 3 nominal values in terms of their curvature (R=12 in., R=14 in., and R=22 in.). Accordingly, three sets of

inner walls were designed and manufactured. The drawings of the end and sidewalls for R=14 in. are in Figures 3.6 and 3.7.

As can be seen from Figure 3.6, the front and rear walls have a curved bottom edge, and are of same curvature as the particular pipe. The sidewalls also have a bevel at their bottom edge to “fit” the surface of the particular pipe as shown in Figure 3.7. This compatible design prevents additional friction forces and leakage of particulate material.

A plan view of the shear box with the inner walls attached to the outer walls is given in Figure 3.8. The nominal thickness of the walls is 0.375 inch to have necessary stiffness but decreases to 0.1875 inch at a small portion next to the surface to reach the target ratio of $A_{boundary}/A_{soil}$. The inner walls are attached to the outer frame by 28 screws. A photograph of the underside of the box is shown in Figure 3.9. A coupon of wet-cast concrete pipe and the shear box on top of the pipe is given in figure 3.10. All technical drawings are given in Appendix A.

The shear load is applied via a threaded stud attached to the outer frame. The point of shear load application was chosen as close as possible to the interface in order to decrease the moment resulting from the eccentricity between the point of force application and the point of the resistant frictional force at the interface.

The normal load is applied via a steel ball at the center of a rigid, 0.75 inch thick load plate. These drawings of the load plate are given in Appendix A

The shear box described above is integrated with the large displacement interface shear device described in Section 5.2.3. This device was previously used to test geosynthetic-soil interfaces. To gain space for the pipe instead of geosynthetics, the

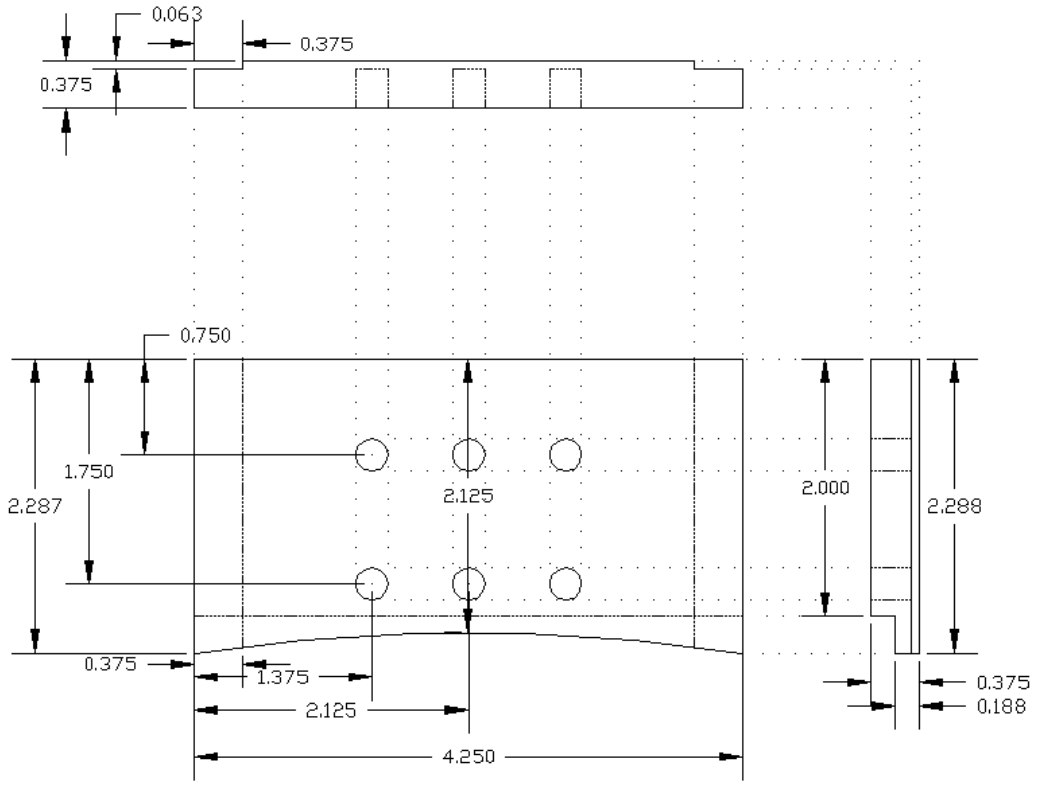


Figure 3.6 Inner End Wall for R=14 in. (all dimensions are in inch)

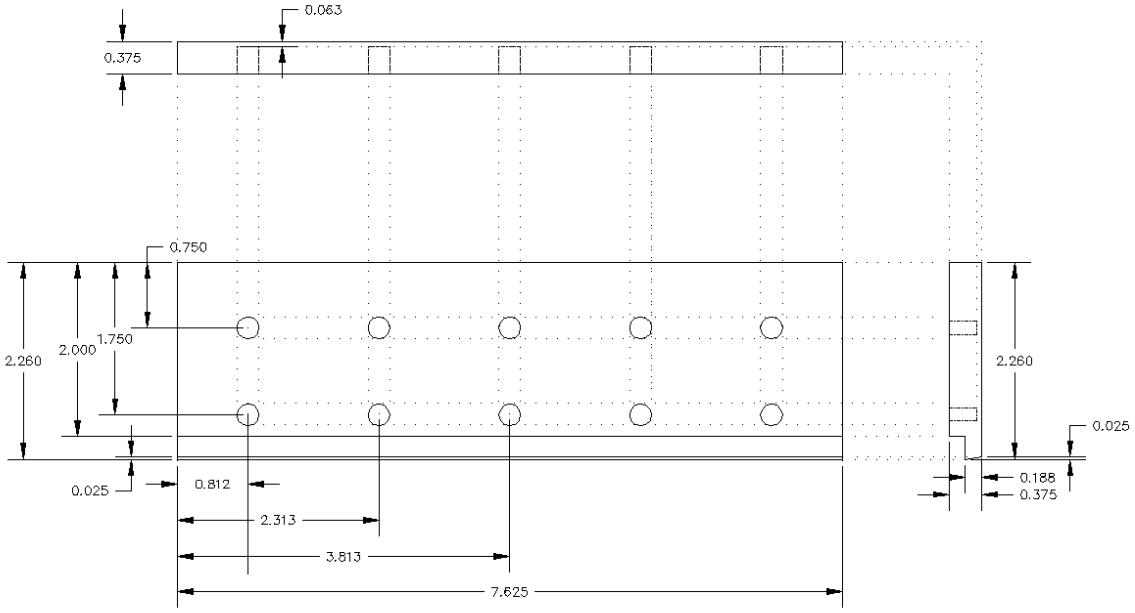


Figure 3.7 Inner Sidewall for R=14 in. (all dimensions are in inch)

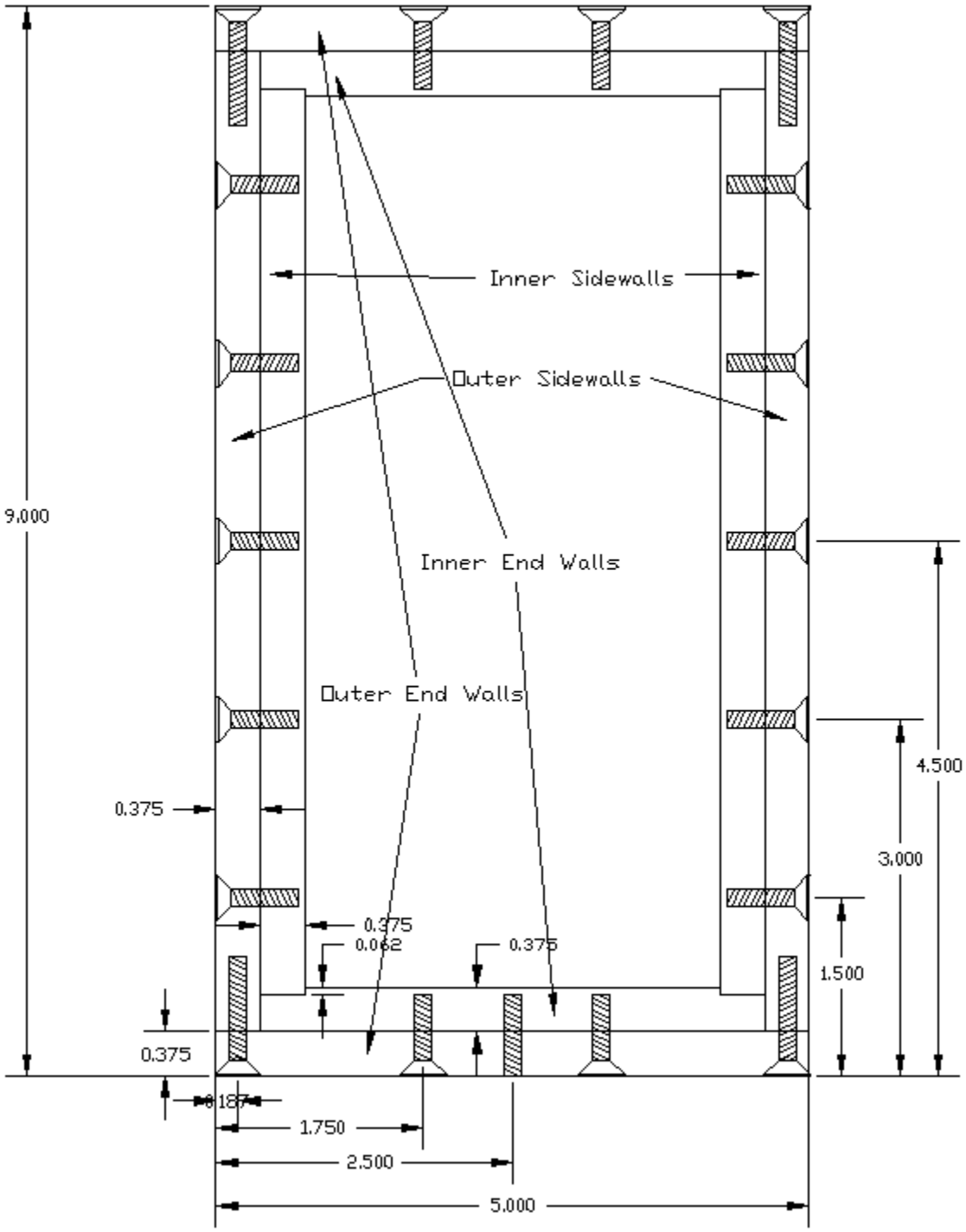


Figure 3.8 The Plan View of the New Shear Box (all dimensions are in inch)

aluminum box used to fix the geosynthetics was replaced with a new aluminum pipe container. This container has two functions: (a) to secure the pipe to the table and (b) to serve as a “bentonite pool” for future test purposes, since bentonite is used as a lubricant in some pipe-jacking applications.

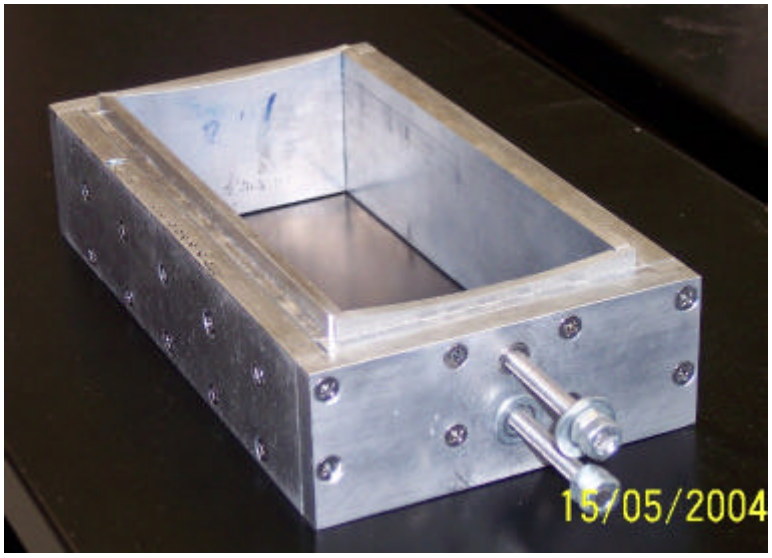


Figure 3.9 Photograph of the Underside of the Shear Box

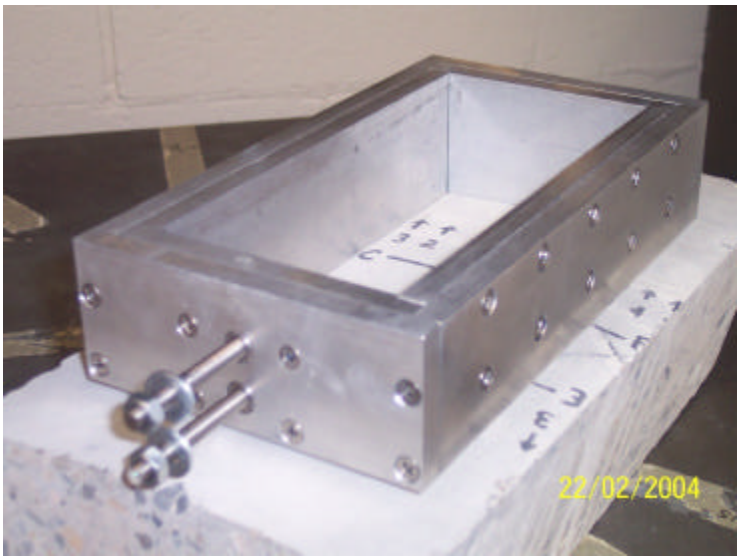


Figure 3.10 Shear Box on Top of the Pipe Coupon

To fit the pipes inside the container, they have been cut to proper dimensions. The cuttings were performed by a wet-concrete saw, which is normally used to cut concrete blocks.

The shear box, the pipe container and other related equipment was manufactured in the machine shop of the School of Civil and Environmental Engineering of Georgia Institute of Technology except the curved profiles of the inner walls of the shear box, which were manufactured in the industry. The main material used was Aluminum Alloy 2024 due to its low unit weight and corrosion resistance. Connections were made via steel screws.

A picture from the top of the modified interface shear device can be seen in Figure 3.11.

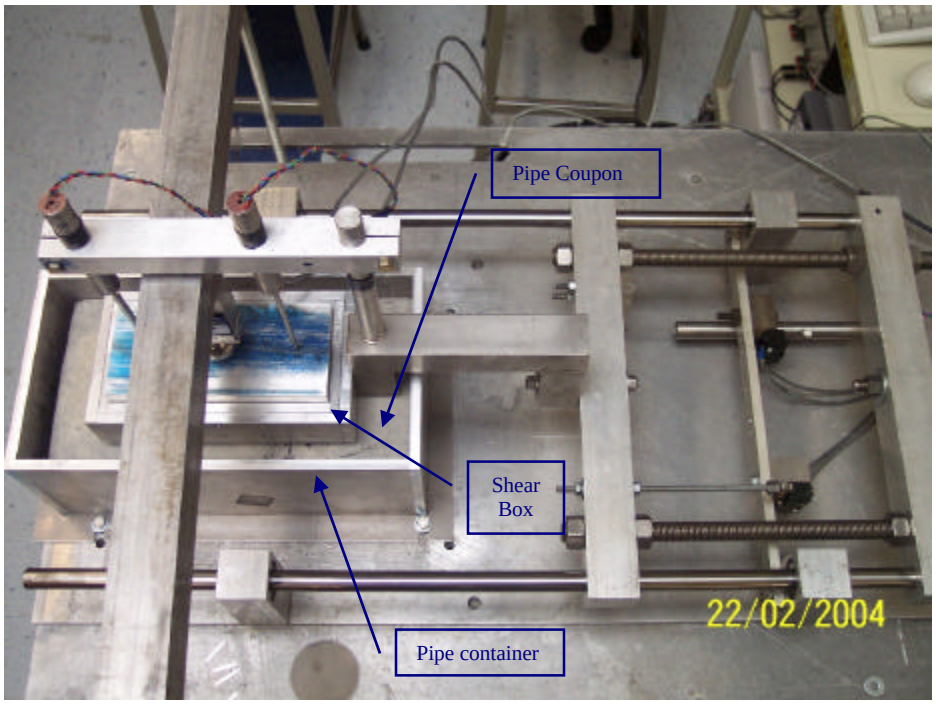


Figure 3.11 The New Design Integrated with the Large-Displacement Interface Shear Apparatus

# CHAPTER 4

# SURFACE TOPOGRAPHY CHARACTERIZATION

## 4.1 Introduction

Various researchers have investigated the relation between surface roughness and interface shear strength (Potyondy, 1961, Brumund & Leonards, 1973, Uesugi & Kishida, 1986, Paikowski et al., 1995, Frost et al., 2002). They concluded that the surface roughness is the predominant parameter that determines the interface shear behavior and strength.

These findings led the author to investigate the effect of roughness on the shear behavior of pipe-soil interfaces. The pipes used in this study have different surface characteristics, which can be quantified by various parameters such as $R_a$, $R_t$, $R_q$, $R_{sk}$, $\Delta a$, $\Delta q$, S, $\lambda_q$, $S_m$, and $L_0$. Among them, $R_a$ (average roughness) is the universally recognized, and most used, international parameter of roughness. It is defined as:

$$R_a = \left( \int_0^L |z(x)| dx \right) / L \qquad (4.1)$$

This chapter focuses only on average roughness parameter $R_a$ because $R_a$ is used to relate the surface topography with the interface shear strength in this study.

## 4.2 Experimental Program

The pipes used in this study, Hobas™ FRP, polycrete, steel, wet-cast concrete, Packerhead™ concrete, and vitrified clay, had different surface characteristics. These characteristics also showed variation for a given pipes. To account for this variability and to check for repeatability, 54 stylus profilometer surface quantification tests were performed on each pipe: 6 Series (A, B, C, D, E, F) with 5 different locations (1,2,3,4,5) within each series, were determined on each pipe surface. The locations of the series were distributed randomly on the pipe surfaces. To check the reproducibility of the tests, the test at location 1 was rerun four times. Accordingly, 9 tests were performed at each series yielding a total of 54 test results per pipe.

Later it was decided to "fabricate" two rougher pipes for use in the testing program because the existing commercial pipe interfaces were not rough enough to result in a failure in the soil body. For this purpose, artificial very rough pipe surfaces were created by gluing sandpaper No.60 and No.36 to outer surface of Hobas™ FRP pipes using Epoxy.

## 4.3 Testing Equipment

The equipment used in roughness measurements was a Taylor-Hobson™ Talysurf Series-2 stylus profilometer. This device is computer-controlled and connected to a data acquisition system. Its stylus has a 120 mm-RS-3120-stylus arm with a 2μm / 60° diamond tip and a maximum travel distance of 50 mm.

A vertical gauge range of 2.1 mm providing a 32 nm vertical resolution and a horizontal increment distance of 0.001 mm between successive readings was used during

the tests. The minimum traverse speed was chosen (0.5 mm/sec) to improve the sensitivity.

During the measurements, the profilometer table was supported on four inflated rubber supports to prevent the effect of external vibrations and noise. A photograph of the profilometer test system is given in Figure 4.1.

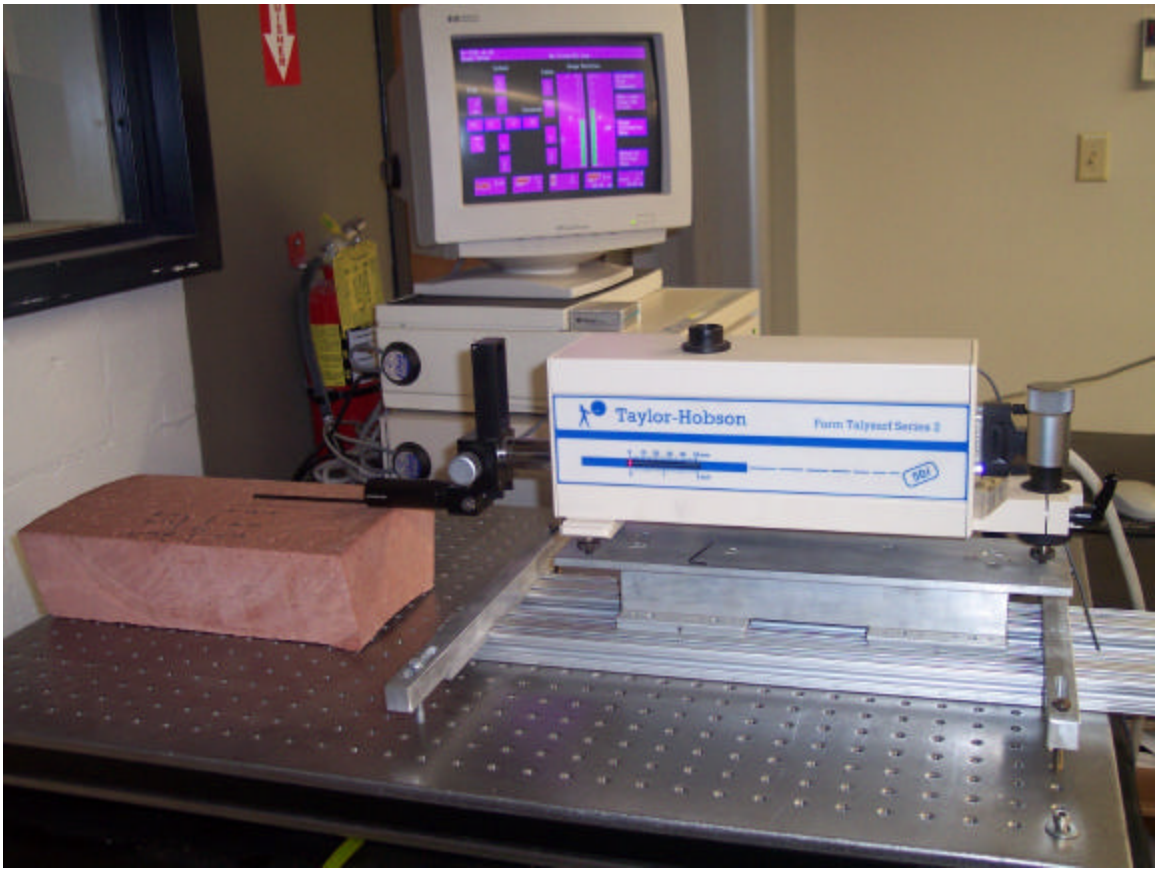


Figure 4.1 Taylor-Hobson™ Talysurf Series-2 Stylus Profilometer

After some initial tests were performed and compared to previous measurements, an inconsistency was observed. This led the author to check the calibration and the condition of the equipment. After it was clear that this inconsistency was not due to the

uncalibrated equipment, the stylus was examined under a microscope. The microscope picture of the stylus tip is given in Figure 4.2 (a). The gray piece on top of the yellow stylus is the 60° conical diamond tip, which is supposed to be sharp enough (in this case with a radius of 2μm) to detect the asperities on a profile. As it is clearly seen from the microscope photograph, the diamond tip was worn away. Figure 4.2 (b) shows a microscope image after the repair and calibration. The difference in sharpness is obvious.

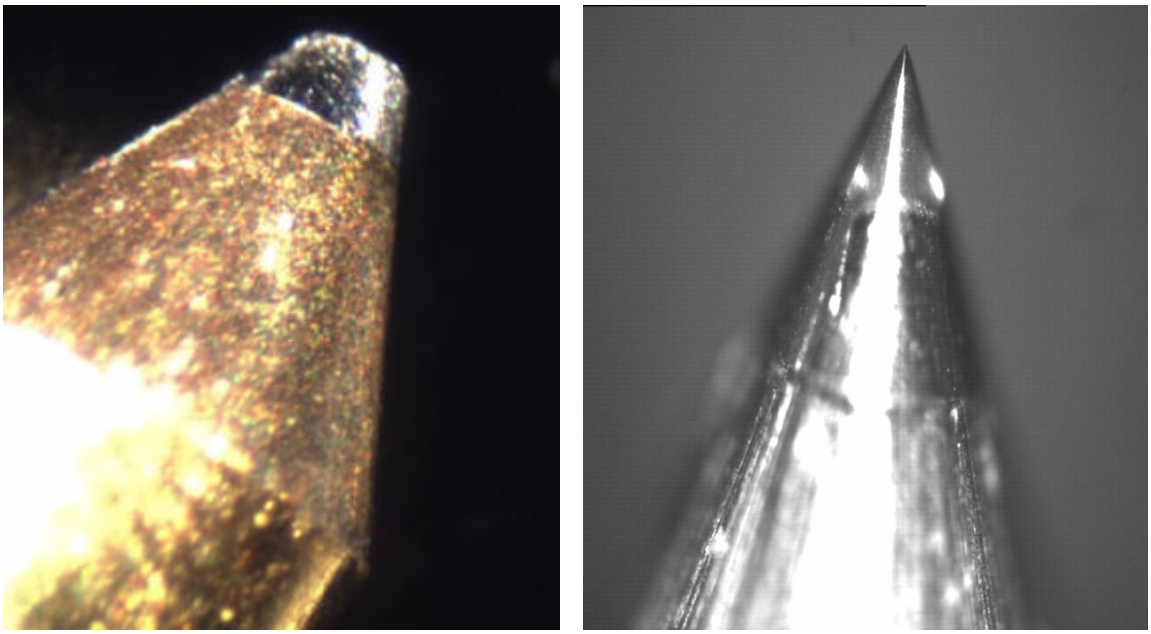

(a) (b)

Figure 4.2 Stylus Tip (a) Before Repair (b) After Repair

The equipment was then calibrated using the “three-line calibration standard”. This standard employs a standard specimen with three tiny linear grooves next to each other with an exact groove depth of 2.07 μm for the middle one. A test is performed on

this specimen and the software automatically calibrates the system according to nominal depth of the groove.

## 4.4 Test Results and Discussion

The surface profile of each individual pipe showed a variation both qualitatively and quantitatively. Asperity features like size, shape, and spacing were different. This can be seen in Figure 4.3, where the surface profiles of 50 mm traverses can be seen. All profiles are plotted with the same vertical scale.

The results are summarized in Figure 4.4, which shows the average roughness values at each particular series for each pipe. Some pipes (i.e. wet-cast concrete or polycrete) have high variation whereas others (i.e. Hobas$^{TM}$ FRP) have a small variation over the surface area. The artificially created surfaces sandpaper No.60 and sandpaper No.36 have just two series A and B instead of six because their size were smaller than the other pipes. All results are given in Table 4.1.

The results of all surface roughness measurements are further summarized in a single plot (Figure 4.5), which demonstrates the average surface roughness of the pipes with corresponding error bars. The Hobas$^{TM}$ FRP pipe is the smoothest pipe with smallest absolute variability. Other commercial pipes show similar variability in absolute terms except the wet-cast concrete pipe, which has a coefficient of variation of 78.5 %. Vitrified clay pipe is shown to have the highest average roughness value among other commercial pipes. It lies between the values of the artificial pipes Sandpaper No.60 and No.36.

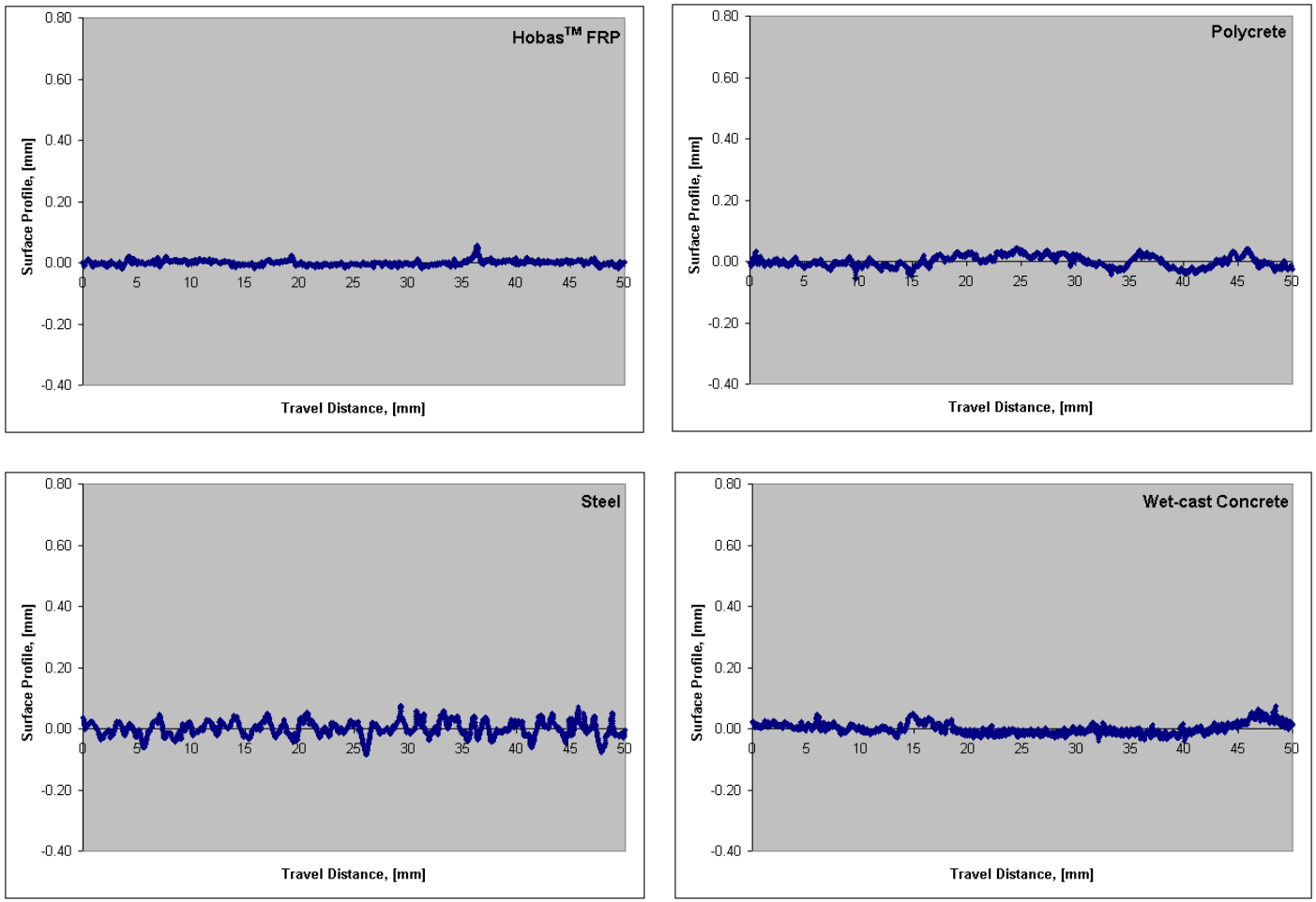


Figure 4.3 Typical Surface Profiles of Hobas™ FRP, Polycrete, Steel, Wet-cast Concrete Pipes

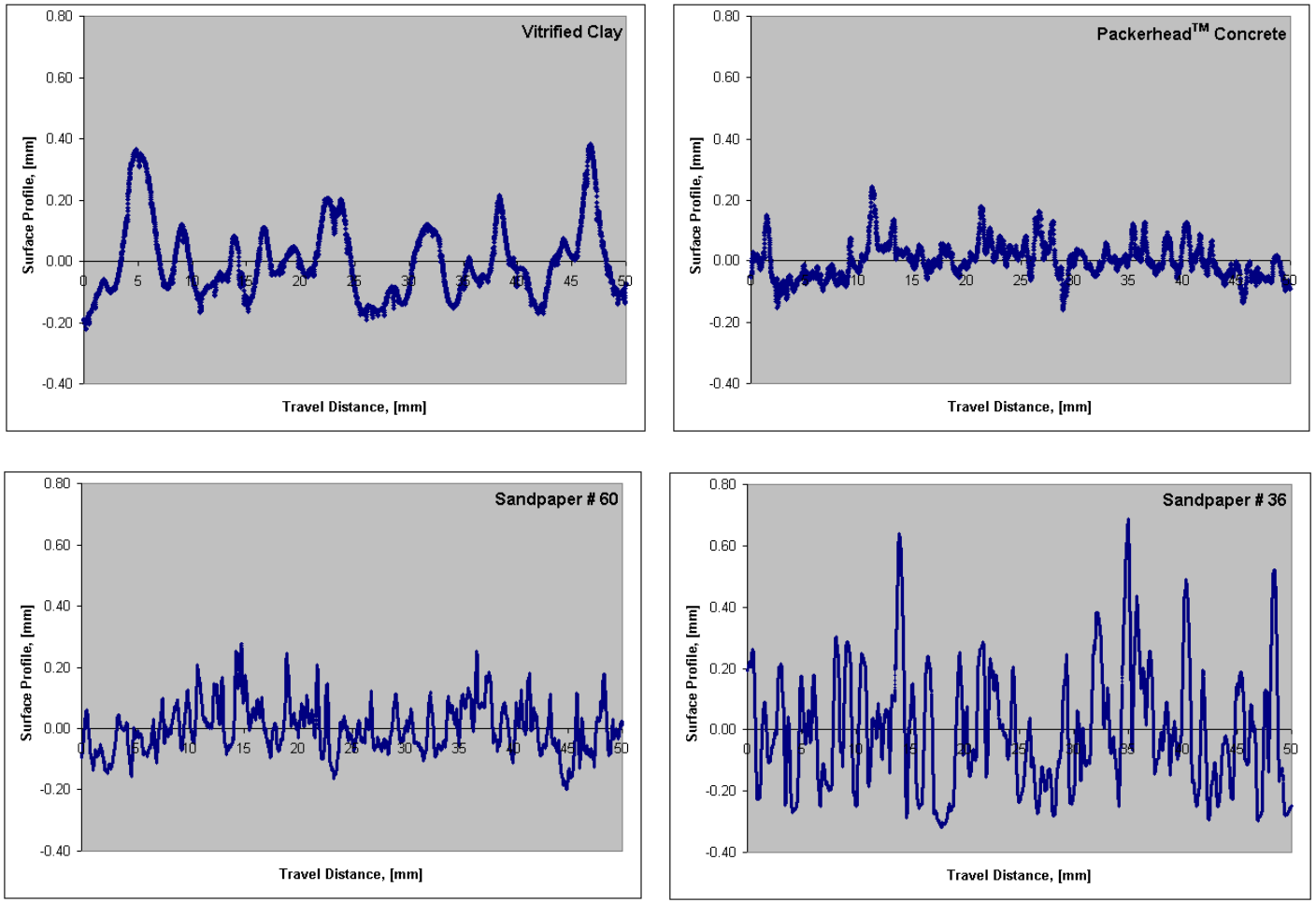


Figure 4.3 (continued) Typical Surface Profiles of Vitrified Clay, Packerhead ™, Sandpaper No.60 and, Sandpaper No.36 Pipes

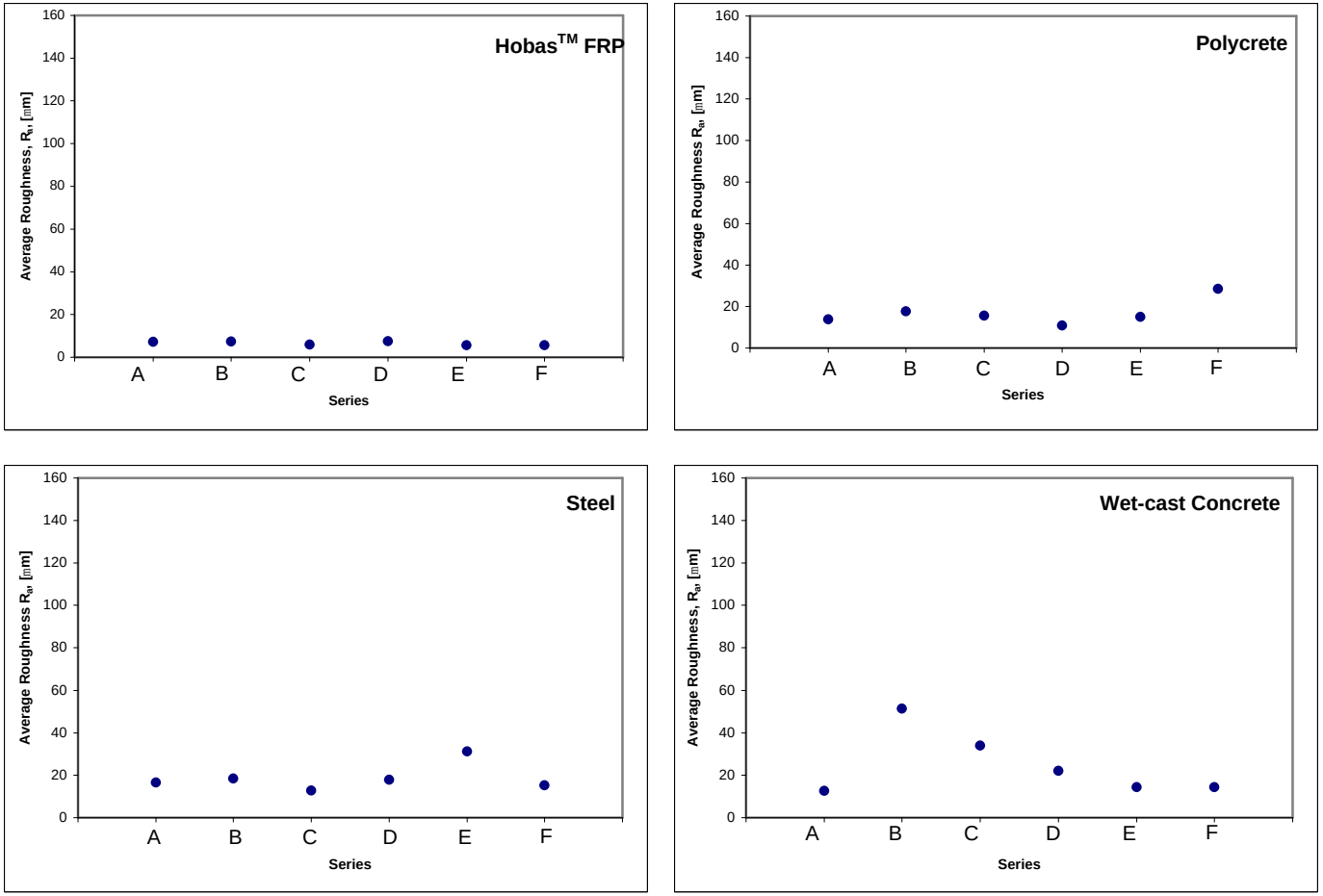


Figure 4.4 The $R_a$ Values at each Particular Series for Different Pipes

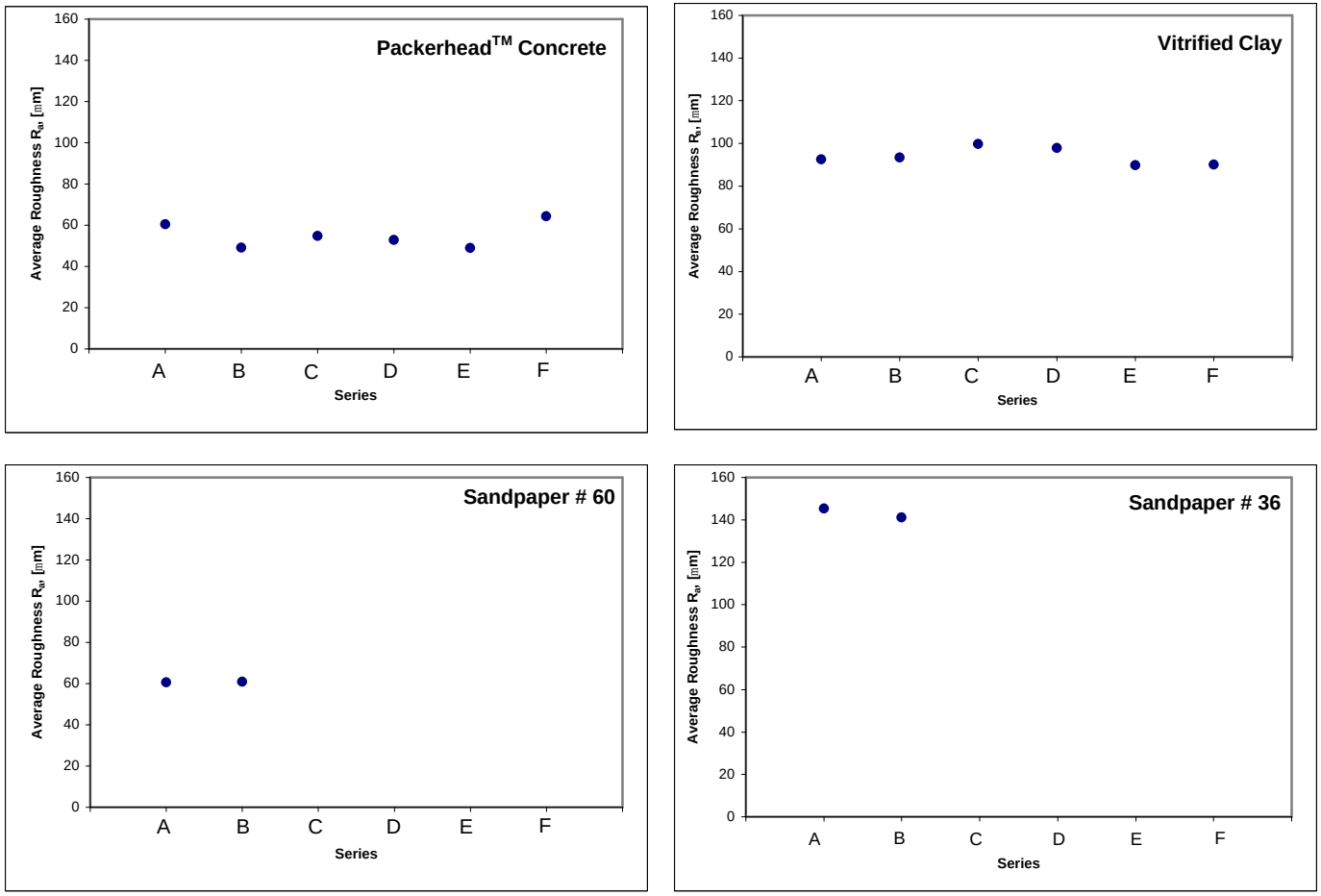


Figure 4.4 (continued) The $R_a$ Values at each Particular Series for Different Pipes

Table 4.1 The Results of the Average Roughness Tests on Pipes

| Test No. | Hobas™ FRP $R_a$ [mm] | Polycrete $R_a$ [mm] | Steel $R_a$ [mm] | Wet-cast Con. $R_a$ [mm] | Packerhead™ $R_a$ [mm] | Vitrified Clay $R_a$ [mm] | SP No.60 $R_a$ [mm] | SP No.36 $R_a$ [mm] |
|---|---|---|---|---|---|---|---|---|
| **$A1_{average}$** | 7.8 | 16.9 | 18.9 | 11.1 | 76.5 | 85.5 | 64.9 | 123.2 |
| **A2** | 5.9 | 15.4 | 19.9 | 14.1 | 44.5 | 98.1 | 62.9 | 156.6 |
| **A3** | 7.6 | 12.5 | 19.5 | 10.0 | 54.1 | 95.2 | 60.2 | 147.0 |
| **A4** | 8.9 | 9.1 | 14.5 | 11.2 | 59.7 | 97.4 | 57.5 | 173.7 |
| **A5** | 5.7 | 15.6 | 9.9 | 17.1 | 67.6 | 85.9 | 57.6 | 126.1 |
| **$B1_{average}$** | 7.2 | 35.4 | 22.1 | 63.6 | 58.0 | 96.5 | 62.0 | 150.9 |
| **B2** | 8.3 | 14.6 | 17.9 | 66.2 | 56.6 | 99.1 | 64.9 | 139.0 |
| **B3** | 6.6 | 14.7 | 23.5 | 61.0 | 42.9 | 79.6 | 54.6 | 128.4 |
| **B4** | 7.5 | 14.9 | 12.1 | 50.3 | 49.7 | 95.6 | 66.4 | 150.8 |
| **B5** | 6.8 | 8.8 | 16.9 | 16.2 | 38.6 | 96.2 | 56.5 | 136.6 |
| **$C1_{average}$** | 7.0 | 13.9 | 11.1 | 14.4 | 48.7 | 82.8 | - | - |
| **C2** | 5.7 | 19.1 | 12.4 | 16.8 | 61.9 | 124.0 | - | - |
| **C3** | 6.3 | 18.6 | 13.1 | 34.6 | 63.4 | 105.3 | - | - |
| **C4** | 4.1 | 14.0 | 12.6 | 20.8 | 51.7 | 82.0 | - | - |
| **C5** | 6.2 | 12.3 | 14.9 | 83.5 | 48.2 | 104.6 | - | - |
| **$D1_{average}$** | 8.2 | 11.1 | 18.6 | 15.1 | 53.4 | 114.6 | - | - |
| **D2** | 7.1 | 9.4 | 16.5 | 27.5 | 48.8 | 100.5 | - | - |
| **D3** | 7.0 | 11.0 | 19.2 | 22.3 | 64.3 | 93.3 | - | - |
| **D4** | 8.3 | 10.9 | 16.9 | 23.6 | 43.8 | 93.3 | - | - |
| **D5** | 6.9 | 12.0 | 18.1 | 22.0 | 54.5 | 87.2 | - | - |
| **$E1_{average}$** | 5.8 | 13.2 | 59.3 | 13.9 | 46.1 | 88.7 | - | - |
| **E2** | 5.1 | 12.5 | 26.0 | 14.2 | 52.5 | 84.9 | - | - |
| **E3** | 5.9 | 14.5 | 21.9 | 12.3 | 43.1 | 104.4 | - | - |
| **E4** | 6.6 | 17.4 | 25.2 | 12.9 | 59.9 | 100.3 | - | - |
| **E5** | 4.6 | 17.4 | 23.9 | 18.4 | 43.0 | 70.4 | - | - |
| **$F1_{average}$** | 6.4 | 16.5 | 15.8 | 15.4 | 53.1 | 76.6 | - | - |
| **F2** | 4.7 | 14.9 | 17.2 | 11.7 | 60.6 | 97.2 | - | - |
| **F3** | 4.9 | 49.0 | 15.6 | 15.8 | 85.7 | 68.9 | - | - |
| **F4** | 5.5 | 43.8 | 9.4 | 11.5 | 69.5 | 105.4 | - | - |
| **F5** | 6.4 | 18.1 | 17.9 | 17.3 | 52.8 | 101.8 | - | - |
| **Average** | **6.5** | **16.9** | **18.7** | **24.8** | **55.1** | **93.8** | **60.8** | **143.2** |
| **STDEV** | **1.2** | **9.4** | **8.8** | **19.5** | **10.6** | **12.2** | **4.1** | **15.7** |
| **% Stdev / Aver** | **18.3%** | **55.3%** | **47.2%** | **78.5%** | **19.2%** | **13.0%** | **6.7%** | **11.0%** |
| **Repeatability** | **2.7%** | **1.5%** | **4.4%** | **3.7%** | **2.5%** | **1.9%** | **5.7%** | **1.3%** |

The repeatability for a single pipe, which is defined as the ratio of standard deviation to the mean in percentage, was satisfactory in the experiments and ranged between 1.5 % and 4.4 %, where 0 % represents “perfect repeatability”.

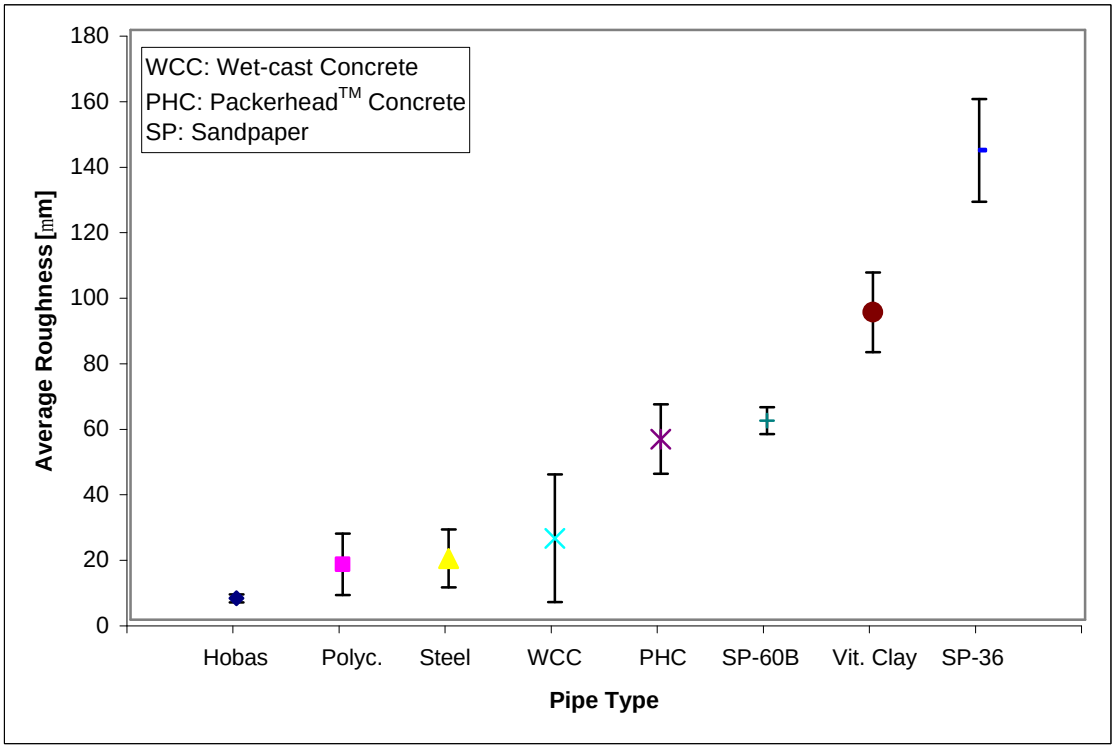


Figure 4.5 The Average Surface Roughness ($R_a$) of Various Pipes

# CHAPTER 5

# INTERFACE SHEAR TESTS

## 5.1 Introduction

This chapter summarizes the results of interface shear testing conducted as part of this study. To relate surface roughness, particle angularity, relative density, and normal stress with the interface shear behavior, various series were performed and are discussed herein. Additional details of the equipment and materials used are described.

## 5.2 Experimental Program

In this study, the shear behavior of various pipe-sand interfaces was investigated. Eight different types of pipes (Hobas™ FRP, polycrete, steel, wet-cast concrete, Packerhead™ concrete, vitrified clay, and two artificially created pipes covered with sandpaper on their surface) were employed. Two different types of sand (Ottawa 20/30 sand and Atlanta blasting sand) were used in the tests. Additional tests were performed to investigate the repeatability of the tests and to evaluate the effect of the normal stress and relative density.

During the tests, the shearing rate was constant and equal to 1 mm/min (0.04 inch/min). The horizontal displacement range was about 58 mm (2.3 inch). Measurements were recorded every two seconds; approximately 1800 readings were recorded for each test. Tests with Ottawa sand were performed at normal stresses 40 kPa, 80 kPa and 120 kPa and tests with Atlanta blasting sand were performed at 80 kPa. To evaluate the effect of the normal stress on interface shear behavior, two stress levels,

namely 160 kPa and 200 kPa, were added to the test program. All the tests noted above were conducted at a target relative density of 80%. Additional tests were performed at four different relative densities ranging from 48 % to 96 % to see the effect of relative density on the behavior. Test repeatability was evaluated with additional tests on Packerhead™ concrete, Hobas™ FRP and vitrified clay pipes. The complete testing program and test results are summarized in Table 5.7 in Section 5.3.5.

### 5.2.1 Particulate Material Properties

To study the effect of particle shape, two different types of sand were used. These are subrounded Ottawa 20/30 quartz sand and angular Atlanta 20/30 blasting quartz sand. Their index properties and standard methods used to determine them are summarized in Table 5.1.

Table 5.1 Soil Index Properties

| **Sand** | **$D_{50}$ [mm]** | **$C_u$ [1]** | **$C_c$ [2]** | **$G_s$ [3]** | **$e_{max}$ [4]** | **$e_{min}$ [5]** |
|---|---|---|---|---|---|---|
| Ottawa 20/30 | 0.64 | 1.46 | 0.96 | 2.65 | 0.747 | 0.501 |
| Atlanta Blasting | 0.82 | 1.38 | 0.77 | 2.65 | 1.092 | 0.734 |

Note: 1. $C_u=D_{60}/D_{10}$
2. $C_c=D_{30}^2/(D_{10}*D_{60})$
3. AASHTO T133
4. ASTM D4254-91, Method B
5. ASTM D4253-93, Method 2A

Typical images of the particulate materials and their grain size distributions are shown in Figures 5.1 and 5.2.

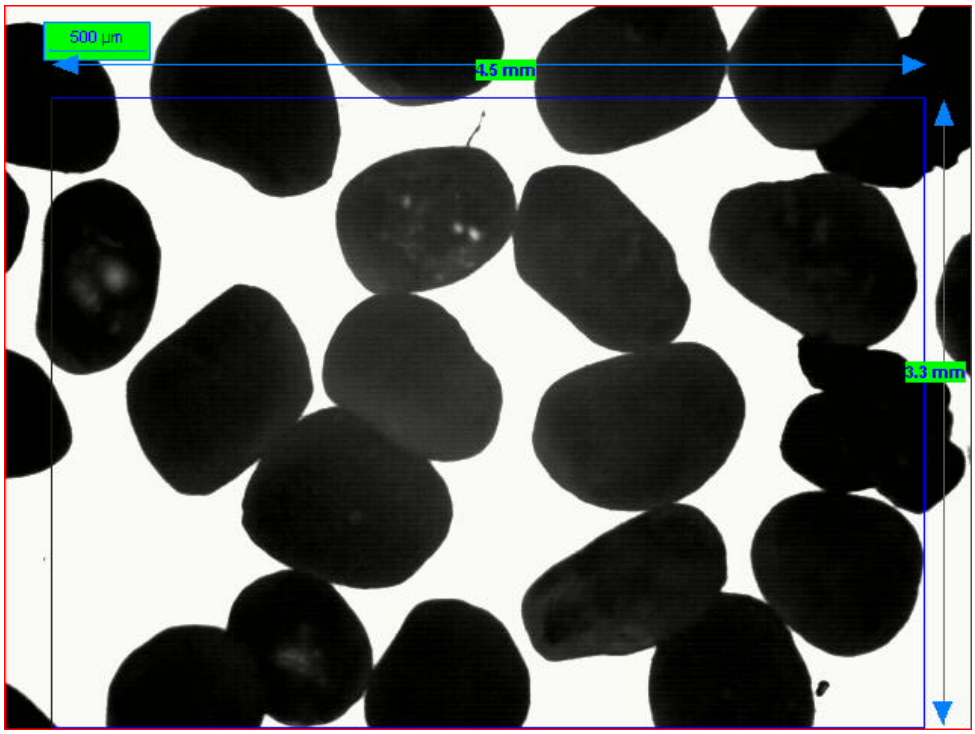


(a)

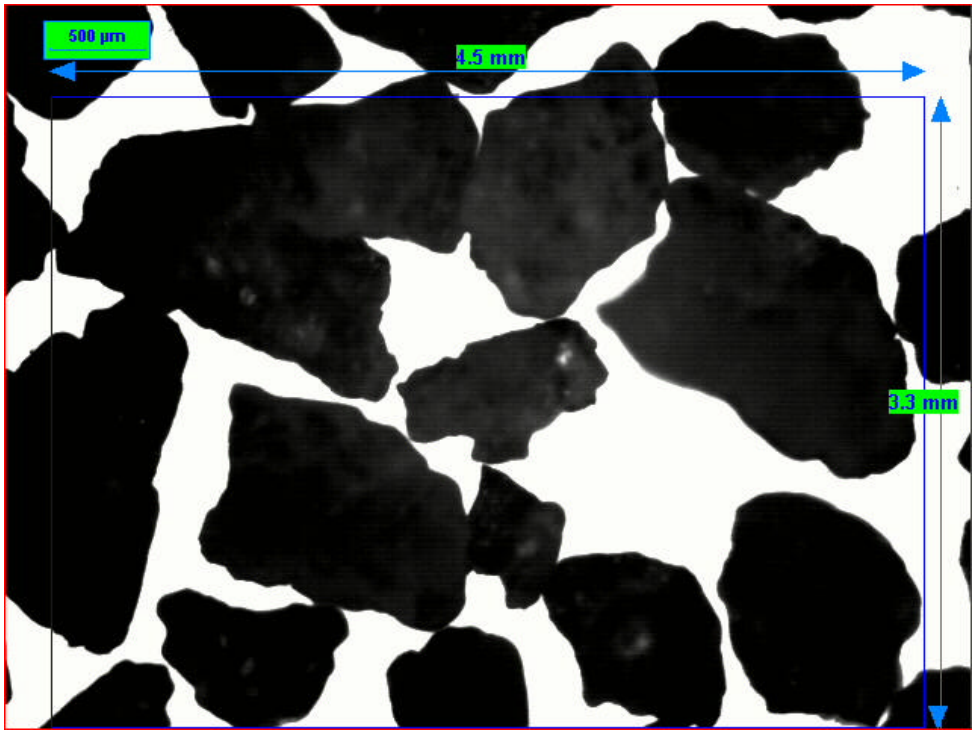


(b)

Figure 5.1 Particle Image for (a) Ottawa 20/30 Sand (b) Atlanta blasting sand

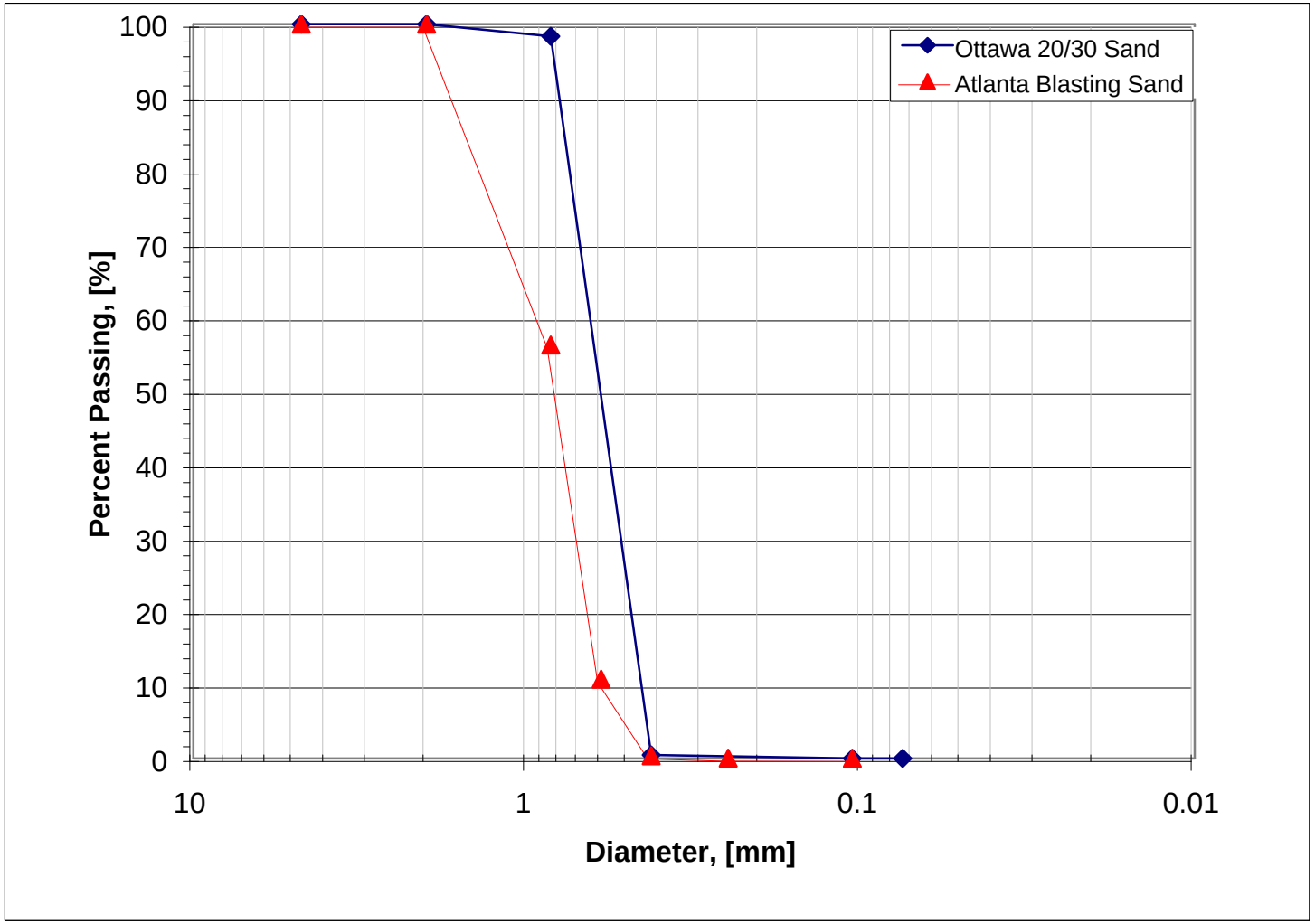


Figure 5.2 The Particle Size Analysis for Ottawa 20/30 Sand and Atlanta Blasting Sand

5.2.2 Continuum Material Properties

The pipes or sections of pipes used in this study are illustrated below in Figure 5.3.

(a) Hobas™ FRP


(b) Polycrete

(c) Steel


(d) Wet-cast Concrete

(e) Vitrified Clay

(f) Packerhead™ Concrete

Figure 5.3 Types of Pipes Used


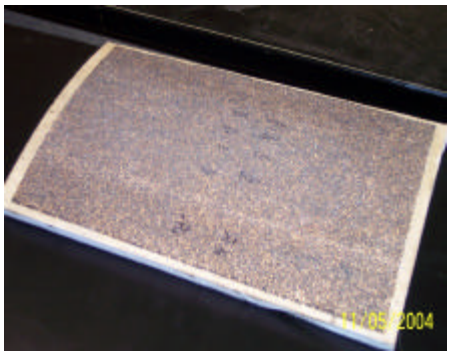

(g) Sandpaper No.60 (h) Sandpaper No.36

Figure 5.3 (continued) Types of Pipes Used

5.2.3 Interface Shear Test Equipment

The interface shear tests were performed using a large-displacement constant-stress apparatus. This apparatus was adopted from an existing device at Georgia Institute of Technology (Zettler, 1999). A plan view drawing of the equipment and photographs from end, side and plan views are given in Figures 5.4, 5.5, 5.6, and 5.7, respectively.

The shear box is driven by a Bodine® 130 Volt DC motor. Gear reducers allow the user to achieve relatively low speeds. The system is controlled electronically by a Dynapar® Series H20 encoder and Dart® speed control system. Two end switches limit the travel of the shear box and stop the motor automatically when the desired shear displacement is achieved.

The normal load is applied by an air-pressurized piston mounted under the shear table. The piston is able to move horizontally on rails when the shear box moves. The pressure is set manually through a control panel and kept constant with a pressure regulator. Its magnitude is determined and monitored via the vertical load cell mounted between the load crosshead and the loading plate.

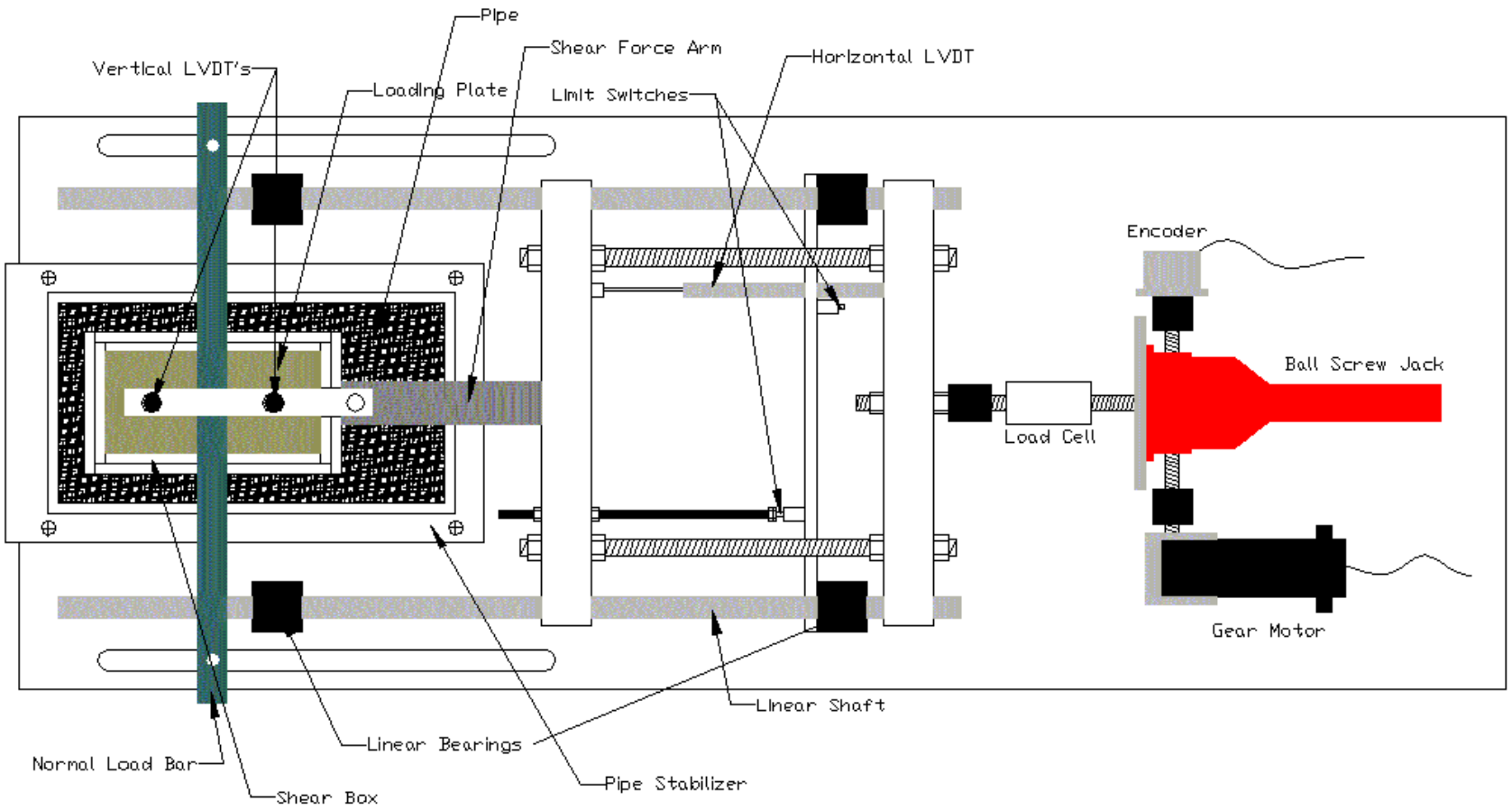


Figure 5.4 The Plan View of Interface Shear Device

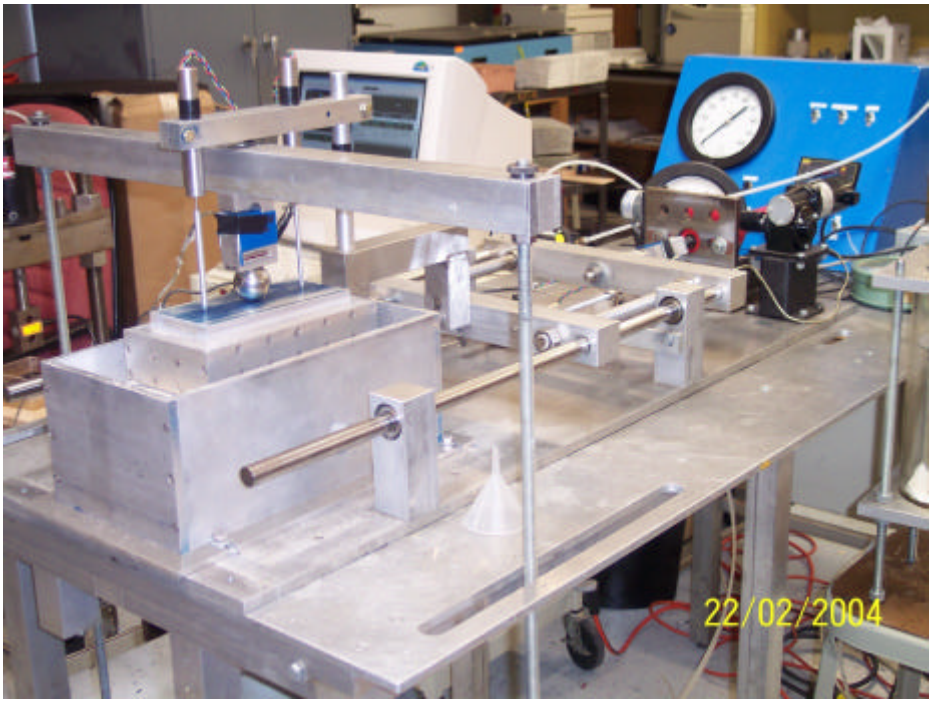


Figure 5.5  Interface Shear Device (End View)


Figure 5.6  Interface Shear Device (Side View)

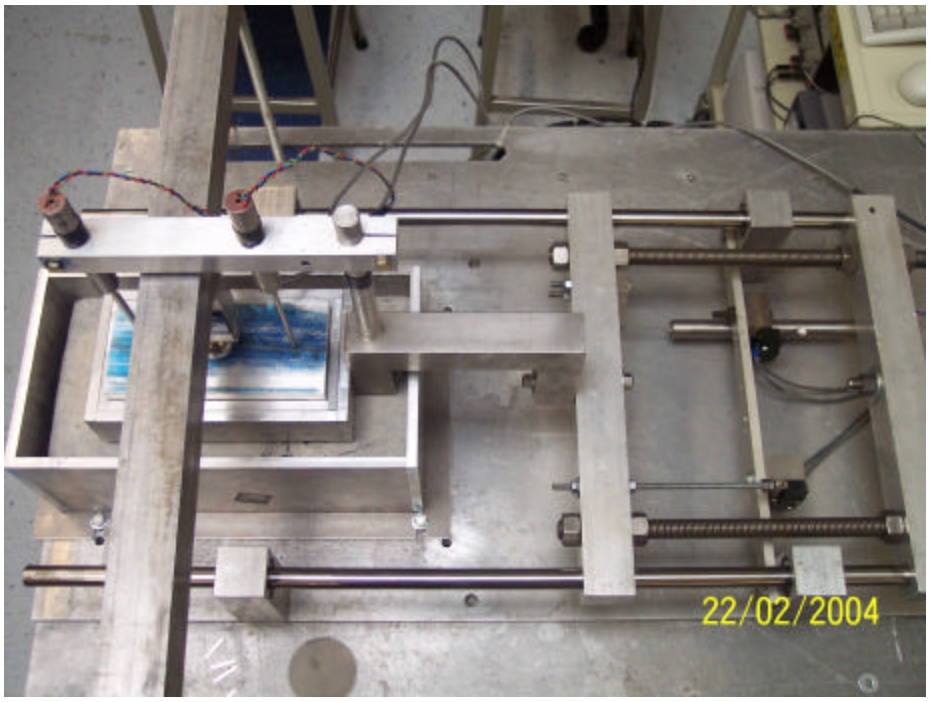


Figure 5.7 Interface Shear Device (Plan View)

The continuum material (pipe) was fixed with an aluminum container / stabilizer which can be used as a “lubricant pool” for future purposes. Details of the shear box were provided in Chapter 3.

Five different data sets were collected electronically. These were vertical (normal) load, horizontal (shear) load, two vertical displacements and horizontal displacement. Vertical and horizontal load measurements were taken with Interface Force® Series SM-1000 load cells with a range of 1000 lbf. Vertical displacement measurements were taken with Trans-Tek® Series 0244 LVDT’s (linear variable differential transformer) with a maximum usable range of ±1.5 inches (±38.1 mm), and horizontal displacements were taken with Trans-Tek® Series 0245 LVDT with a maximum usable range of ±2.75 inches (±69.8 mm).

Agilent® 34970A data acquisition/switch unit and HP BenchLink Data Logger software were used to collect, process, display and save the data. The device has a maximum resolution of $6_{1/2}$ digits (22 bits) with 0.004% basic 1-year dcV accuracy. $5_{1/2}$ digits (18 bits) resolution was used in this study. The resolution of the measurement systems are ±0.5 lbf for the load cells and ±0.05 mm for the displacement transducers. The area of shearing was constant during the tests because the test coupons of the pipes were longer than the length of the box plus the shearing distance.

### 5.2.4 Specimen Preparation

Specimens were prepared using an air pluviation technique. This technique gives uniform specimens (Mulilis et al., 1977, Rad and Tumay, 1987, Frost and Park, 2003), is simple and repeatable. Two main factors affecting the relative density of the specimen are the fall height of the particles and the opening size of the sieve (or the deposition intensity) (Rad and Tumay, 1987). Increase in fall height results in an increase in impact energy and consequently a higher density in the specimen. A smaller sieve size allows a more dispersed sand rain and particles have a higher opportunity to fill the gaps between each other.

The sand rainer used in this study had four holes and the opening size could be changed via a shaft that was connected to a disc on top of the hole plate. Maximum diameter of the openings was 0.5 inch. Photographs of the sand rainer and the hole pattern are given in Figure 5.8.

In this study, the sieve opening size was changed to reach desired target densities. The fall height was kept constant. Trials were performed to determine the appropriate opening size to achieve the desired relative density.

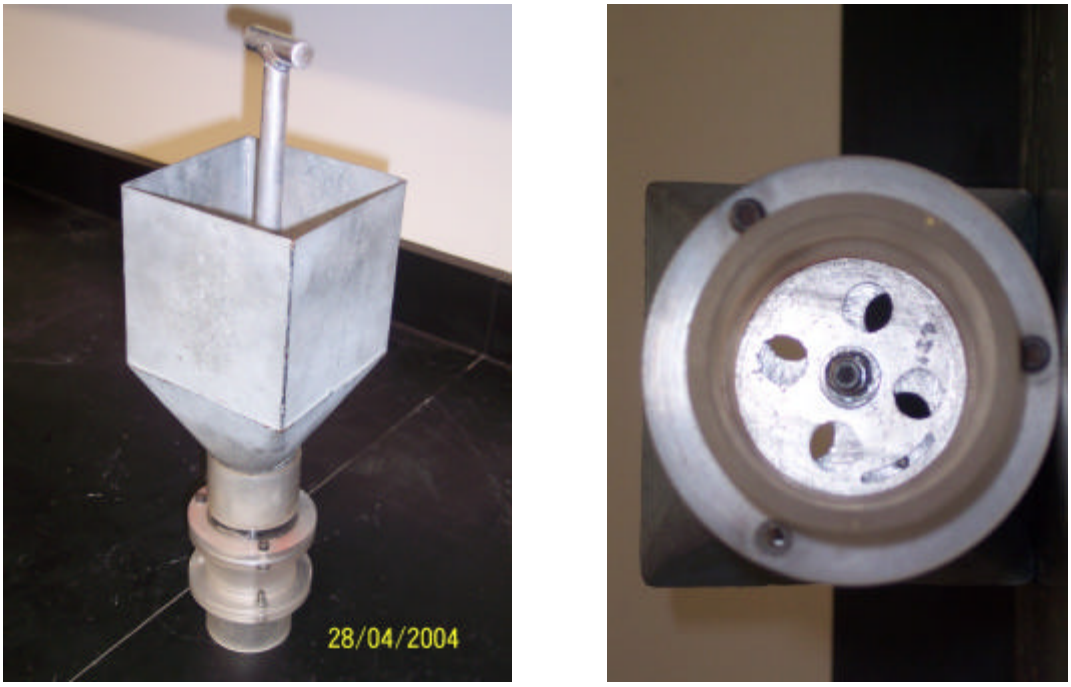


(a) (b)

Figure 5.8 (a) The Sand Rainer (b) The Opening Pattern

The average relative density was 79.7% ±3.8% for the Ottawa 20/30 sand and 81.3% ± 2.5% for the Atlanta blasting sand. Also, additional tests were performed within a density range of 47%-98% to evaluate the effect of void ratio on the interface shear behavior.

To determine $e_{max}$ and $e_{min}$, the standard procedure of the ASTM D4253-93 and ASTM D4254-91 was followed.

### 5.2.5 Experimental Error

Some minor difficulties and problems were encountered when performing interface shear tests including some minor tilting of the loading plate. Although the point of shear load application was designed as close as possible to the interface, a couple still existed between the shear load and friction at the surface. This couple tries to rotate the sand specimen in the box and causes the tilting. It was more pronounced at higher horizontal displacements and rougher pipes, since the moment increases with roughness. Different solutions were investigated to prevent it, such as plane loading instead of point loading, eccentric loading, performing the test in reverse direction (pushing the box instead of pulling). Detailed investigation of these tests showed that the tilting does not have an important effect on the interface shear strength both at peak and residual.

Another minor problem was the leakage or loss of the particulate media from the rear part of the box. This leakage was more pronounced at rougher pipes. The reasons were (1) the tilting effect described above and (2) the surface topography of the pipes. It is almost impossible to keep all sand particles in the box because the grooves in the surface profiles allow the sand particles to move through, especially at rougher pipes. Solutions to prevent this including attaching an elastic rubber band at the boundary were evaluated but these created new friction forces between the box and the pipe and were not used during the test program. The amount of sand lost during the tests was negligible.

Tests were performed under constant-stress conditions. The validity of this statement was checked and some instability in the normal stress was observed during the tests. An example of this is illustrated in Figure 5.9. There was slight increase in the normal load after the test was initiated however this increase gradually dissipated and the

value stabilized at its initial value for the rest of the test. This was attributed to a problem in the air-piston creating the normal load. Tilting of the loading bar imposes additional friction between the piston and the surrounding hollow pressure cylinder and hinders the free movement of the piston. The piston had been modified before this study but the problem was not completely solved. To compensate the effect of this relatively small fluctuation, the coefficient of friction was used instead of shear force in interpreting the results. Further, this small fluctuation does not have a significant effect on the results.

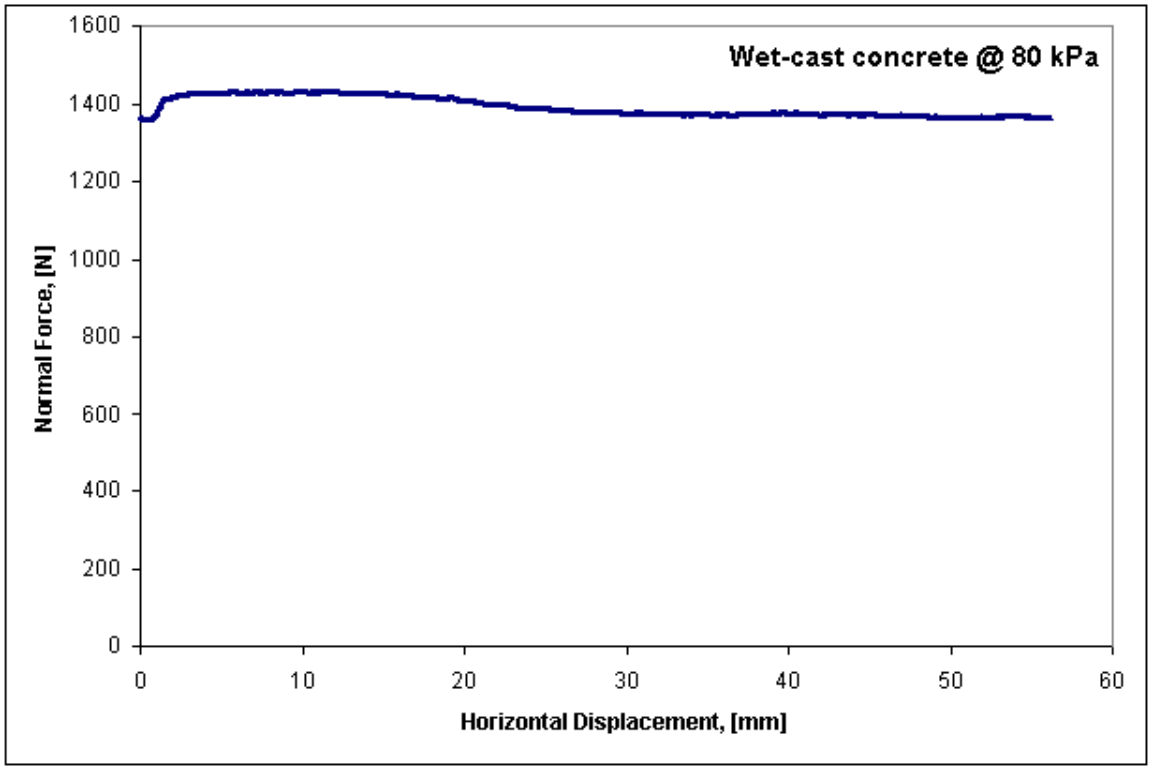


Figure 5.9 The Distribution of the Normal Force During the Wet-cast Concrete Pipe-Ottawa Sand Test @ 80 kPa

5.2.6 Direct Shear Tests

To compare the interface friction behavior with internal shear characteristics of the soil itself, direct shear tests were performed on the sands used in this study. Three tests were conducted for each sand type at normal stresses 80 kPa, 120 kPa and 160 kPa. The same specimen preparation method and shearing rate noted above were used. The specimens had a diameter of 63.5 mm (2.5 in.) and a height of approximately 2.54 cm (1.0 in.). The equipment used was a fully automated Geocomp ShearTrac II Direct/Residual Shear Device with a 10 kN (2000 lb) loading capacity, horizontal travel range of ±12.5 mm (±0.5 inch) resolved to 0.0013 mm and a vertical travel range of 12.5 mm (0.5 inch) resolved to 0.0013 mm.

The shear force at peak and steady state versus normal force curves for both sands are summarized in Figures 5.10 and 5.11. The slope of these graphs gives the friction angles. The related data and friction angles are summarized in Table 5.2. All shear force versus horizontal displacement curves for Ottawa 20/30 and Atlanta blasting sands at 80 kPa, 120 kPa, and 160 kPa are given on Appendix B.

The peak and residual friction values of the angular Atlanta blasting sand is higher than the sub-rounded Ottawa sand because the angular particles are more interlocked and resistant than the sub-rounded ones.

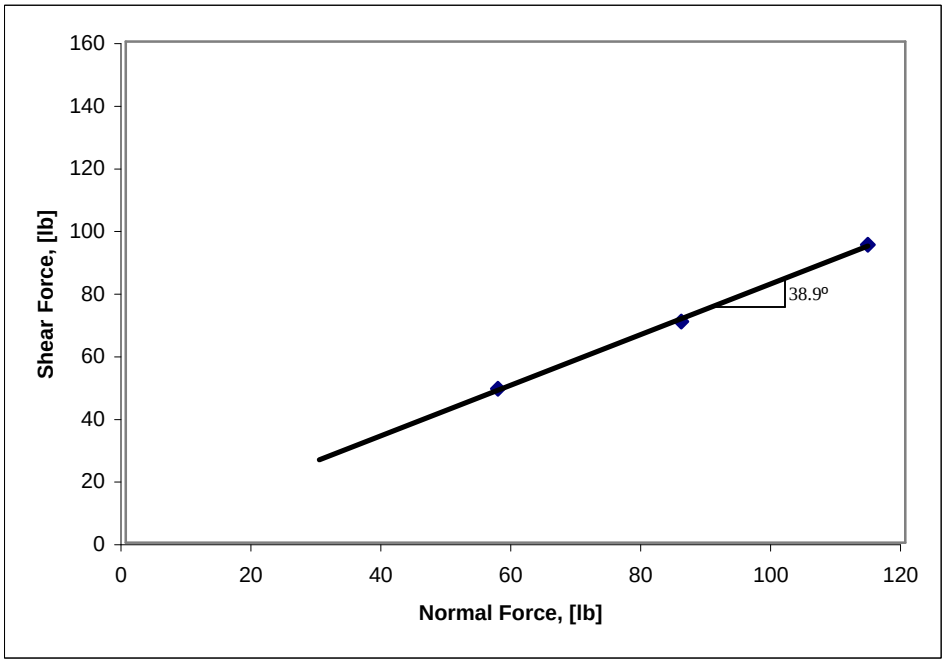


(a)

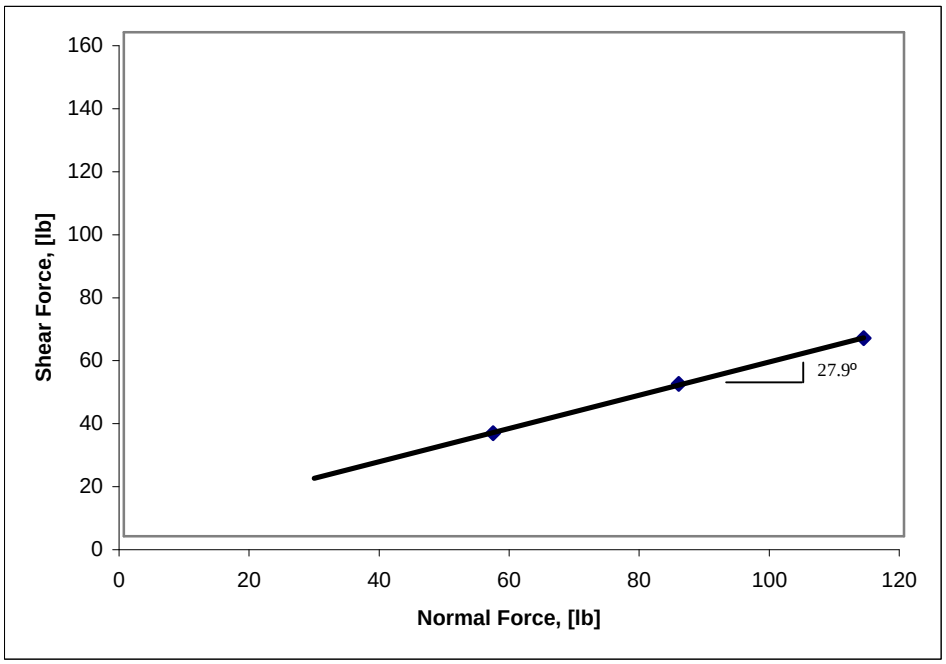


(b)

Figure 5.10 The Shear Force at Different Normal Stresses of Ottawa 20/30 Sand (a) At Peak (Friction Angle = 38.9º) (b) At Steady-state (Friction Angle = 27.9º)

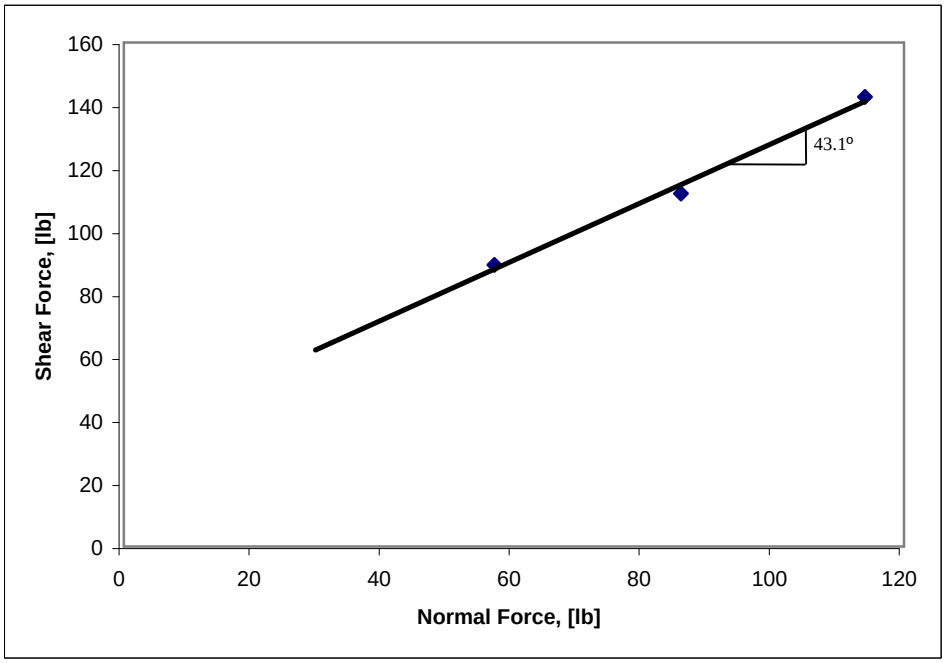


(a)

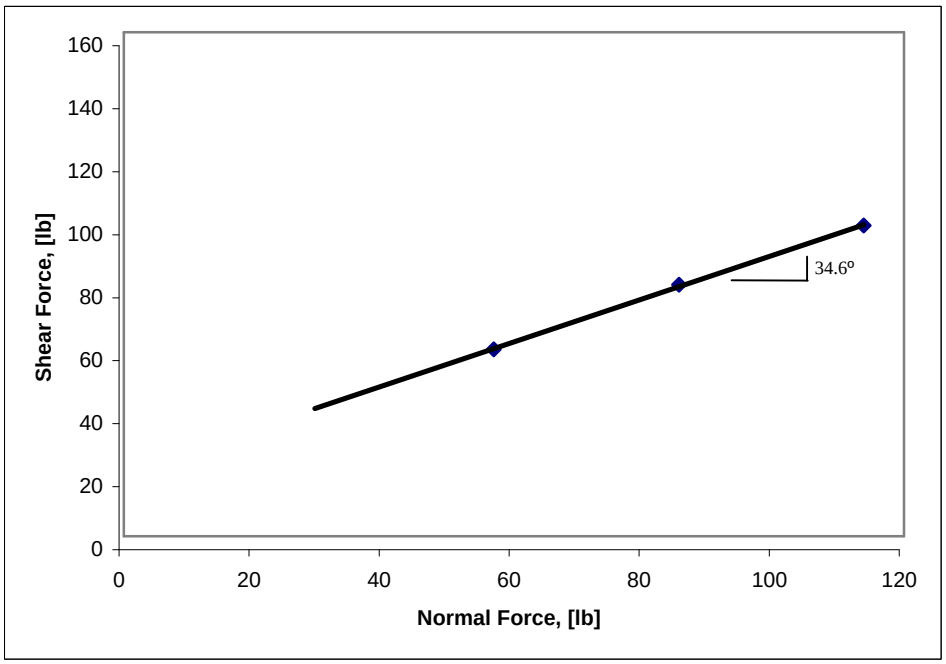


(b)

Figure 5.11 The Shear Force at Different Normal Stresses of Atlanta Blasting Sand (a) At Peak (Friction Angle = 43.1º) (b) At Steady-state (Friction Angle = 34.6º)

Table 5.2 The Peak and Residual Friction Values of Direct Shear Tests

| Sand Type | Normal Stress [kPa] | Relative Density [%] | Peak Force | | Residual Force | | Friction Angle | |
|---|---|---|---|---|---|---|---|---|
| | | | Normal [lb] | Shear [lb] | Normal [lb] | Shear [lb] | Peak | Res. |
| **Ottawa 20/30** | 80 | 81.3 | 57.3 | 49.1 | 56.8 | 32.7 | **38.9** | **27.9** |
| | 120 | 73.0 | 85.5 | 70.6 | 85.3 | 48.3 | | |
| | 160 | 77.8 | 114.2 | 95.1 | 113.8 | 62.8 | | |
| **Atlanta Blasting** | 80 | 78.0 | 57.0 | 89.4 | 56.9 | 59.3 | **43.1** | **34.6** |
| | 120 | 80.1 | 85.7 | 112.1 | 85.4 | 79.8 | | |
| | 160 | 75.4 | 114.0 | 142.7 | 113.8 | 98.6 | | |

## 5.3 Interface Direct Shear Test Results and Discussion

### 5.3.1 Effect Of Pipe Type (Roughness)

As discussed earlier, the pipes used in this study have different surface characteristics. The tests demonstrated below aim to evaluate the effect of surface roughness on the interface shear behavior. They were performed at normal stresses of 40 kPa, 80 kPa, and 120 kPa with Ottawa 20/30 sand. A total of 24 plots of coefficient of friction versus horizontal displacement are given below in Figures 5.12 - 5.23. The average relative density for the tests is 79.7 % ± 3.8 %. The relative density of each test is demonstrated on the particular figure subtitle.

The frictional behavior was different for each particular pipe. For the same test conditions (normal stress, type of sand and relative density), the coefficient of friction values increase with the increase in pipe surface roughness. The peak friction coefficient was 0.50 for the smooth Hobas$^{TM}$ FRP pipe ($R_a$=6.5 μm) whereas it was 0.73 for the

rough Packerhead$^{TM}$ concrete pipe ($R_a$=55.1 μm). All friction values are summarized in Table 5.3. The peak friction occurred within 0.8 to 3.3 millimeters of horizontal displacement. The smoother the pipe the less displacement was required before the peak friction was reached.

The pipes with intermediate roughness (steel, wet-cast concrete) and high roughness values (Packerhead concrete, vitrified clay, sandpaper #60 and #36) showed a clear post-peak softening whereas the smoother pipes (Hobas FRP and Polycrete) did not have an obvious one. This can be attributed to the shearing mechanism involved in the process. Sliding was the predominant mechanism at the interface of smoother pipes. On the other hand, particles slipped, rolled, moved vertically and rearranged at the interface of rougher pipes and reached a stable "minimum-friction" condition, which is the residual part of the shearing behavior.

The main trend in interface shear behavior of various pipes at different normal stresses was the same. The details of the effect of normal stress will be presented in Section 5.3.4.

The variability in the friction-displacement data was more pronounced at the lowest normal stress level of 40 kPa. This was considered as "normal material response" and was attributed to more "freedom" of the particles under lower stresses. The fluctuations at the steady-state part of the curves were more visible at the smooth and intermediate smooth pipes and were attributed to the mechanism (sliding versus rolling, moving vertically and, rearranging) involved in the process.

Table 5.3 The Coefficient of Friction at Various Pipe-Ottawa 20/30 Sand Interfaces

| Pipe Type | Coefficient of Friction | | | | | |
|---|---|---|---|---|---|---|
| | N = 40 kPa | | N = 80 kPa | | N = 120 kPa | |
| | peak | residual | peak | residual | peak | Residual |
| **Hobas™ FRP** | 0.51 | 0.43 | 0.50 | 0.44 | 0.48 | 0.42 |
| **Polycrete** | 0.50 | 0.42 | 0.49 | 0.43 | 0.47 | 0.43 |
| **Steel** | 0.68 | 0.49 | 0.62 | 0.44 | 0.62 | 0.47 |
| **Wet-cast Con.** | 0.68 | 0.49 | 0.65 | 0.48 | 0.63 | 0.45 |
| **Vitrified Clay** | 0.71 | 0.50 | 0.63 | 0.48 | 0.65 | 0.49 |
| **Packerhead™ Con.** | 0.81 | 0.54 | 0.73 | 0.53 | 0.73 | 0.52 |
| **Sandpaper No.60** | 0.80 | 0.60 | 0.77 | 0.55 | 0.75 | 0.55 |
| **Sandpaper No.36** | 0.82 | 0.61 | 0.76 | 0.56 | 0.74 | 0.54 |

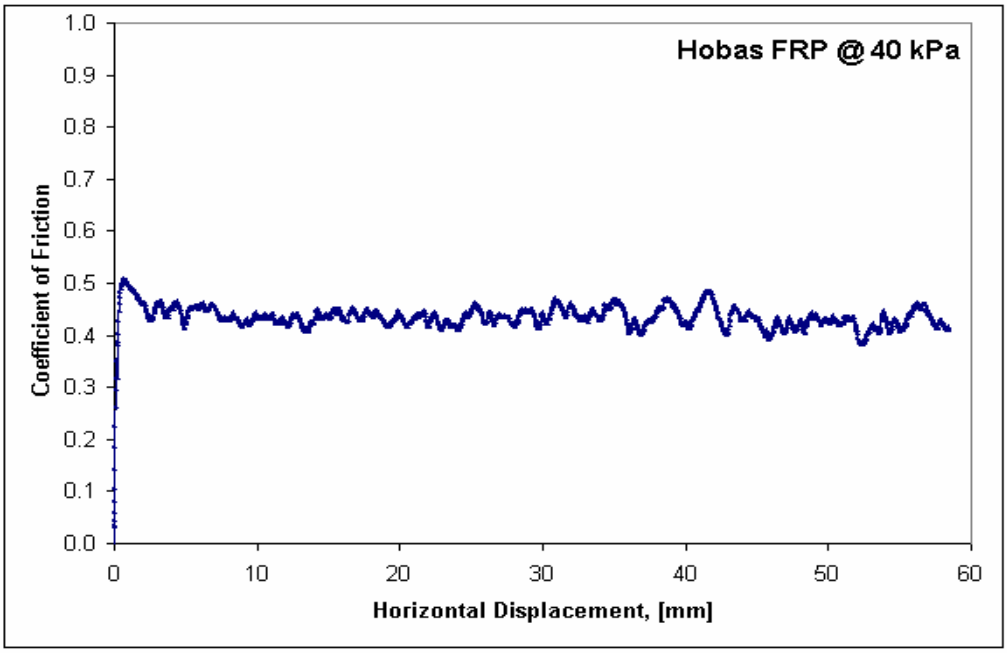


(a)

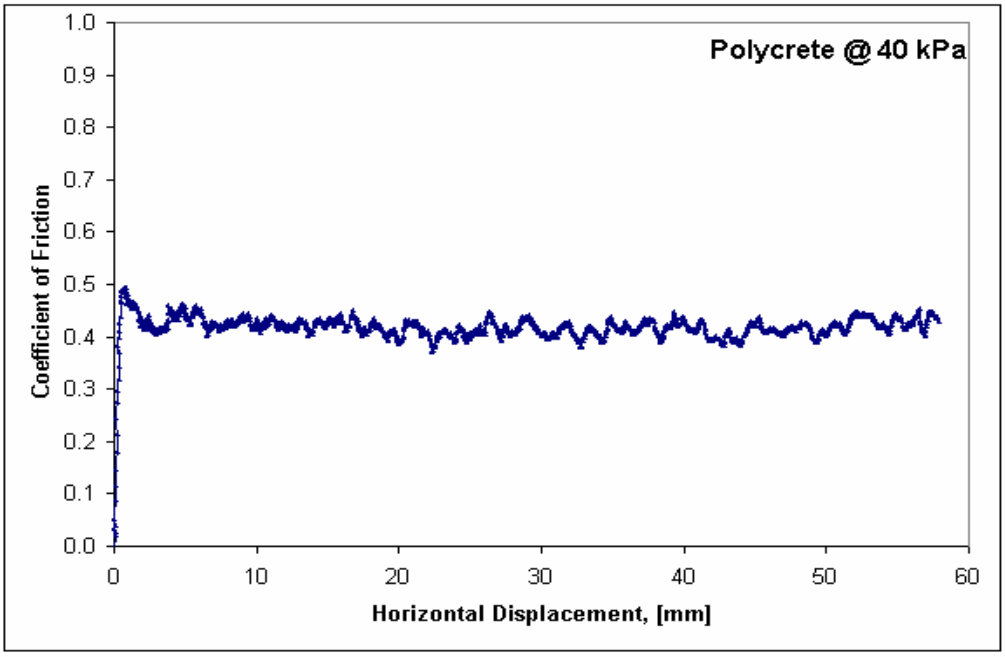


(b)

Figure 5.12 Coefficient of Friction versus Horizontal Displacement Curves of Ottawa 20/30 Sand with (a) Hobas$^{TM}$ FRP ($D_R$=%81) (b) Polycrete ($D_R$=%83) Pipes at 40 kPa.

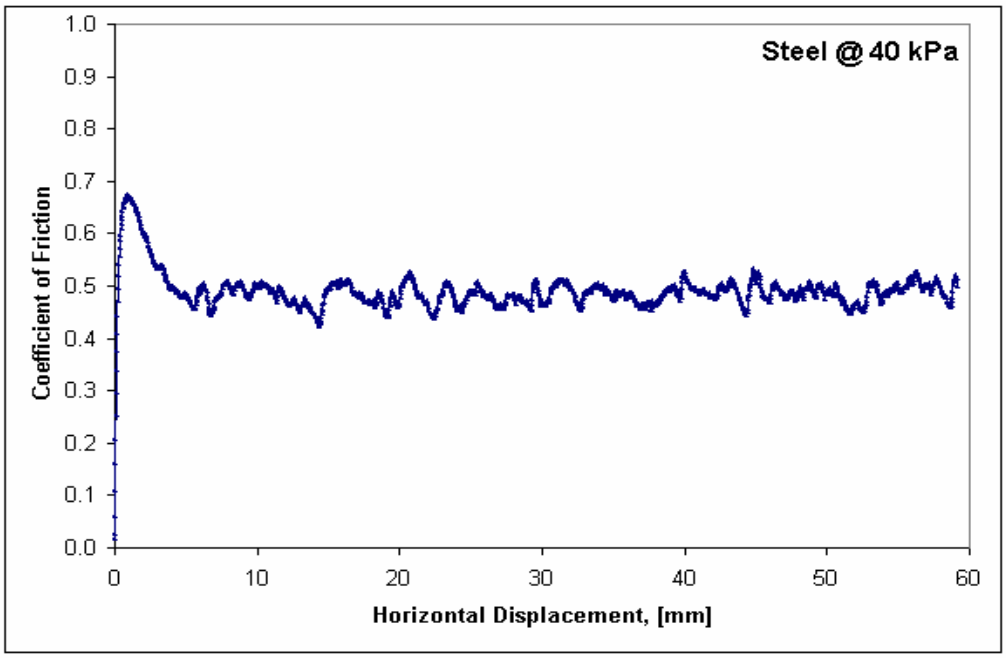


(a)

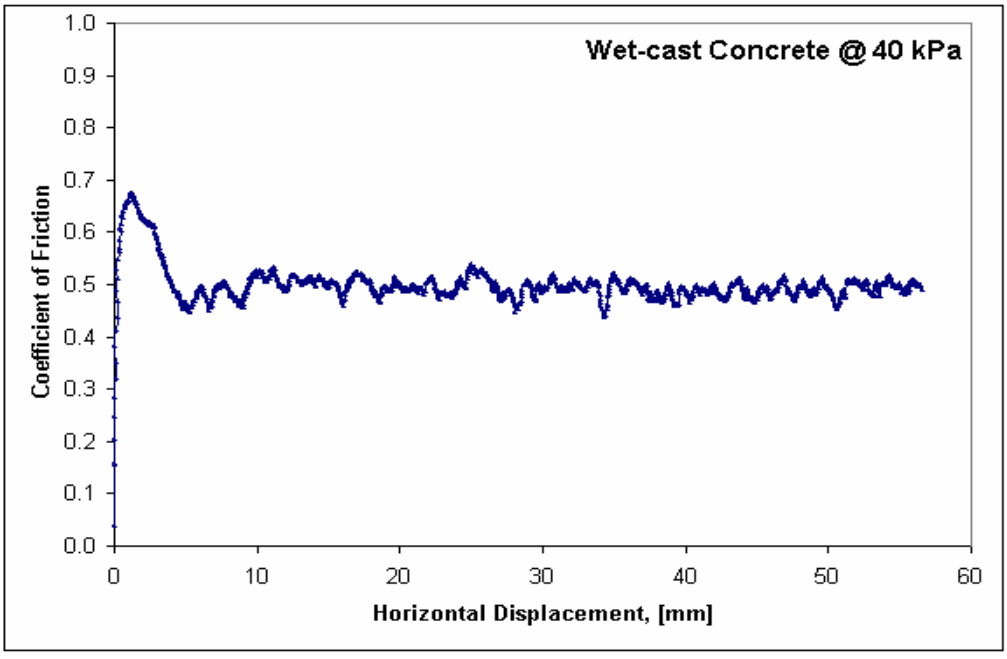


(b)

Figure 5.13 Coefficient of Friction versus Horizontal Displacement Curves of Ottawa 20/30 Sand with (a) Steel ($D_R$=%87) (b) Wet-cast Concrete ($D_R$=%76) Pipes at 40 kPa.

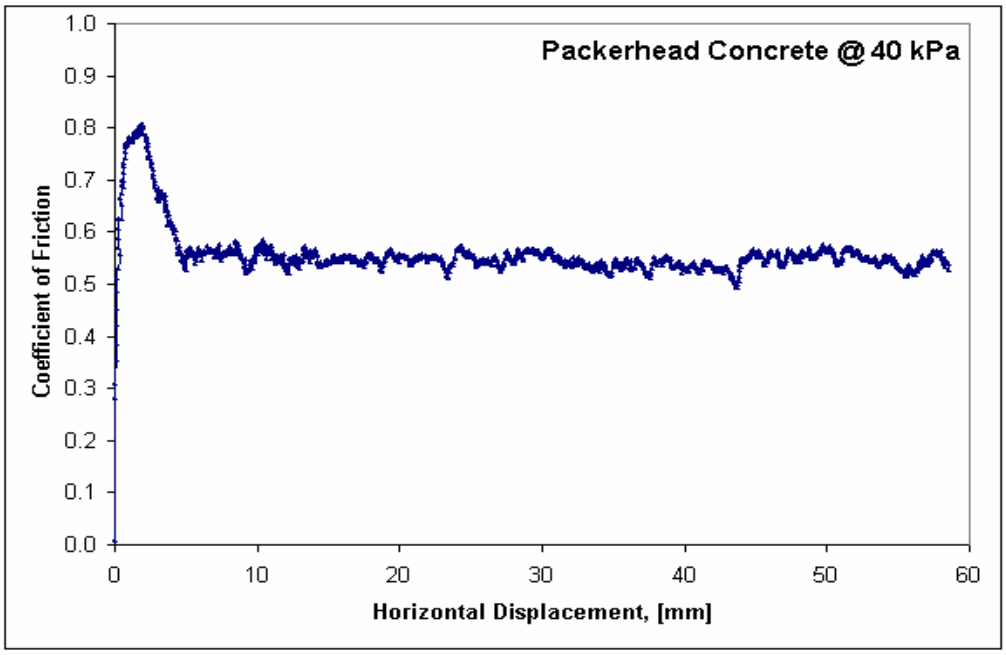


(a)

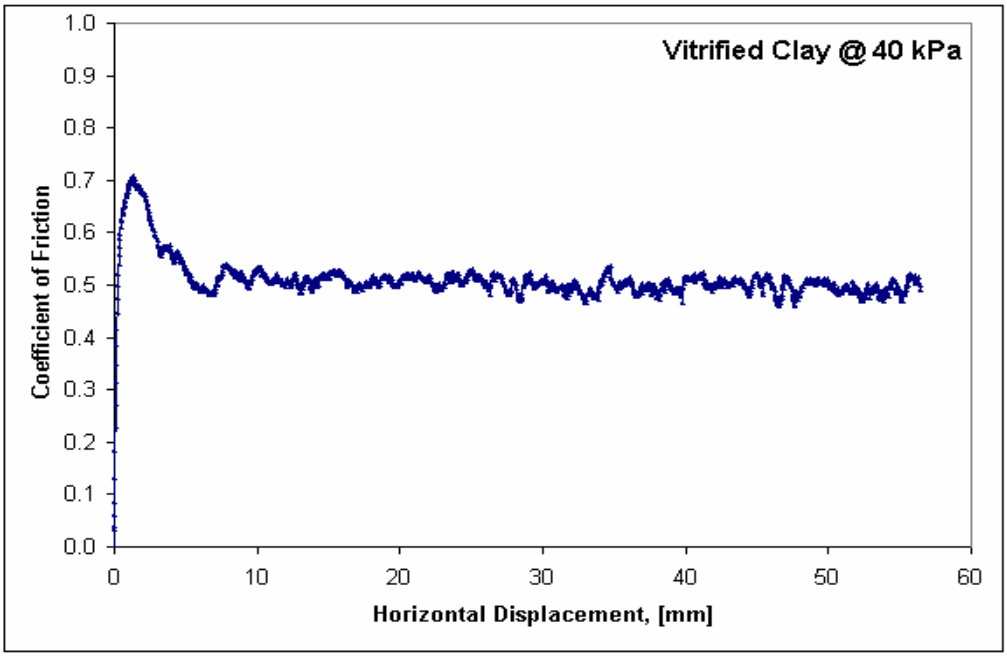


(b)

Figure 5.14 Coefficient of Friction versus Horizontal Displacement Curves of Ottawa 20/30 Sand with (a) Packerhead$^{TM}$ Concrete ($D_R$=%83) (b) Vitrified Clay ($D_R$=%79) Pipes at 40 kPa.

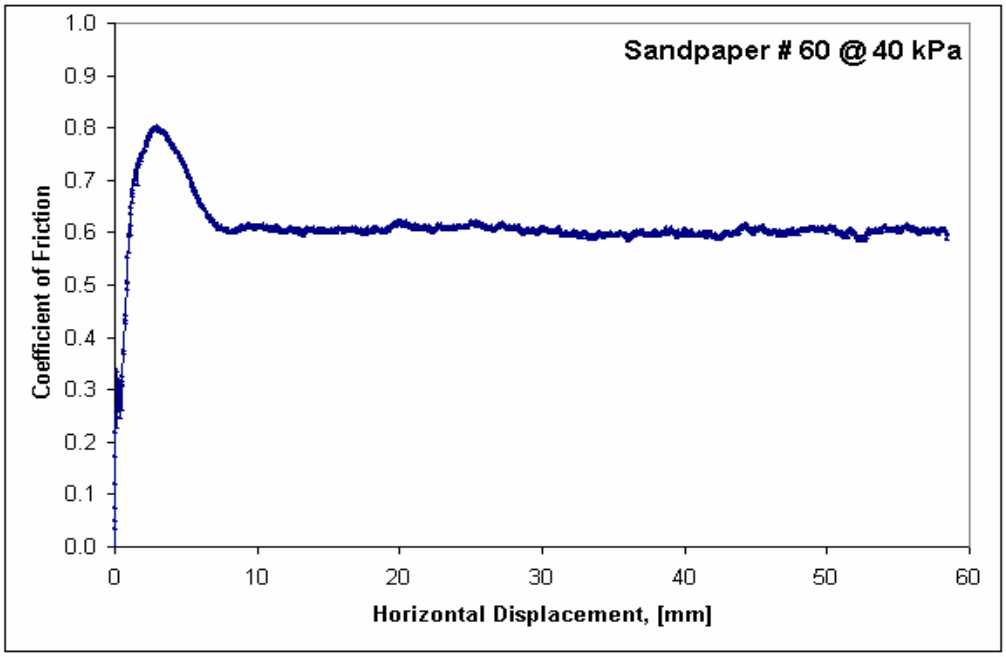


(a)

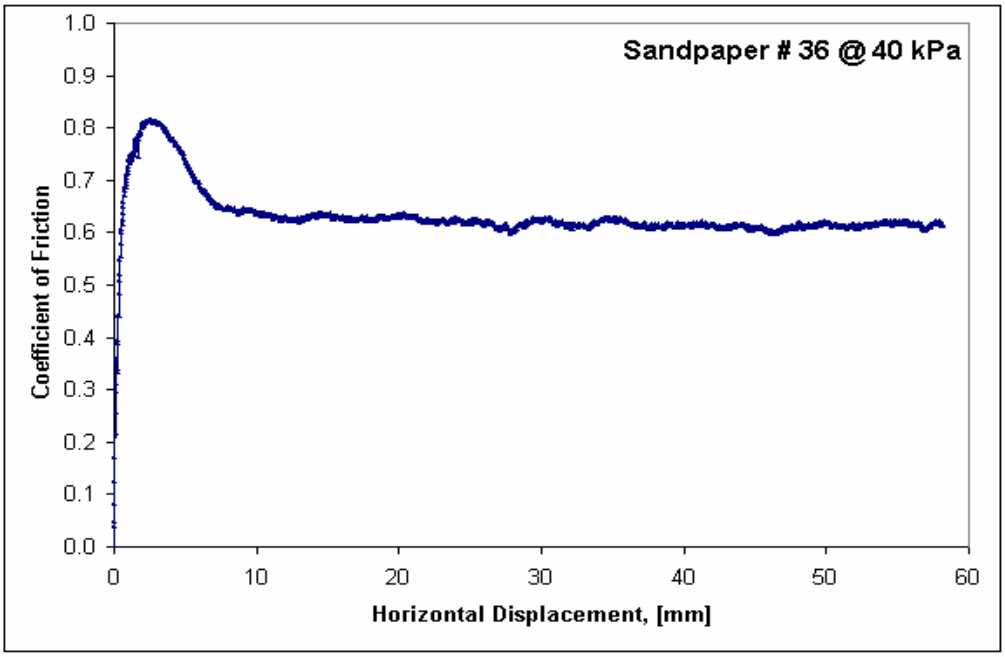


(b)

Figure 5.15 Coefficient of Friction versus Horizontal Displacement Curves of Ottawa 20/30 Sand with Artificial Sandpaper (a) No.60 ($D_R$=%81) (b) No.36 ($D_R$=%83) Pipes at 40 kPa.

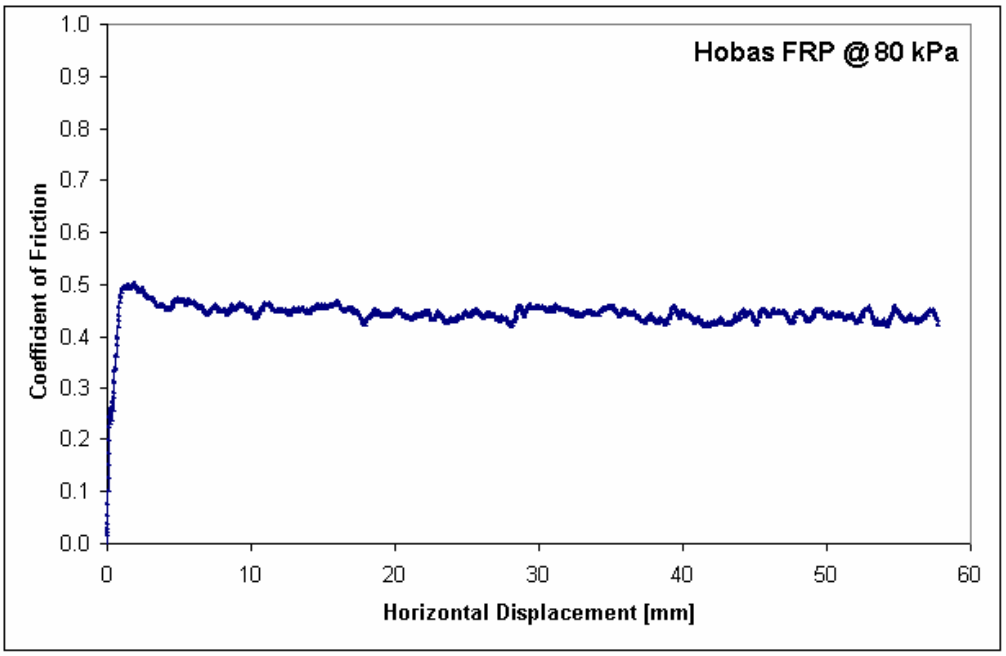


(a)

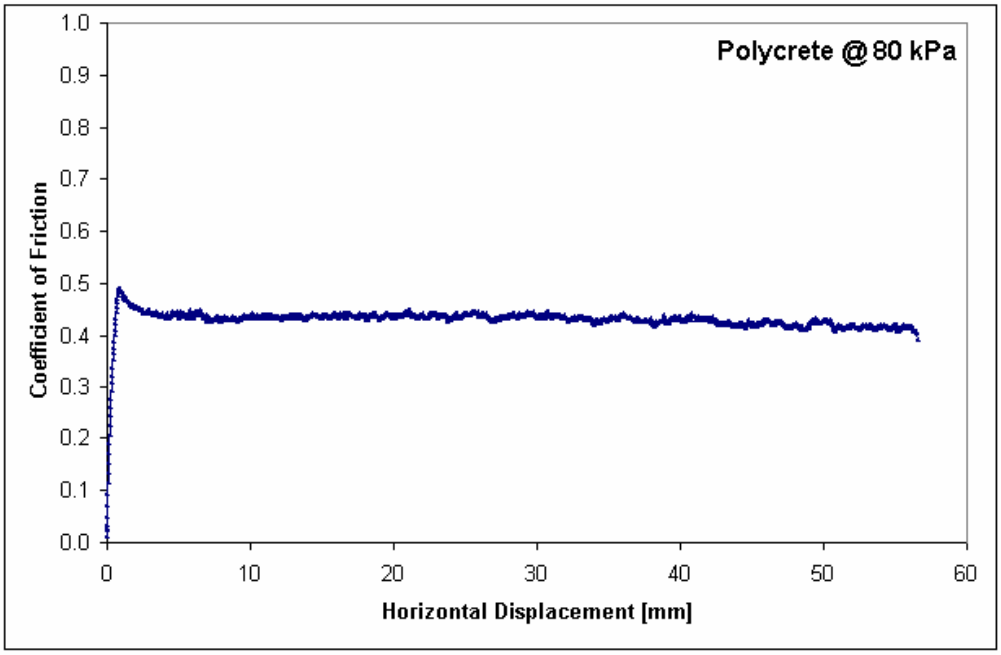


(b)

Figure 5.16 Coefficient of Friction versus Horizontal Displacement Curves of Ottawa 20/30 sand with (a) Hobas$^{TM}$ FRP ($D_R$=%79) (b) Polycrete ($D_R$=%79) pipes at 80 kPa.

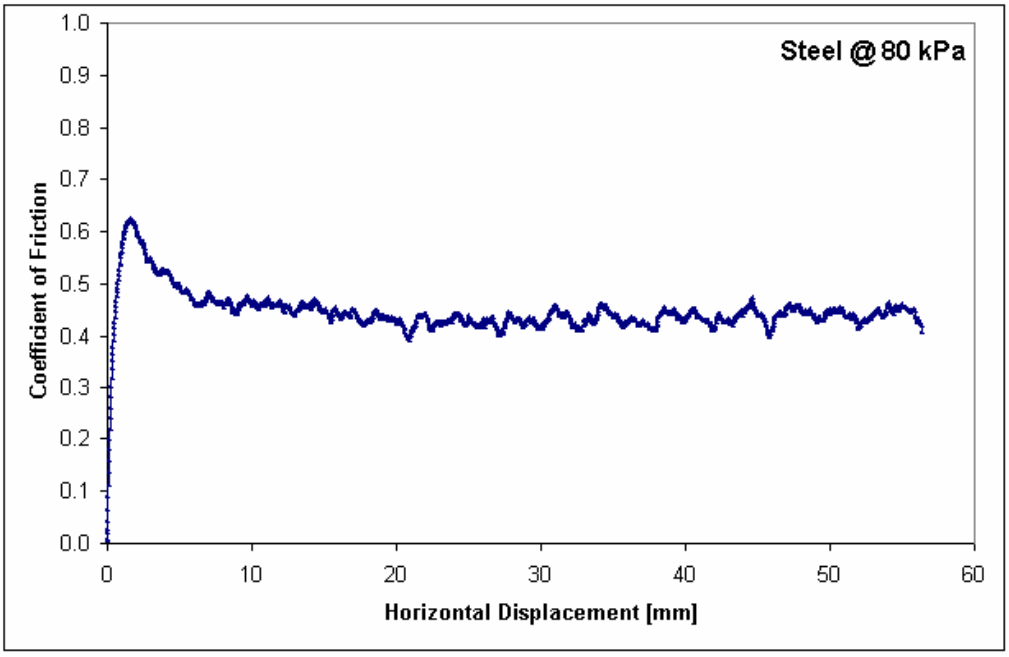


(a)

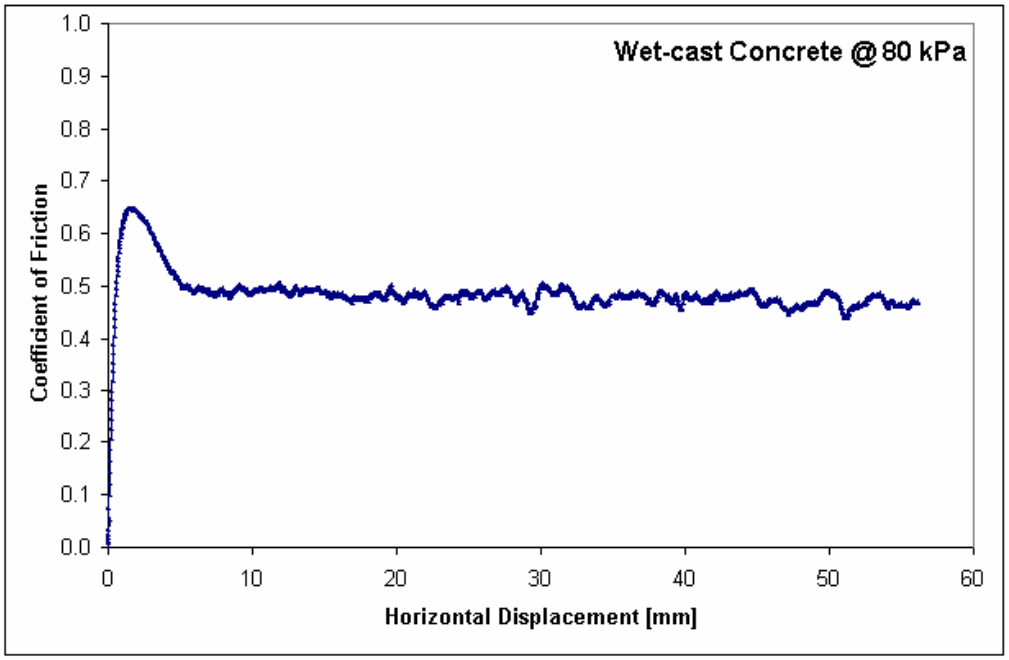


(b)

Figure 5.17 Coefficient of Friction versus Horizontal Displacement Curves of Ottawa 20/30 Sand with (a) Steel ($D_R$=%80) (b) Wet-cast Concrete ($D_R$=%77) Pipes at 80 kPa.

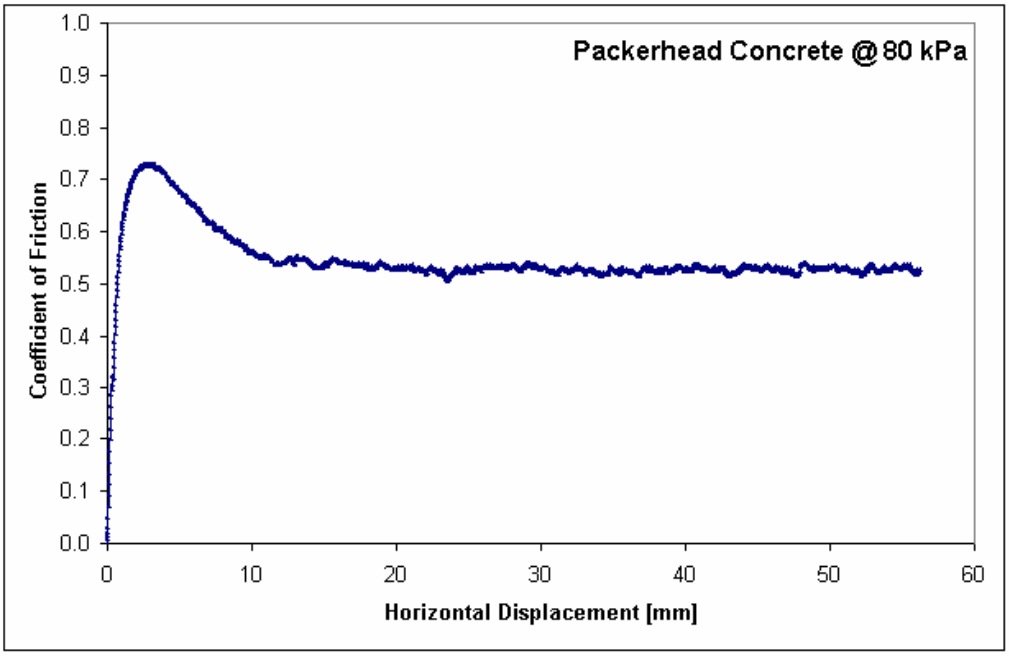


(a)

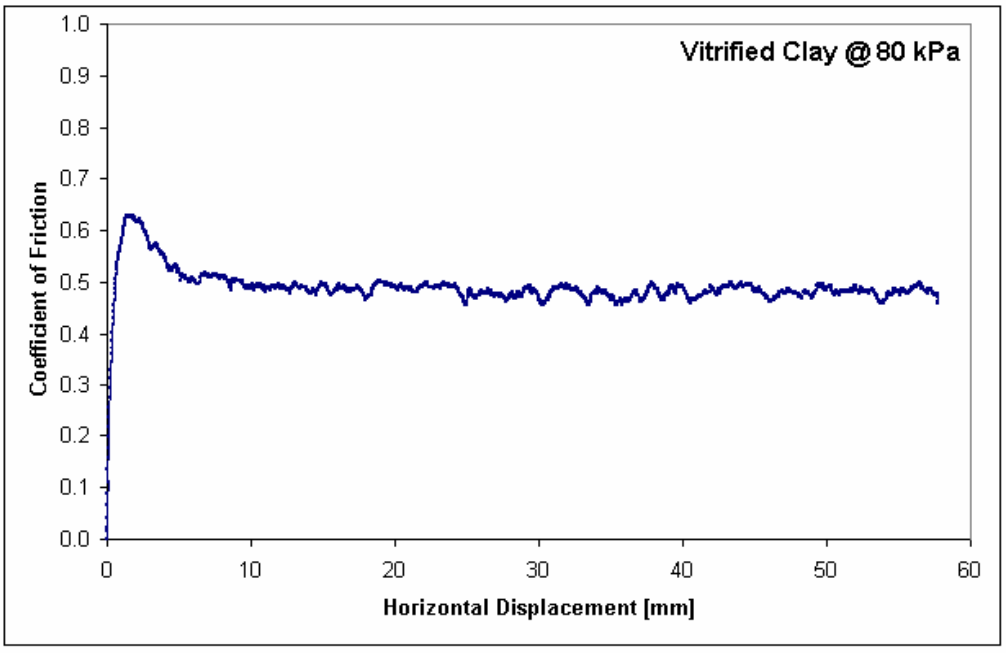


(b)

Figure 5.18 Coefficient of Friction versus Horizontal Displacement Curves of Ottawa 20/30 Sand with (a) Packerhead™ Concrete ($D_R$=%80) (b) Vitrified Clay ($D_R$=%66) Pipes at 80 kPa.

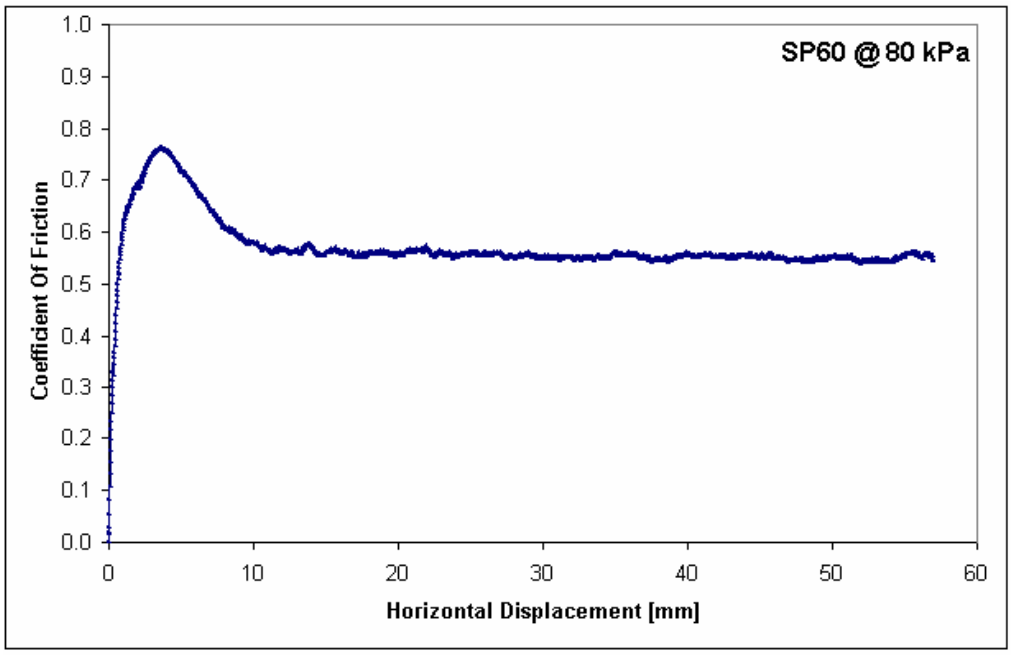


(a)

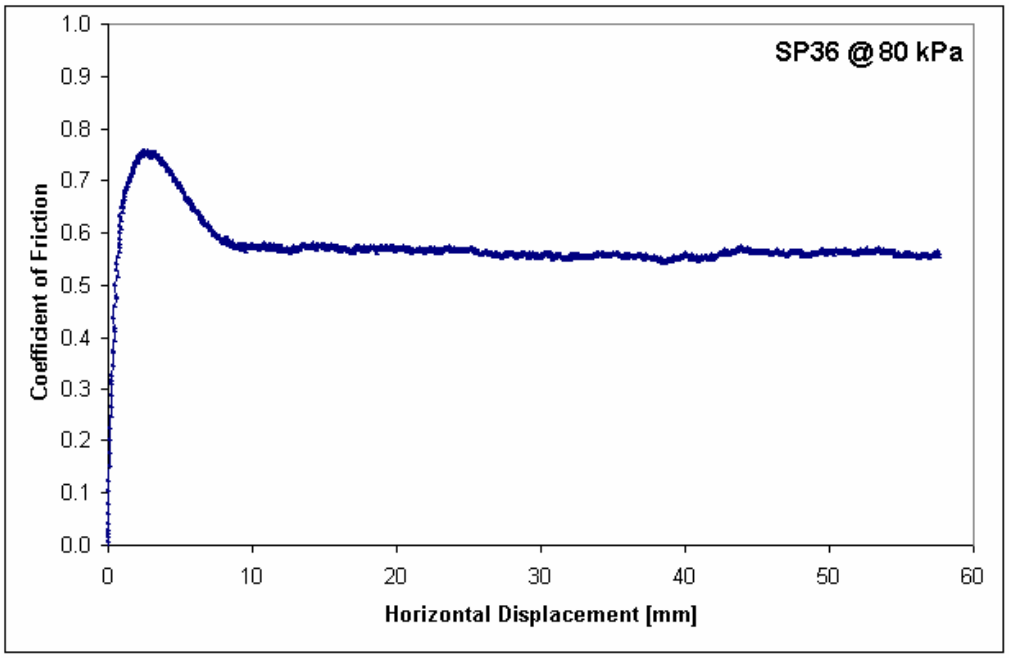


(b)

Figure 5.19 Coefficient of Friction versus Horizontal Displacement Curves of Ottawa 20/30 sand with Artificial Sandpaper (a) No.60 ($D_R$=%76) (b) No.36 ($D_R$=%80) Pipes at 80 kPa.

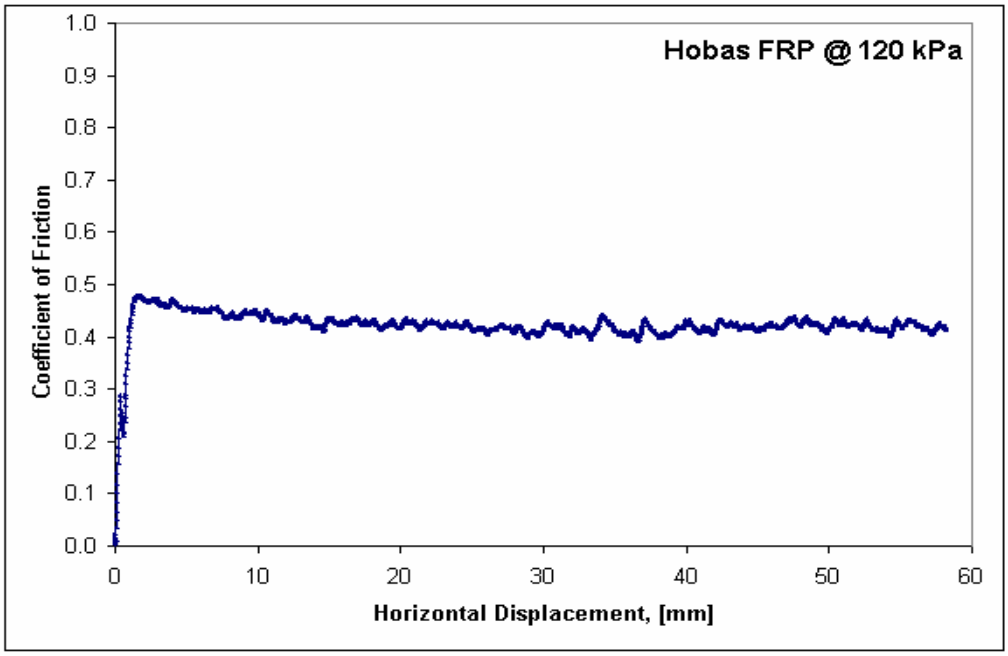


(a)

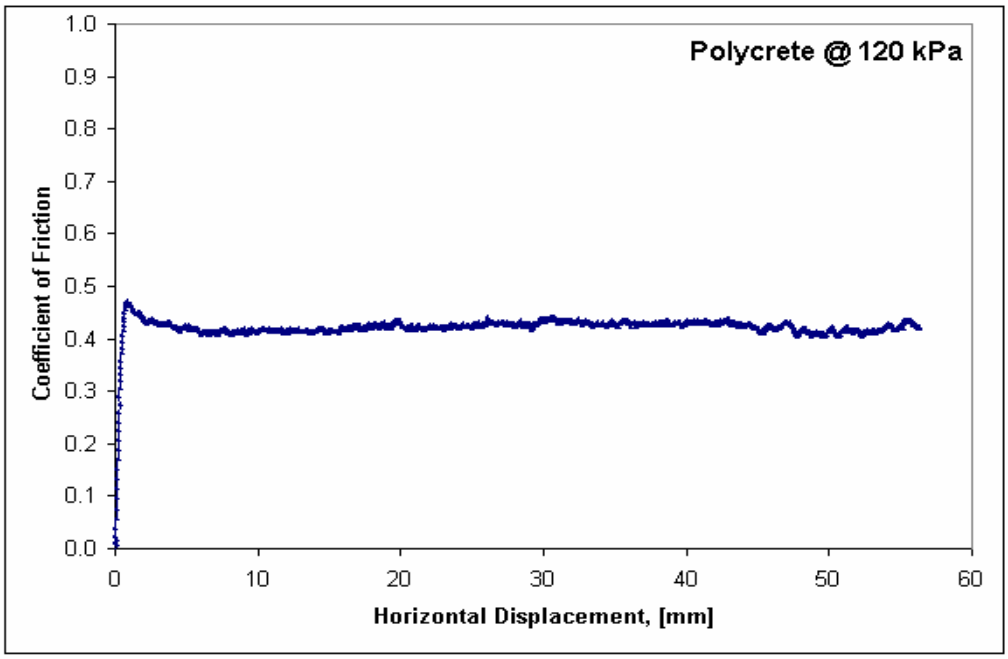


(b)

Figure 5.20 Coefficient of Friction versus Horizontal Displacement Curves of Ottawa 20/30 Sand with (a) Hobas$^{TM}$ FRP ($D_R$=%78) (b) Polycrete ($D_R$=%77) Pipes at 120 kPa.

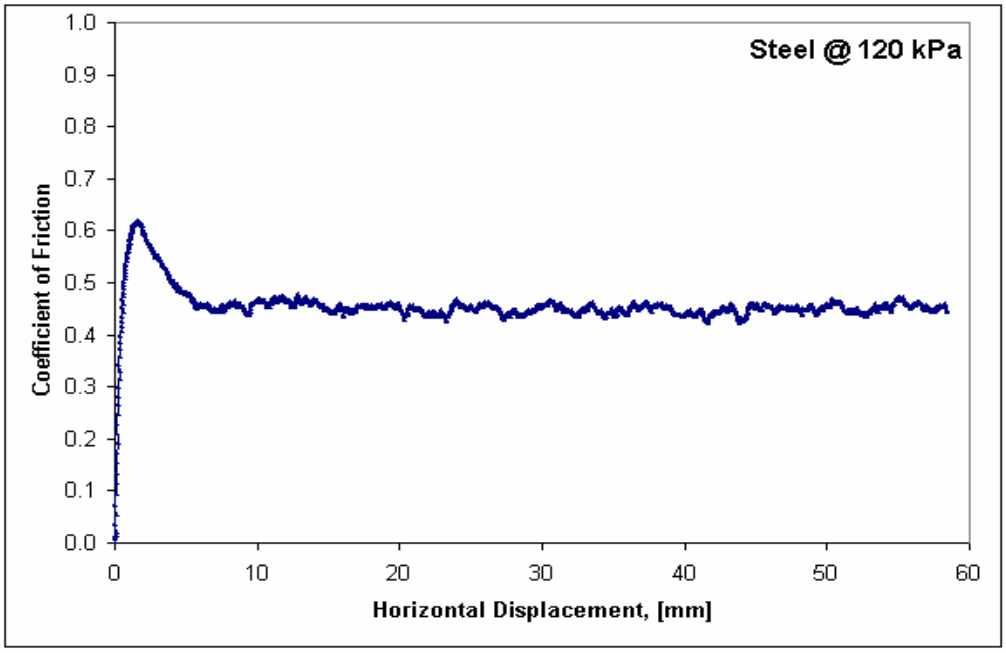


(a)

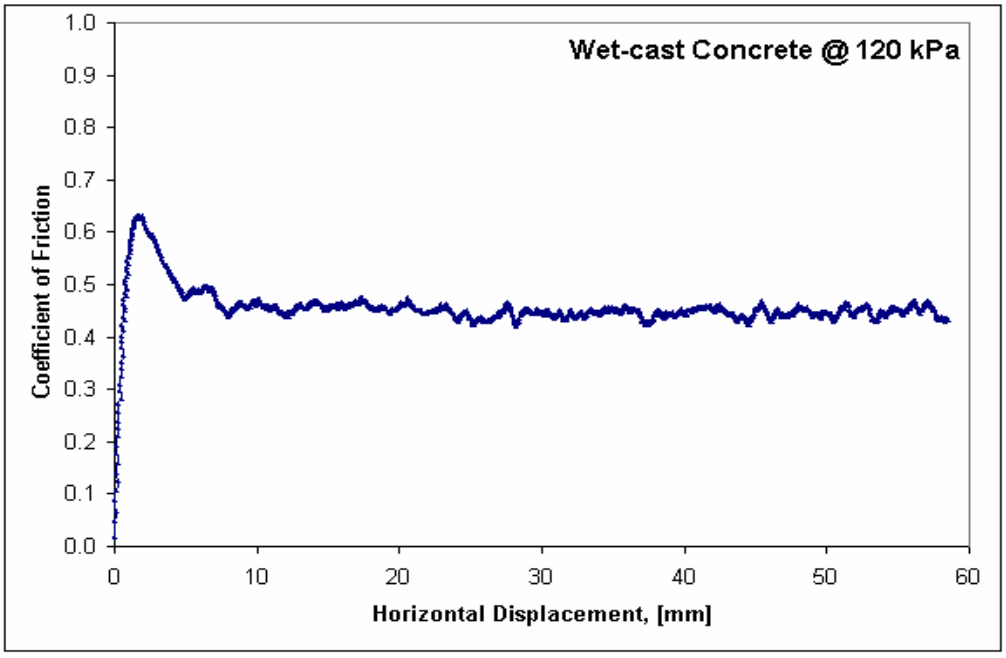


(b)

Figure 5.21 Coefficient of Friction versus Horizontal Displacement Curves of Ottawa 20/30 Sand with (a) Steel ($D_R$=%82) (b) Wet-cast concrete ($D_R$=%78) Pipes at 120 kPa.

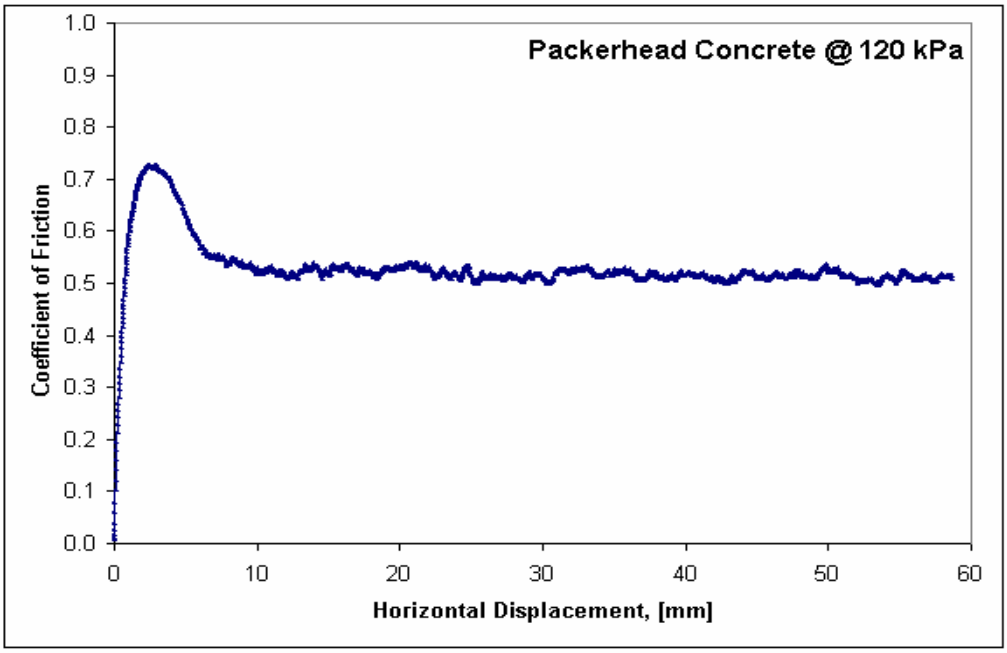


(a)

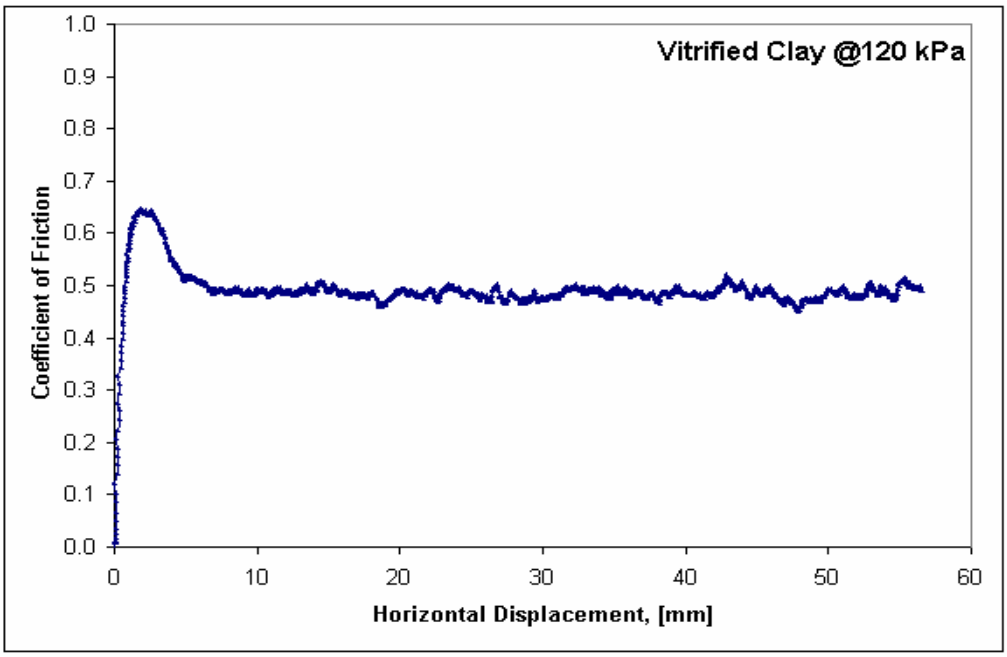


(b)

Figure 5.22 Coefficient of Friction versus Horizontal Displacement Curves of Ottawa 20/30 Sand with (a) Packerhead$^{TM}$ Concrete ($D_R$=%82) (b) Vitrified Clay ($D_R$=%77) Pipes at 120 kPa.

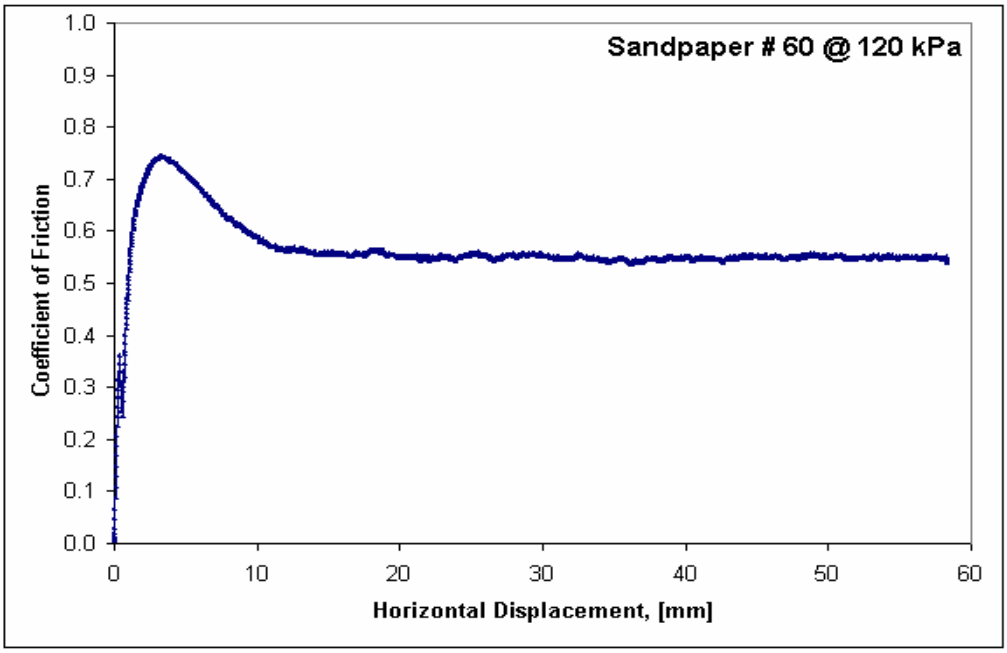


(a)

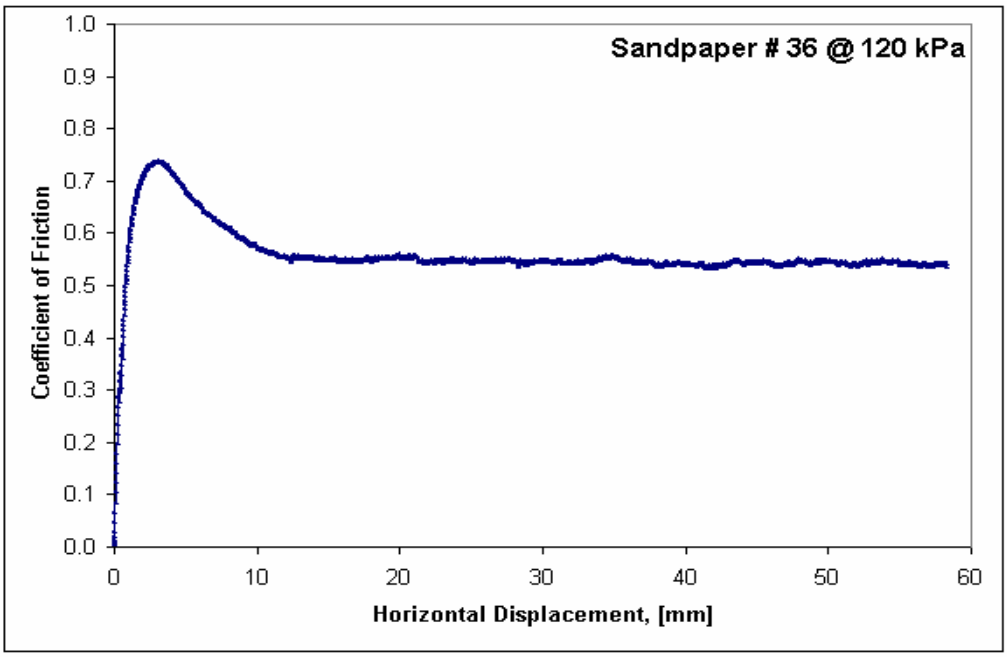


(b)

Figure 5.23 Coefficient of Friction versus Horizontal Displacement Curves of Ottawa 20/30 Sand with Artificial Sandpaper (a) No.60 ($D_R$=%77) (b) No.36 ($D_R$=%83) Pipes at 120 kPa.

5.3.2 Effect Of Sand Type (Angularity)

The tests presented and discussed in Section 5.3.1 were performed with the sub-rounded Ottawa 20/30 sand. A similar series of tests were performed for the angular Atlanta blasting sand at 80 kPa to evaluate the effect of particle angularity. Both sands had similar gradation curves and $D_{50}$ values (see Section 5.2.1).

A total of 8 plots of coefficient of friction versus horizontal displacement are given below in Figures 5.24 - 5.27. The average relative density for the tests was 81.3 % ± 2.5 %. The relative density of each test is indicated on the particular figure subtitle.

For the same test conditions (normal stress, type of sand and relative density) the same, the coefficient of friction values increased with the increase in surface roughness. The peak friction coefficient was 0.58 for the smooth Hobas$^{TM}$ FRP pipe ($R_a$=6.5 μm) whereas it was 0.86 for the rough Packerhead$^{TM}$ concrete pipe ($R_a$=55.1 μm). These compared with the values of 0.50 and 0.73 presented previously for Ottawa 20/30 tested against the same pipe materials. All friction values are summarized in Table 5.4. It is concluded that the friction values increased with the increase of particle angularity because angular particles have a stronger interlock with the pipe and within themselves. The peak friction occurred within 5.0 millimeters of horizontal displacement in all tests. The smoother the pipe, the less displacement was required before the peak friction was reached.

The interface shear behavior of Atlanta blasting sand was similar to Ottawa sand regarding the post-peak softening. Smoother pipes (Hobas$^{TM}$ FRP and Polycrete) did not experience an obvious decrease after the peak, which was attributed to the shearing mechanism involved in the process.

Table 5.4 The Coefficient of Friction at Various Pipe-Atlanta Blasting Sand Interfaces

| | **Hobas™ FRP** | **Poly-crete** | **Steel** | **Wet-cast Conc.** | **Vitr. Clay** | **Packer. Conc.** | **SP No.60** | **SP No.36** |
|---|---|---|---|---|---|---|---|---|
| **peak** | 0.58 | 0.53 | 0.73 | 0.76 | 0.77 | 0.86 | 0.87 | 0.89 |
| **residual** | 0.56 | 0.49 | 0.58 | 0.59 | 0.61 | 0.62 | 0.66 | 0.67 |

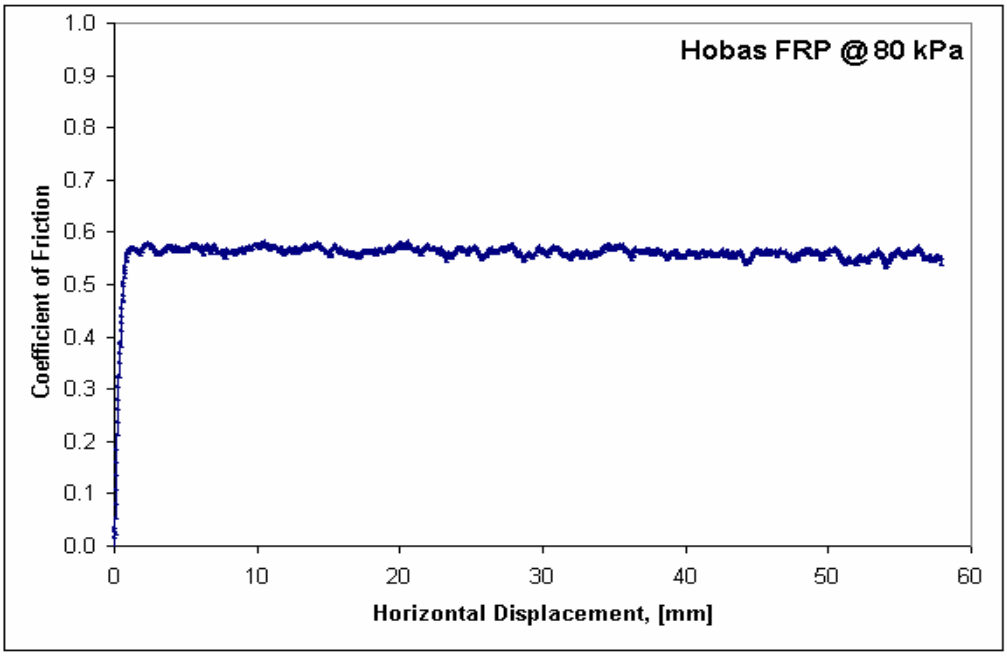


(a)

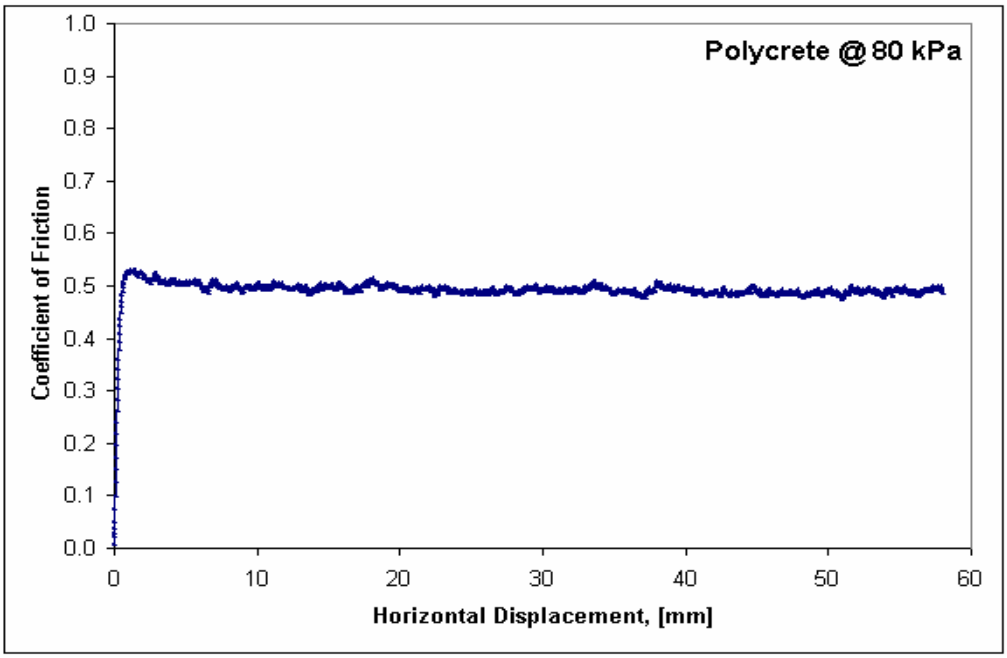


(b)

Figure 5.24 Coefficient of Friction versus Horizontal Displacement Curves of Atlanta Blasting Sand with (a) Hobas$^{TM}$ FRP ($D_R$=%84) (b) Polycrete ($D_R$=%78) pipes at 80 kPa.

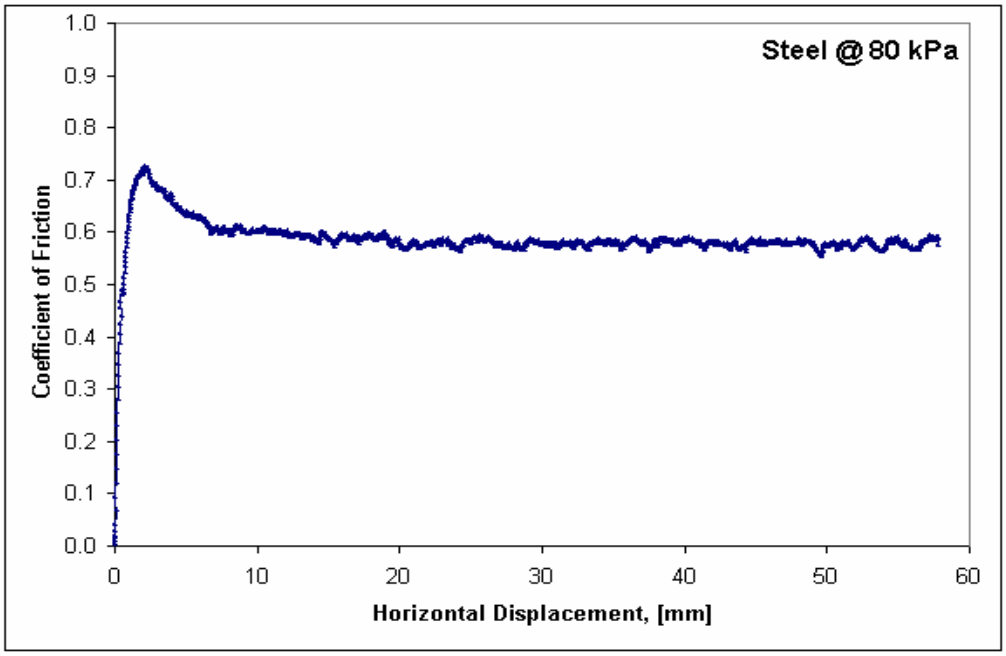


(a)

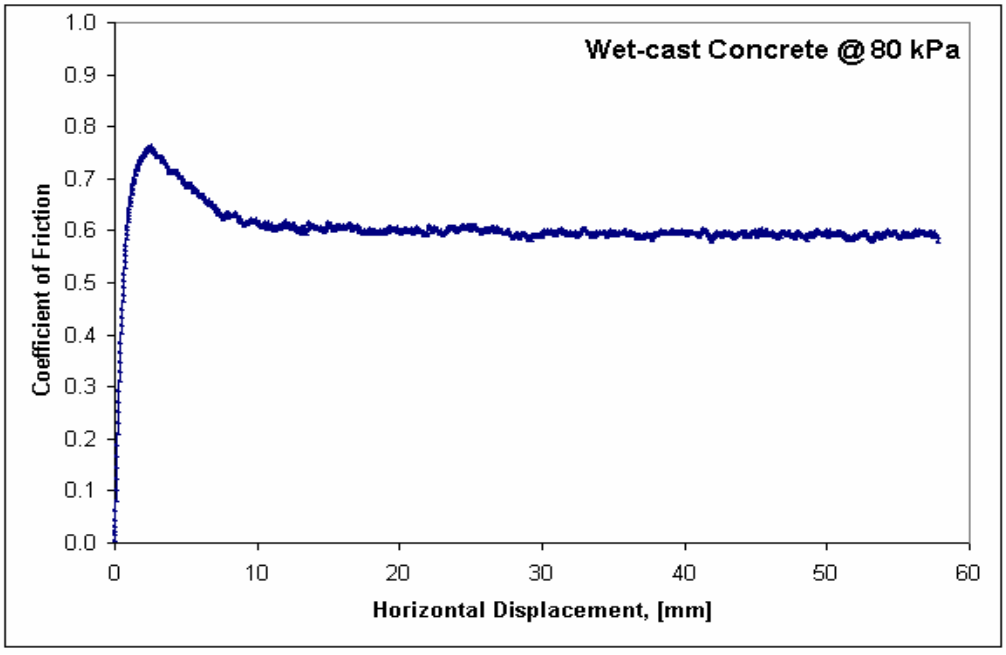


(b)

Figure 5.25 Coefficient of Friction versus Horizontal Displacement Curves of Atlanta Blasting Sand with (a) Steel ($D_R$=%83) (b) Wet-cast concrete ($D_R$=%78) Pipes at 80 kPa.

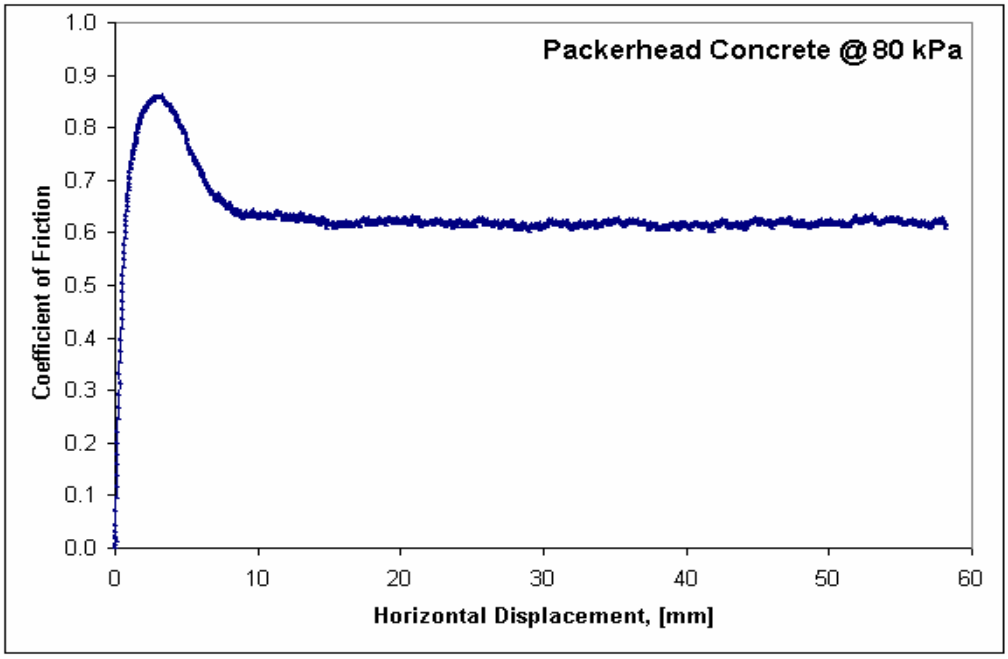


(a)

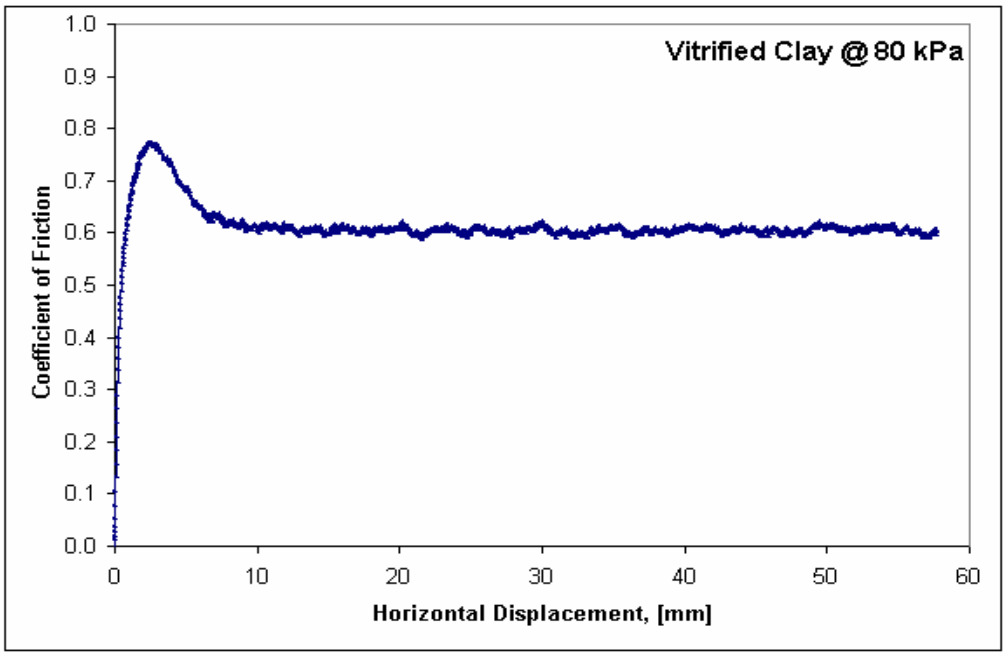


(b)

Figure 5.26 Coefficient of Friction versus Horizontal Displacement Curves of Atlanta Blasting Sand with (a) Packerhead$^{TM}$ Concrete ($D_R$=%85) (b) Vitrified Clay ($D_R$=%82) Pipes at 80 kPa.

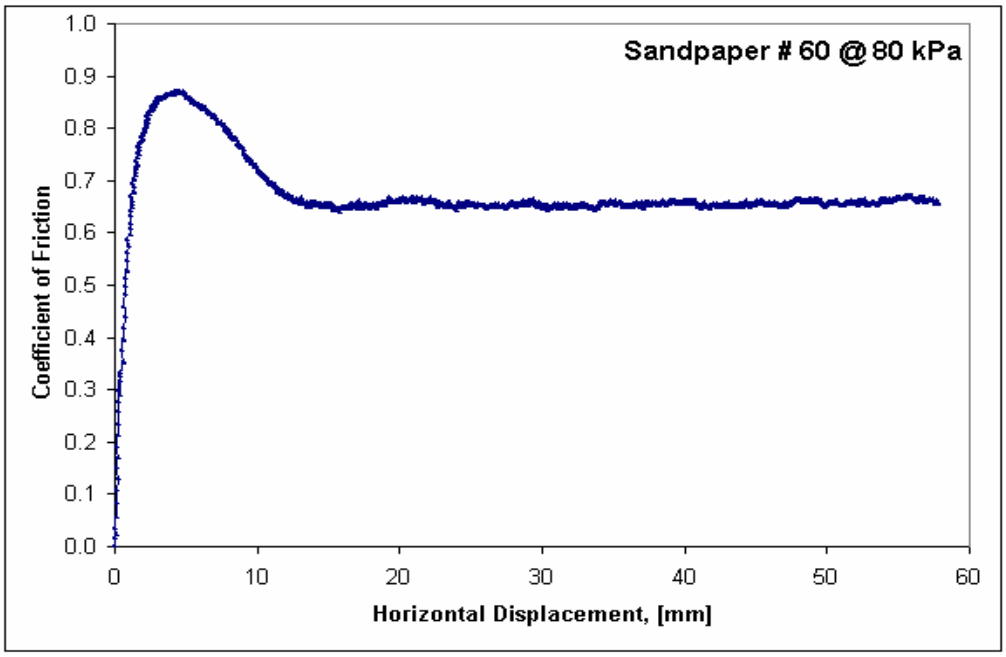


(a)

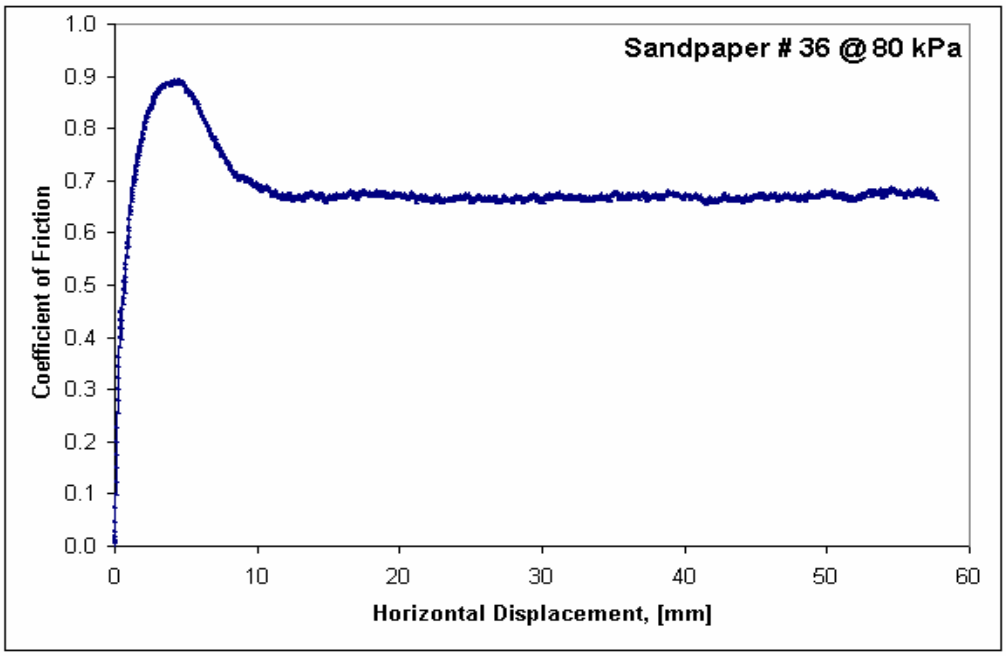


(b)

Figure 5.27 Coefficient of Friction versus Horizontal Displacement Curves of Atlanta Blasting Sand with Artificial Sandpaper (a) No.60 ($D_R$=%80) (b) No.36 ($D_R$=%81) Pipes at 80 kPa.

5.3.3 Effect Of Relative Density

The tests described above were performed at a constant relative density of about 80 %. Previous researchers have found that the compactness of the soil also has an effect on the interface shear characteristics (Butterfield and Andrawes, 1972, Frost and Han, 1999). To evaluate this effect on pipe-soil interaction, a series of tests were performed on Hobas$^{TM}$ FRP, Packerhead$^{TM}$ concrete, and vitrified clay pipes. Each pipe was tested at five different relative densities varying between 47% and 98% and at a normal stress of 80 kPa. Test results are summarized in Table 5.5 and plots showing the change of coefficient of friction with the change of relative density for Ottawa 20/30 sand and Hobas$^{TM}$ FRP, Packerhead$^{TM}$ concrete pipes are given below (Figures 5.28 and 5.29).

Table 5.5 Coefficient of Friction Values at Different Relative Densities

| **Soil Type** | **Pipe Type** | **Normal Stress [kPa]** | **Relative Density [%]** | **tan$\delta_p$** | **tan$\delta_r$** |
|---|---|---|---|---|---|
| Ottawa 20/30 Sand | Hobas | 80 | 46.8 | 0.48 | 0.43 |
| | | | 56.5 | 0.48 | 0.43 |
| | | | 65.9 | 0.47 | 0.42 |
| | | | 95.6 | 0.53 | 0.43 |
| | Packerhead | | 50.0 | 0.63 | 0.50 |
| | | | 58.0 | 0.65 | 0.51 |
| | | | 68.7 | 0.71 | 0.50 |
| | | | 98.3 | 0.82 | 0.50 |
| | Vit. Clay | | 46.7 | 0.58 | 0.50 |
| | | | 55.5 | 0.61 | 0.50 |
| | | | 64.8 | 0.61 | 0.51 |
| | | | 94.4 | 0.74 | 0.50 |

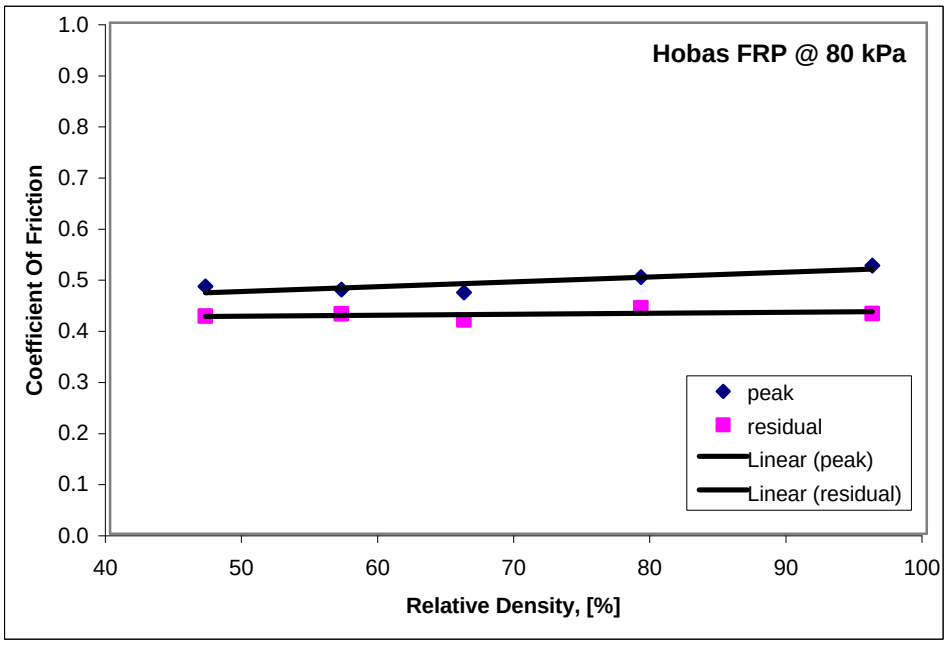


(a)

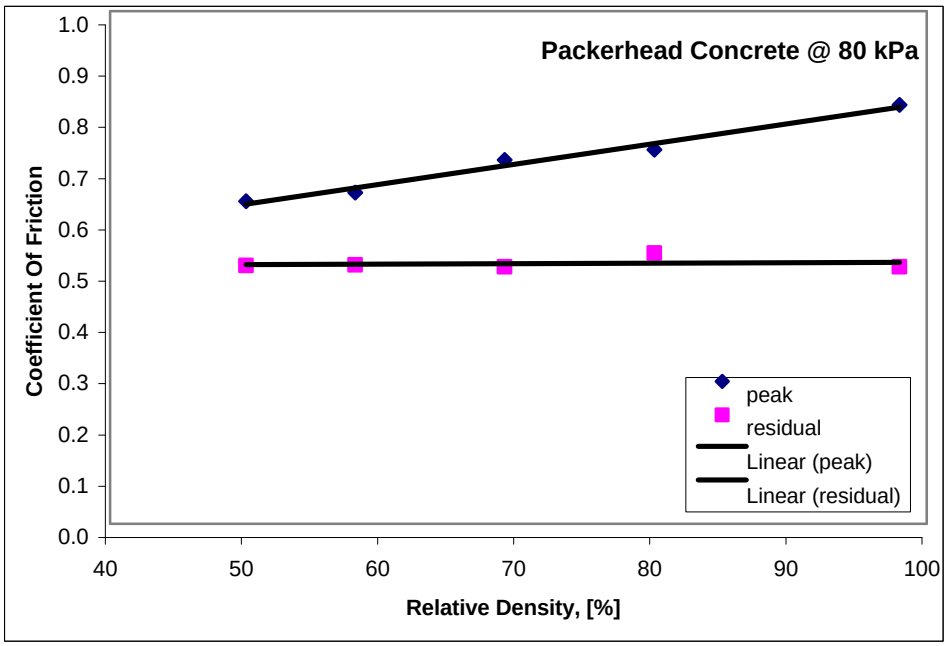


(b)

Figure 5.28 Coefficient of Friction versus Relative Density Curves of Ottawa 20/30 Sand with (a) Hobas™ FRP (b) Packerhead™ Concrete Pipes at 80 kPa

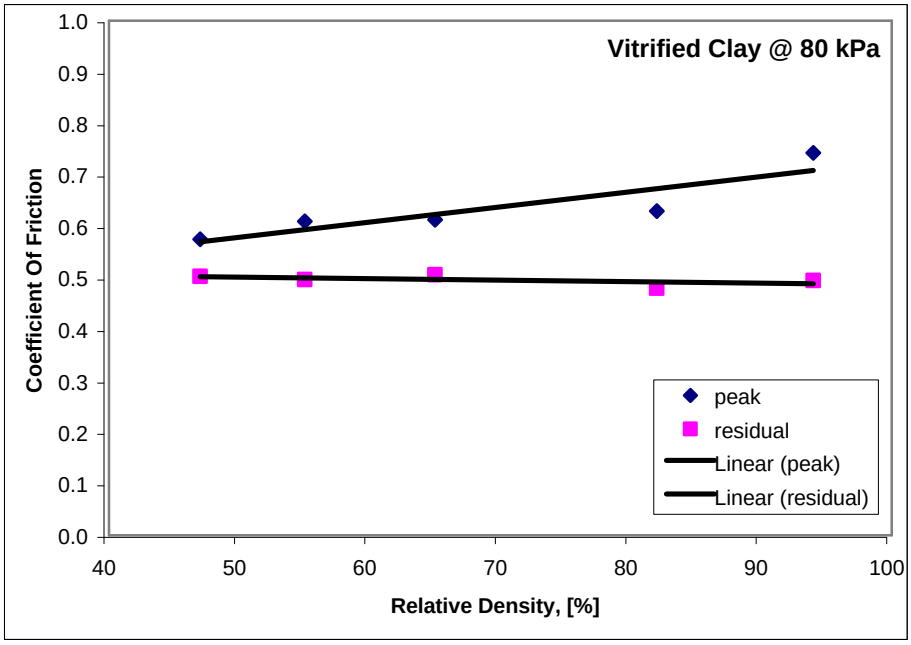


Figure 5.29 Coefficient of Friction versus Relative Density Curve of Ottawa 20/30 sand with Vitrified Clay Pipe at 80 kPa

As can be seen from the graphs, the peak coefficient of friction increased linearly with the increase in the soil density for all pipes. This can be explained by the higher friction and interlocking between the particles and interface. For each pipe, the slope of the trendline was different and was consistent with the individual friction characteristics. In contrast, the residual angle of friction remained constant, which can be explained as follows: After a certain shear displacement, the particle rearrangement is complete, the soil reaches a stable, residual condition and void ratio. This stability is the main reason for the constant friction angles at the residual condition.

5.3.4 Effect Of Normal Stress

In general the shear force is accepted as increasing linearly with the increase in normal force in frictional behavior. This is not a bad approximation for convenient normal stress ranges but previous research work showed that this is not a correct statement in the broad nature of contact mechanics (Archard, 1957, Dove and Frost, 1999).

In this section, the effect of the normal stress on the coefficient of friction was evaluated. Tests at two other stress levels, 160 kPa and 200 kPa, were performed in addition to the three stress levels, 40 kPa, 80 kPa, and 120 kPa, already presented. Tests were run at Hobas™ FRP, Packerhead™ concrete and vitrified clay pipes at a relative density of 80 % on average. Test results are summarized in Table 5.6 and plots showing the change of coefficient of friction with the change of normal stress for Ottawa 20/30 sand and Hobas™ FRP, Packerhead™ concrete, and vitrified clay pipes are given below (Figure 5.30 and 5.31).

Table 5.6 Coefficient of Friction Values at Different Normal Stresses

| **Soil Type** | **Pipe Type** | **Normal Stress [kPa]** | **Relative Density [%]** | **tan$\delta_p$** | **tan$\delta_r$** |
|---|---|---|---|---|---|
| Ottawa 20/30 Sand | Hobas™ FRP | 160 | 83.9 | 0.49 | 0.44 |
| | Packerhead™ | | 80.8 | 0.70 | 0.51 |
| | Vit. Clay | | 79.2 | 0.65 | 0.48 |
| | Hobas™ FRP | 200 | 80.3 | 0.49 | 0.43 |
| | Packerhead™ | | 84.2 | 0.69 | 0.50 |
| | Vit. Clay | | 76.4 | 0.65 | 0.49 |

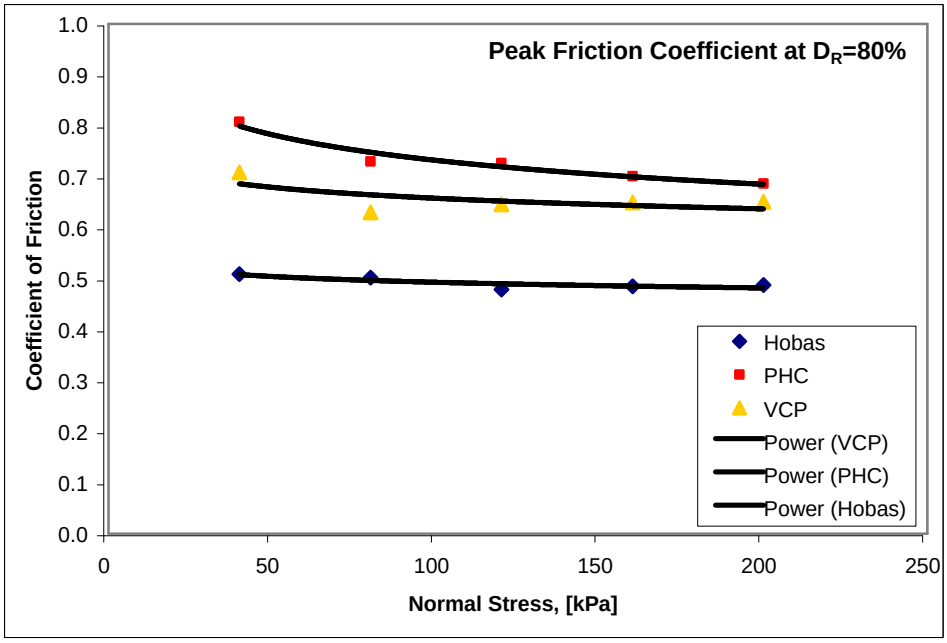


(a)

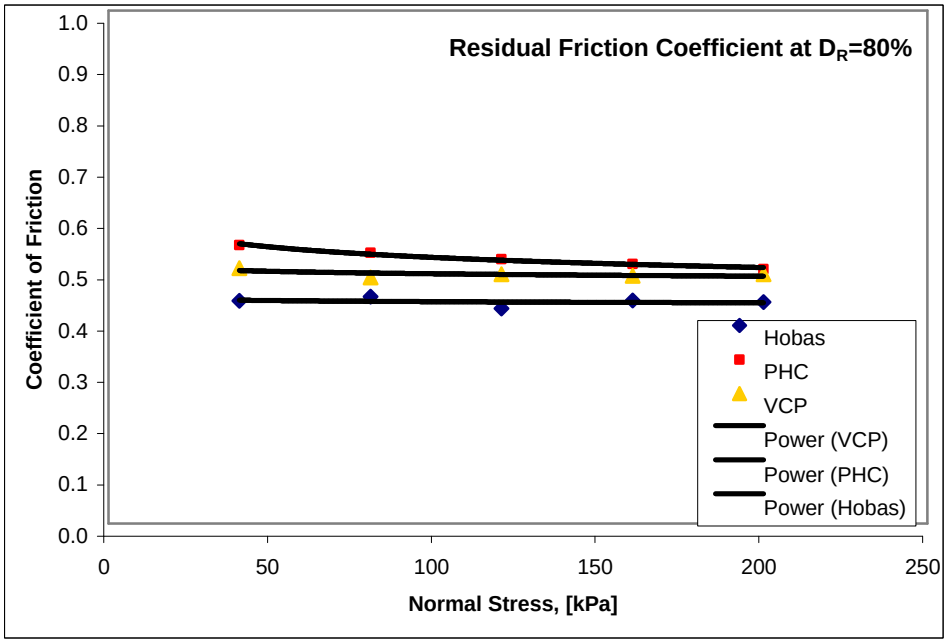


(b)

Figure 5.30 Coefficient of Friction versus Normal Stress of Ottawa 20/30 Sand with Hobas™ FRP, Packerhead™ Concrete and Vitrified Clay Pipes (a) For Peak Coefficient of Friction (b) For Residual Coefficient of Friction

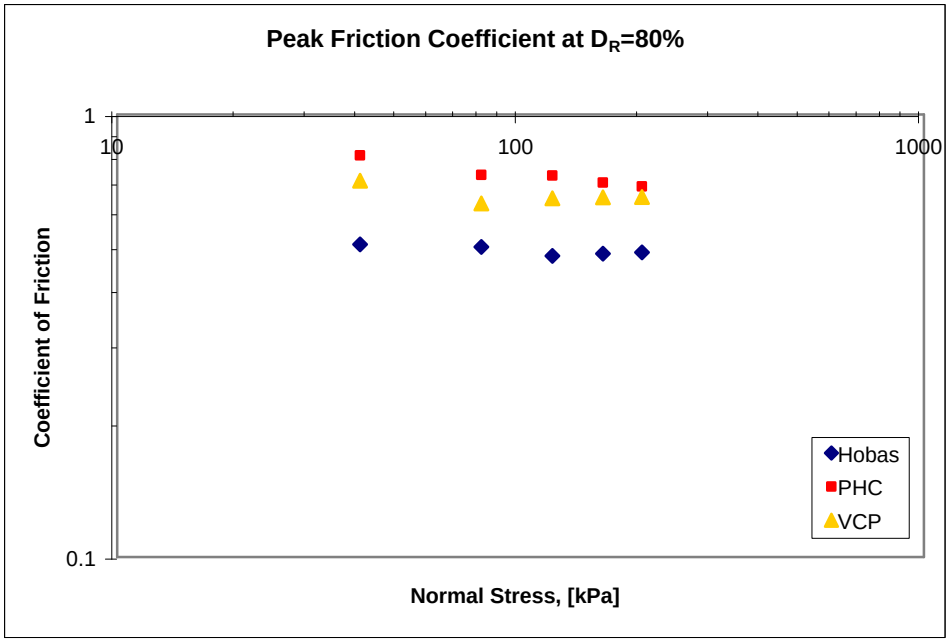


(a)

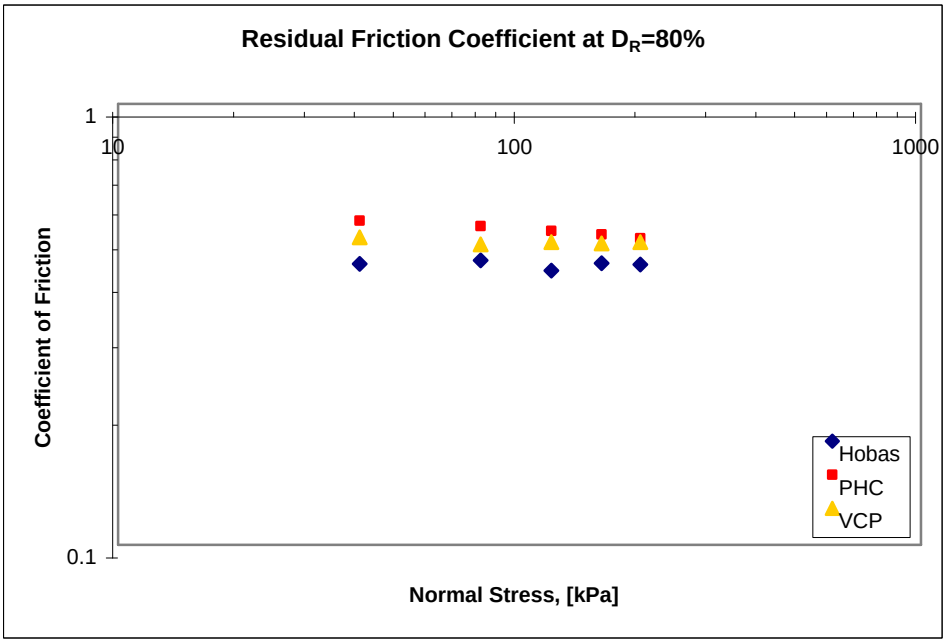


(b)

Figure 5.31 Log-Coefficient of Friction versus Log-Normal Stress of Ottawa 20/30 Sand with Hobas™ FRP, Packerhead™ Concrete and Vitrified Clay Pipes for (a) Peak Coefficient of Friction (b) Residual Coefficient of Friction

The plots in Figure 5.30 showed that the friction values tend to decrease with an increase in normal stress. This tendency is more pronounced with the "high-friction" Packerhead™ concrete pipe and less pronounced with the "low-friction" Hobas™ FRP pipe. The magnitude of decrease is more in the peak curve than the residual curve. A power function trendline is fitted for each data set.

If the same plots are converted to log-log plots (Figure 5.31), it can be seen that, for normal stresses less than approximately 60 kPa, the logarithm of the friction coefficient tends to increase linearly with the decrease of the normal load. This increase can be attributed to non-linear decrease of the contact area with the normal load. Because the contact area does not decrease as fast as the normal load, the coefficient of friction tends to increase (Archard, 1957).

However, for normal stresses greater than approximately 60 kPa, the coefficient of friction tends to stabilize with the increase in normal stress. This is also consistent with the findings of Dove and Frost (1999) for the frictional behavior of smooth geomembrane-Ottawa sand interfaces. This stabilization can be attributed to effect of plowing, where additional friction forces occur at the interface. The effect of plowing is more pronounced by softer vitrified clay and Hobas™ FRP pipes and less pronounced by the harder Packerhead™ concrete pipe.

### 5.3.5 Repeatability

To check the repeatability of the experimental work, several replicate tests were performed and the results were compared with the original ones. The repeatability was investigated at a smooth (Hobas™ FRP) and two rough pipes (Packerhead™ concrete

and vitrified clay). Both sands, Ottawa 20/30 and Atlanta blasting sand, were used in these tests.

The results are demonstrated in Figures 5.32 - 5.34. The repeatability of the tests is considered to be very satisfactory. The reproducability was less for the "low-friction" Hobas™ FRP pipe than the "high-friction" Packerhead™ concrete and vitrified clay pipes. The minor differences were attributed to the mechanism (sliding versus rolling, moving vertically and, rearranging) involved in the process.

The Table 5.7 summarizes the testing program and results of all interface shear tests.

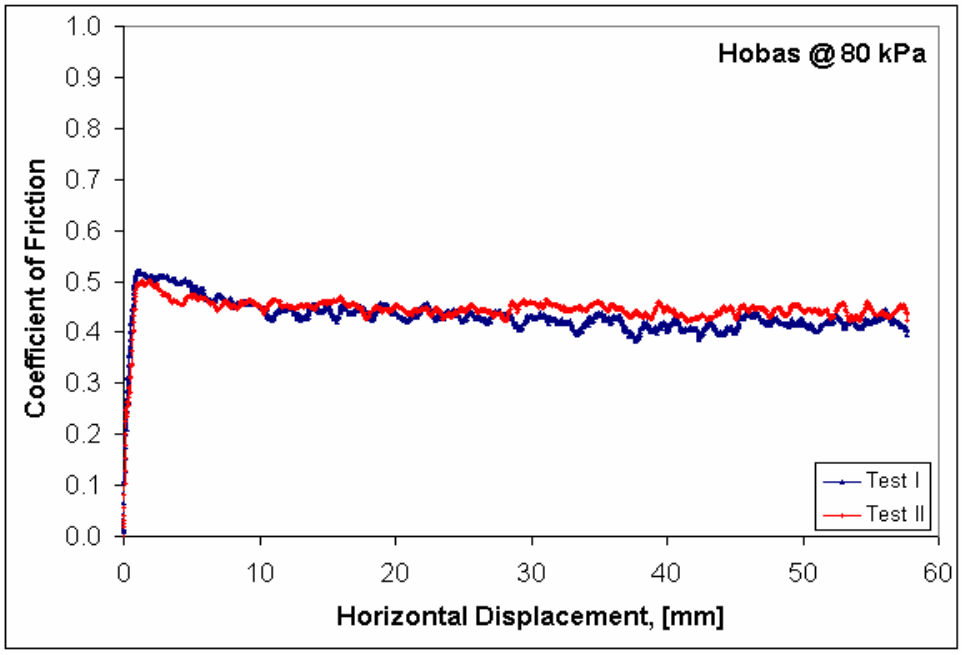


Figure 5.32 Repeatability Tests of Ottawa 20/30 Sand - Hobas™ FRP Pipe Interface

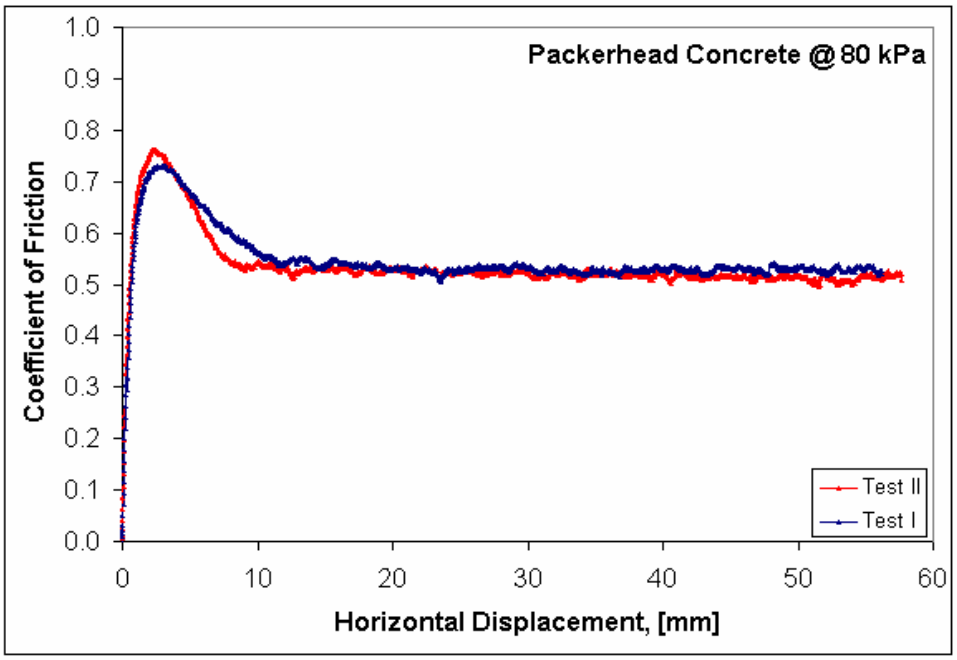


(a)

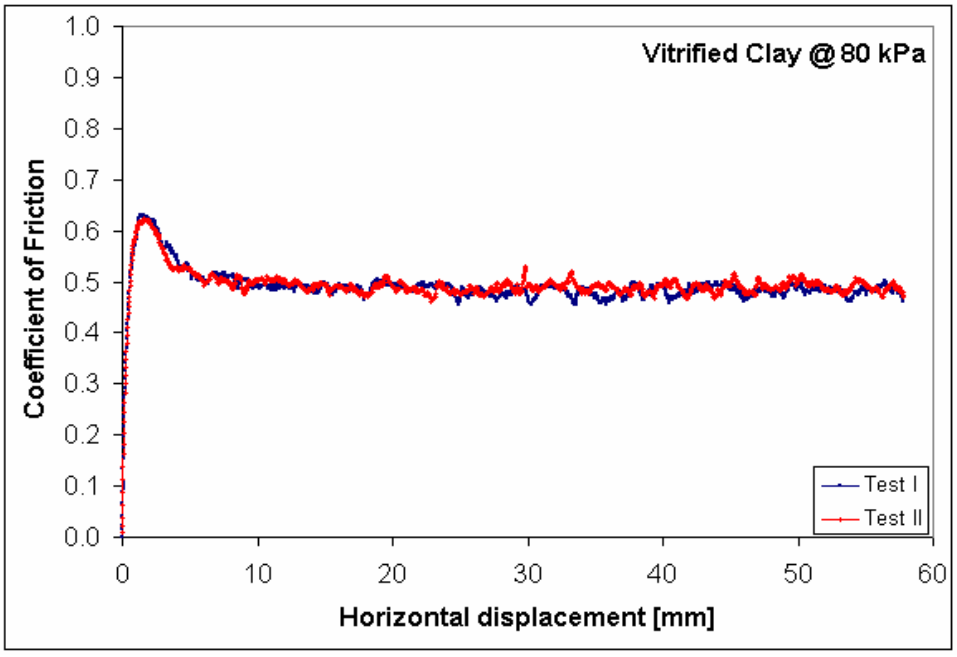


(b)

Figure 5.33 Repeatability Tests of (a) Ottawa 20/30 Sand - Packerhead™ Concrete Pipe and (b) Ottawa 20/30 Sand – Vitrified Clay Pipe Interfaces

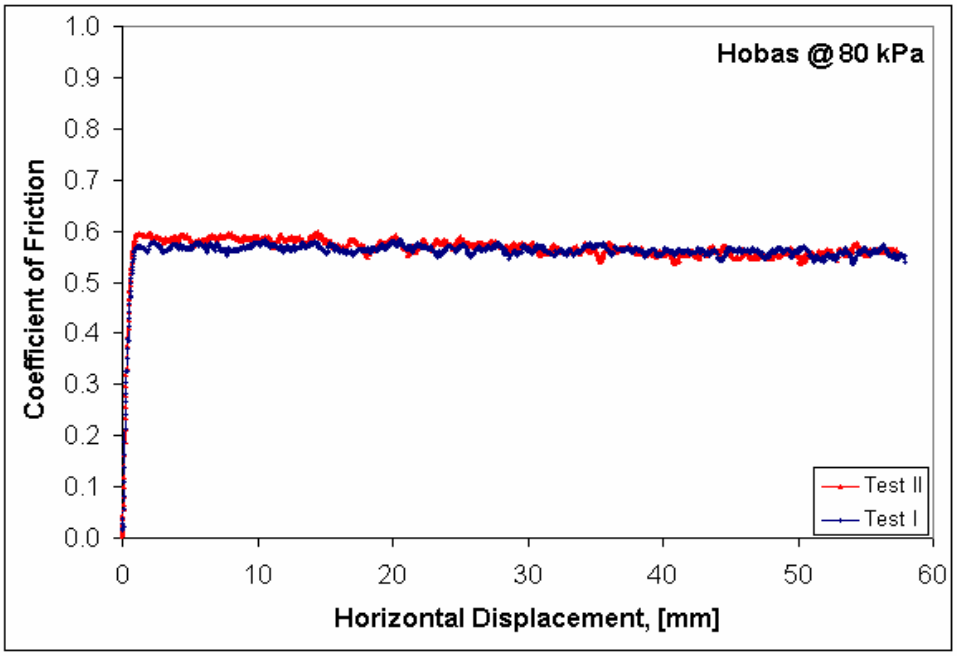


(a)

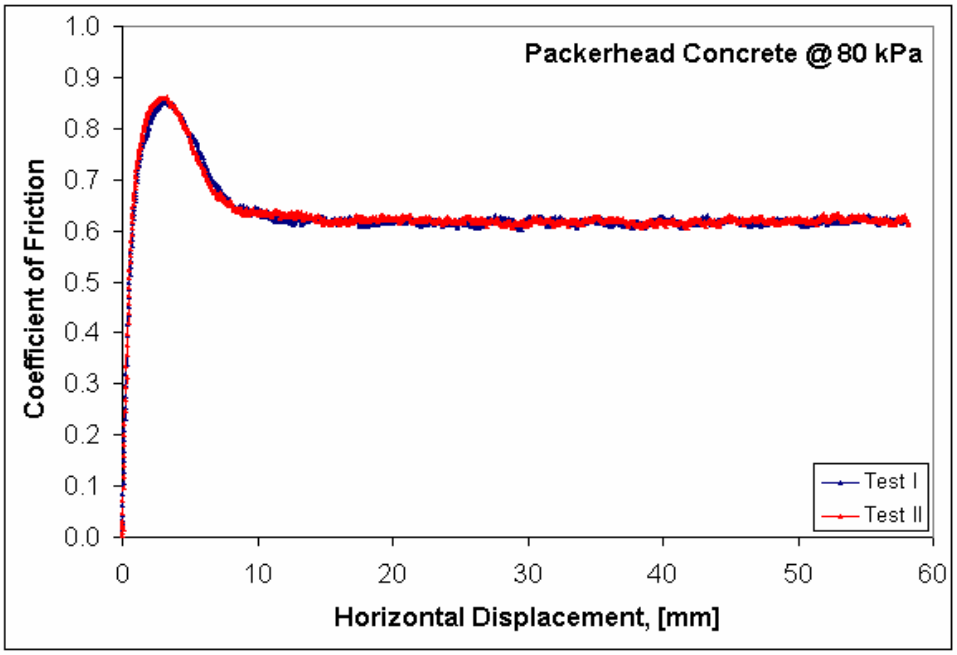


(b)

Figure 5.34 Repeatability Tests of (a) Atlanta Blasting Sand - Hobas™ FRP Pipe and (b) Atlanta Blasting Sand - Packerhead™ Concrete Pipe Interfaces

Table 5.7 Testing Program and Test Results

| Test No. | Soil Type | Pipe Type | Normal Stress [kPa] | Relative Density [%] | Shearing Rate [mm/min] | tan$\delta_p$ | tan$\delta_r$ |
|---|---|---|---|---|---|---|---|
| 1 | Ottawa 20/30 Sand | Hobas™ | 80 | 78.9 | 1.0 | 0.50 | 0.44 |
| 2 | | Hobas™ | | 81.6 | | 0.52 | 0.42 |
| 3 | | Polycrete | | 79.2 | | 0.49 | 0.43 |
| 4 | | Steel | | 80.4 | | 0.62 | 0.44 |
| 5 | | Wet-cast | | 77.0 | | 0.65 | 0.48 |
| 6 | | Packerhead™ | | 80.4 | | 0.73 | 0.53 |
| 7 | | Packerhead™ | | 86.1 | | 0.76 | 0.52 |
| 8 | | Vit. Clay | | 66.0 | | 0.63 | 0.48 |
| 9 | | SP # 60 | | 76.2 | | 0.77 | 0.55 |
| 10 | | SP # 36 | | 80.0 | | 0.76 | 0.56 |
| 11 | Atlanta Blasting Sand | Hobas™ | 80 | 83.7 | 1.0 | 0.58 | 0.56 |
| 12 | | Hobas™ | | 81.1 | | 0.60 | 0.56 |
| 13 | | Polycrete | | 77.8 | | 0.53 | 0.49 |
| 14 | | Steel | | 82.9 | | 0.73 | 0.58 |
| 15 | | Wet-cast | | 78.5 | | 0.76 | 0.59 |
| 16 | | Packerhead™ | | 85.1 | | 0.86 | 0.62 |
| 17 | | Packerhead™ | | 79.3 | | 0.85 | 0.62 |
| 18 | | Vit. Clay | | 81.6 | | 0.77 | 0.61 |
| 19 | | SP # 60 | | 79.9 | | 0.87 | 0.66 |
| 20 | | SP # 36 | | 81.3 | | 0.89 | 0.67 |
| 21 | Ottawa 20/30 Sand | Hobas™ | 40 | 81.1 | 1.0 | 0.51 | 0.43 |
| 22 | | Polycrete | | 82.6 | | 0.50 | 0.42 |
| 23 | | Steel | | 87.3 | | 0.68 | 0.49 |
| 24 | | Wet-cast | | 76.0 | | 0.68 | 0.49 |
| 25 | | Packerhead™ | | 82.8 | | 0.81 | 0.54 |
| 26 | | Vit. Clay | | 79.2 | | 0.71 | 0.50 |
| 27 | | SP # 60 | | 80.7 | | 0.80 | 0.60 |
| 28 | | SP # 36 | | 83.0 | | 0.82 | 0.61 |

Table 5.7 (continued) Testing Program and Test Results

| Test No. | Soil Type | Pipe Type | Normal Stress [kPa] | Relative Density [%] | Shearing Rate [mm/min] | tan$\delta_p$ | tan$\delta_r$ |
|---|---|---|---|---|---|---|---|
| 29 | Ottawa 20/30 Sand | Hobas™ | 120 | 78.2 | 1.0 | 0.48 | 0.42 |
| 30 | | Polycrete | | 76.8 | | 0.47 | 0.43 |
| 31 | | Steel | | 82.5 | | 0.62 | 0.47 |
| 32 | | Wet-cast | | 77.6 | | 0.63 | 0.45 |
| 33 | | Packerhead™ | | 82.3 | | 0.73 | 0.52 |
| 34 | | Vit. Clay | | 79.2 | | 0.75 | 0.55 |
| 35 | | SP # 60 | | 77.0 | | 0.65 | 0.49 |
| 36 | | SP # 36 | | 83.0 | | 0.74 | 0.54 |
| **Effect Of Relative Density** | | | | | | | |
| 37 | Ottawa 20/30 Sand | Hobas™ | 80 | 46.8 | 1.0 | 0.48 | 0.43 |
| 38 | | | | 56.5 | | 0.48 | 0.43 |
| 39 | | | | 65.9 | | 0.47 | 0.42 |
| 40 | | | | 95.6 | | 0.53 | 0.43 |
| 41 | | Packerhead™ | | 50.0 | | 0.63 | 0.50 |
| 42 | | | | 58.0 | | 0.65 | 0.51 |
| 43 | | | | 68.7 | | 0.71 | 0.50 |
| 44 | | | | 98.3 | | 0.82 | 0.50 |
| 45 | | Vit. Clay | | 46.7 | | 0.58 | 0.50 |
| 46 | | | | 55.5 | | 0.61 | 0.50 |
| 47 | | | | 64.8 | | 0.61 | 0.51 |
| 48 | | | | 94.4 | | 0.74 | 0.50 |
| **Effect Of Normal Stress** | | | | | | | |
| 49 | Ottawa 20/30 Sand | Hobas™ | 160 | 83.9 | 1.0 | 0.49 | 0.44 |
| 50 | | Packerhead™ | | 80.8 | | 0.70 | 0.51 |
| 51 | | Vit. Clay | | 79.2 | | 0.65 | 0.48 |
| 52 | | Hobas™ | 200 | 80.3 | | 0.49 | 0.43 |
| 53 | | Packerhead™ | | 84.2 | | 0.69 | 0.50 |
| 54 | | Vit. Clay | | 76.4 | | 0.65 | 0.49 |

## 5.4 Relationship Between Interface Strength and Surface Roughness

The average roughness values of the pipes were summarized in Chapter 4. In this section they are related to the peak and residual coefficient of friction of various pipes. The friction values utilized are from the test results of both Ottawa 20/30 sand and Atlanta blasting sand. Tests of Ottawa sand were performed at normal stresses of 40 kPa, 80 kPa, and 120 kPa whereas tests of Atlanta blasting sand were performed at 80 kPa, only. The plots are demonstrated in Figures 5.35 – 5.38.

All graphs show a bilinear relationship. The interface friction strength increases linearly with average roughness and reaches a maximum value and than remains constant. This maximum value is approximately equal to the internal friction strength of the soil itself. The phenomenon is explained as follows: The upper bound of interface friction is the internal friction of the soil itself because after a certain critical roughness value is reached, the failure is not on the interface anymore; it moves into the soil. This result is consistent with the findings of Uesugi and Kishida in 1986 for planar sand-steel interfaces.

The only pipe whose behavior deviated somewhat from this trend was the vitrified clay pipe. Although it has a rough surface and its $R_a$ value was beyond the critical roughness, the interface shear strength was less than the value of the “plateau”. This observation led the author to question whether other roughness parameters can describe the surface characteristics better. Additional plots were created by replacing $R_a$ with other parameters $\Delta a$, $\Delta q$, S, $\lambda_q$, $S_m$, $L_0$ and $R_{ku}$. Unfortunately, these parameters did not have a correlation with the interface shear strength of the pipe. These plots are given in the Appendix B.

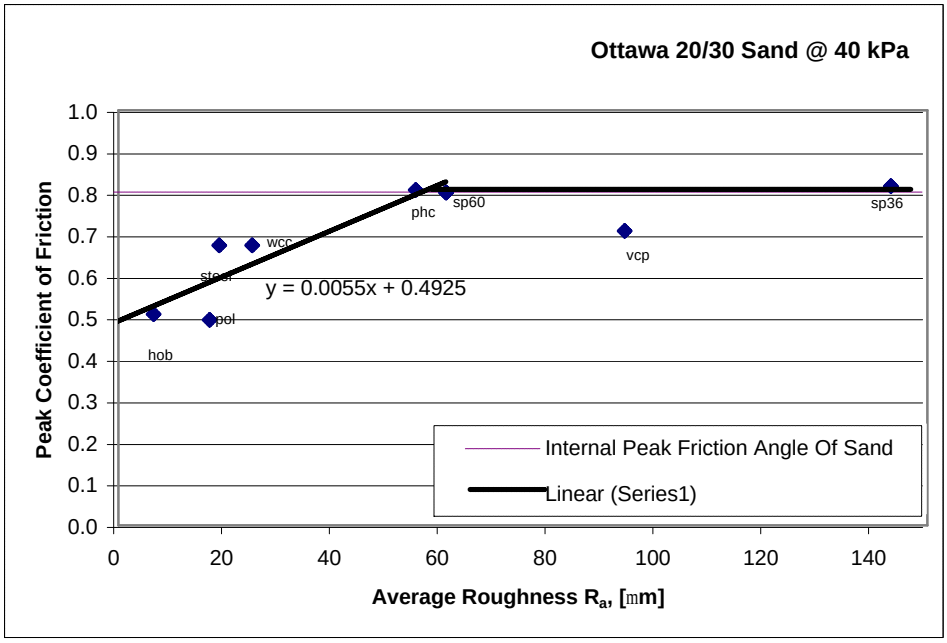


(a)

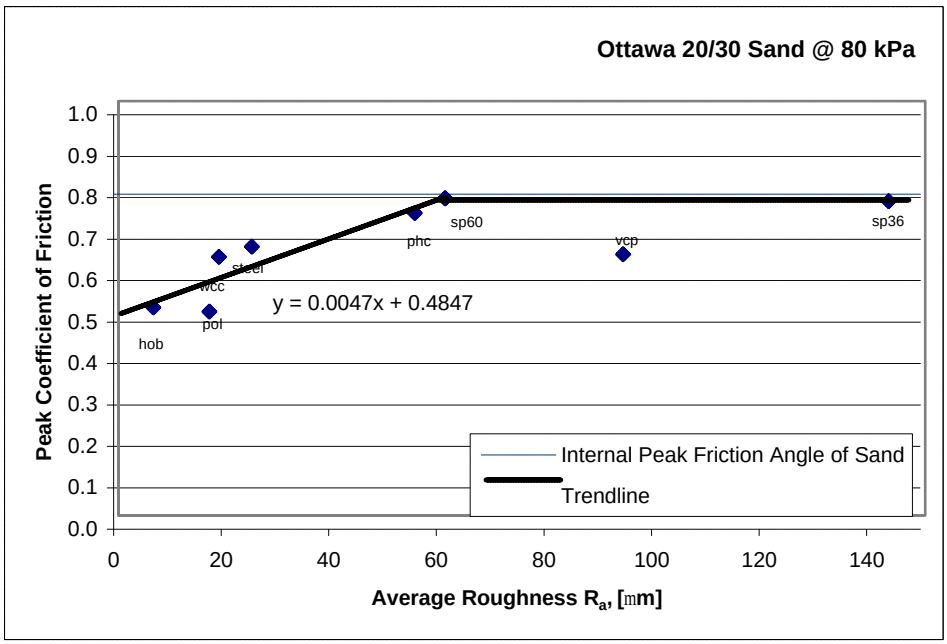


(b)

Figure 5.35 The Change of Peak Coefficient of Friction with Average Roughness for Ottawa 20/30 Sand at (a) 40 kPa (b) 80 kPa.

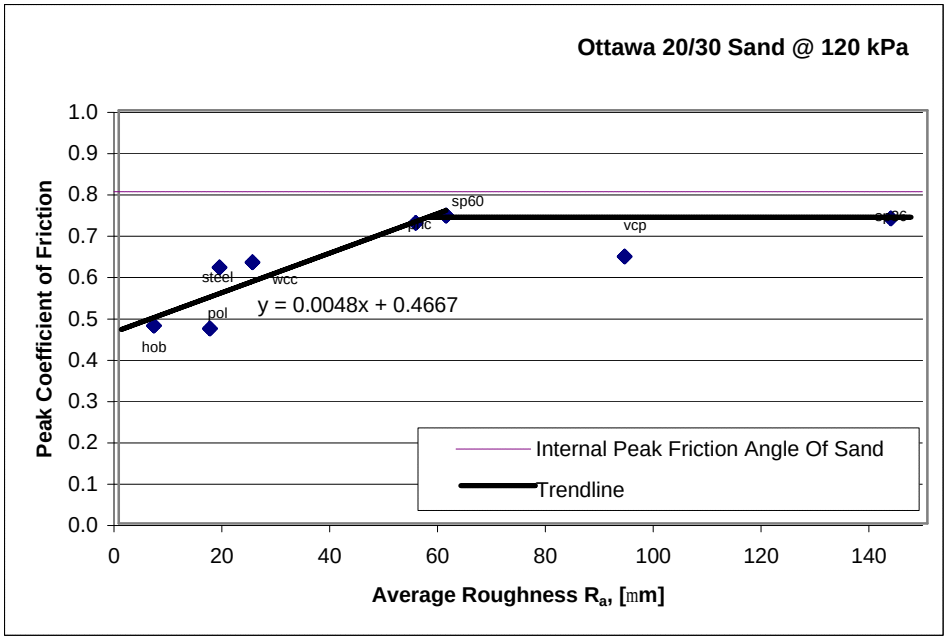


(a)

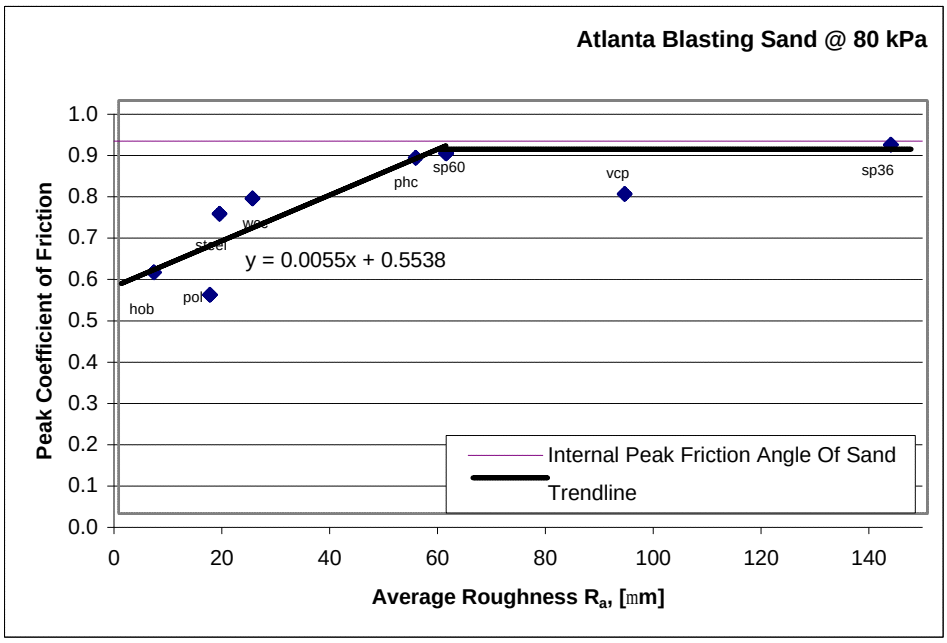


(b)

Figure 5.36 The Change of Peak Coefficient of Friction with Average Roughness for (a) Ottawa 20/30 Sand at 120 kPa (b) Atlanta Blasting Sand at 80 kPa.

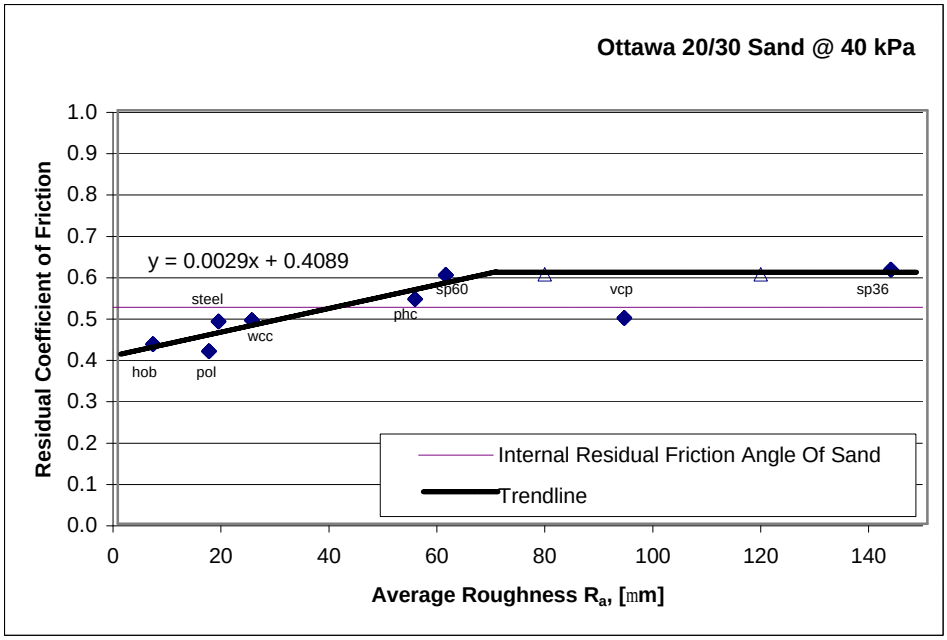


(a)

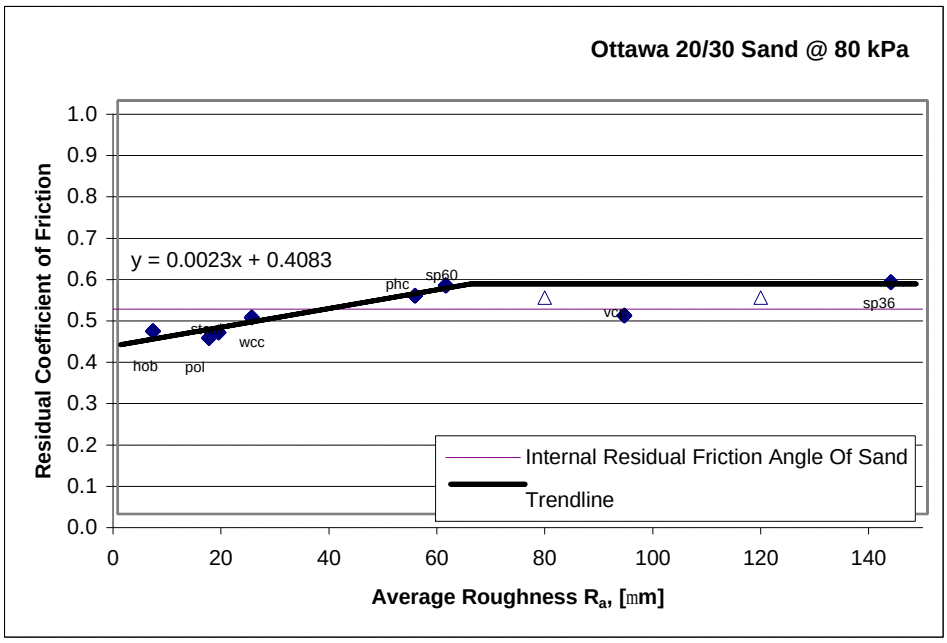


(b)

Figure 5.37 The Change of Residual Coefficient of Friction with Average Roughness for Ottawa 20/30 sand at (a) 40 kPa (b) 80 kPa.

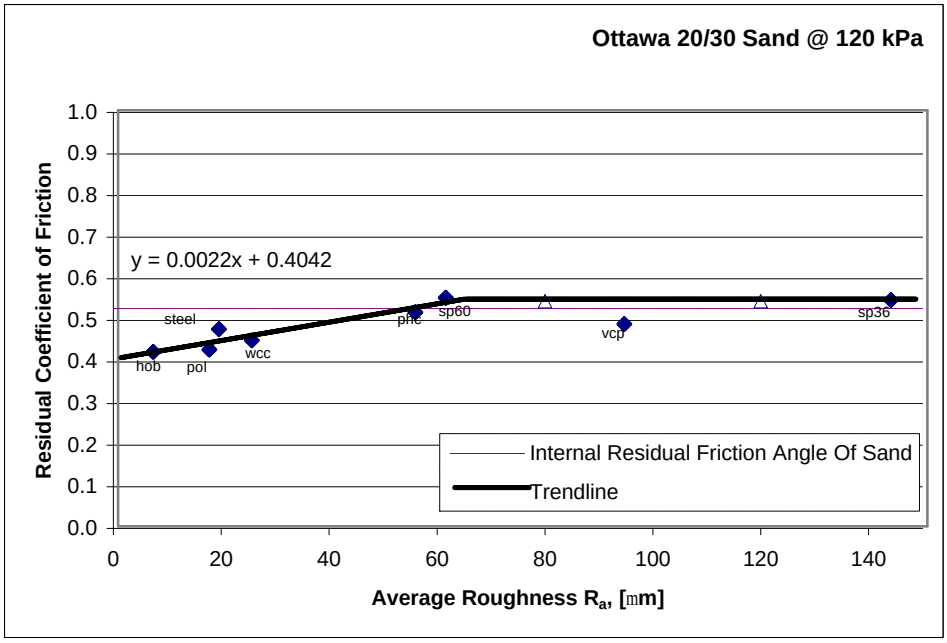


(a)

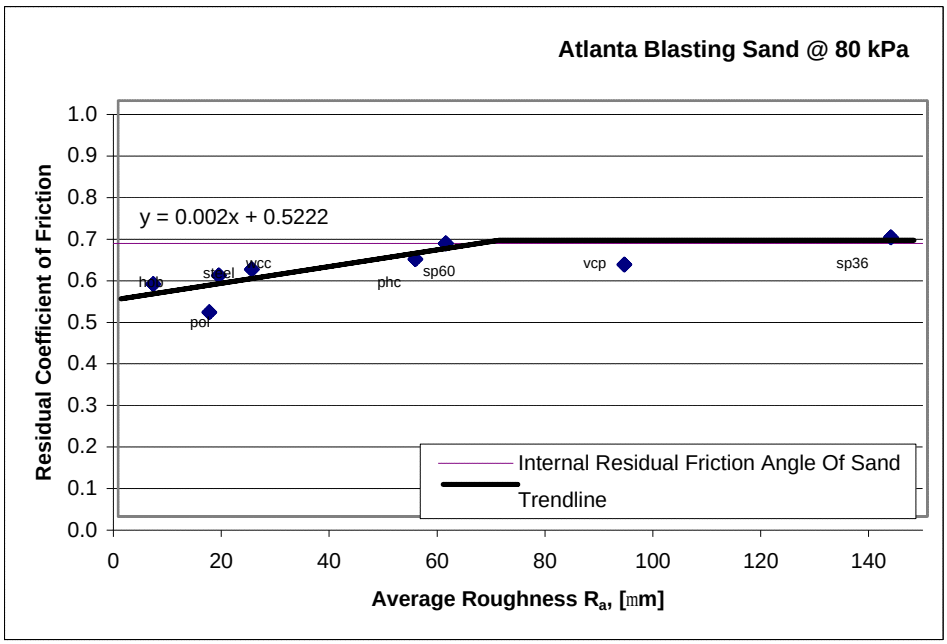


(b)

Figure 5.38 The Change of Residual Coefficient of Friction with Average Roughness for (a) Ottawa 20/30 Sand at 120 kPa (b) Atlanta Blasting Sand at 80 kPa.

The phenomenon noted above was observed at each normal stress and sand type and explained by the surface profile of the vitrified clay pipe: Although this pipe had a high $R_a$ value, the number, dimensions and spacing of asperities were different than other profiles. The profile did not have sharp corners; the transitions from peak to valleys were smooth and rounded. The profile of the vitrified clay pipe in relation with the size of the particle did not create the expected high friction on the interface. This was also confirmed by the field performance of this type of pipe.

The surface profiles for vitrified clay and Packerhead$^{TM}$ concrete pipes are presented in Figure 5.39 to demonstrate the difference of the profile of the vitrified clay pipe. The plots on the top show a profile from 0 mm to 50 mm. The bottom plots magnify the same profile between 20 mm and 25 mm. The particle diameter of Ottawa 20/30 sand is marked with a red line in the bottom profiles. It can be clearly seen from the figure that the profile of vitrified clay pipe has less peaks and valleys and is smoother than the profile of Packerhead$^{TM}$ concrete pipe.

The correlation of the trendline with the internal friction of the soil is higher in the graphs of residual strength. This means that the fluctuations in the data are less for the steady-state friction due to the stability of the condition reached. Fluctuations can be attributed to the variation in roughness characteristics in the pipes.

The internal friction angles of the particular sand used in the tests are also shown on the plots of coefficient of friction versus roughness and are represented by a dashed line. The ultimate strength of the interface does not correspond exactly on top of the internal friction angle of sand. Moreover this difference varies with normal stress. This

difference is illustrated in Figure 5.40, where the x-axis is the normal stress and the y-axis is the ratio of the interface friction angle to the internal friction angle:

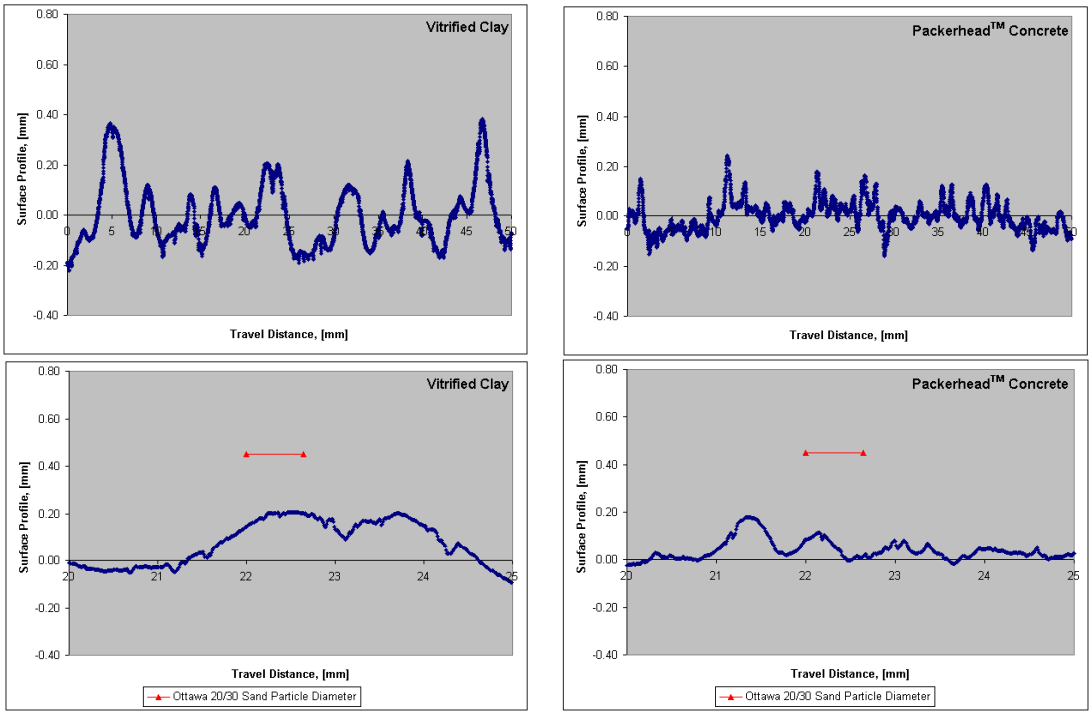


(a) (b)

Figure 5.39 Surface Profiles of (a) Vitrified Clay (b) Packerhead™ Concrete Pipes

As can be seen from the figure, the ratio tends to stabilize with the increase in normal stress. The difference may be attributed to the method of determination of the internal friction angle of sand. It is assumed that the friction angle does not change with the normal stress and the angle was calculated from the slope of the line connecting points of maximum shear stress and maximum normal stress. In reality, this curve is not linear; it is concave downward. Also, the equipments used in both type of tests and the error produced within them, were different.

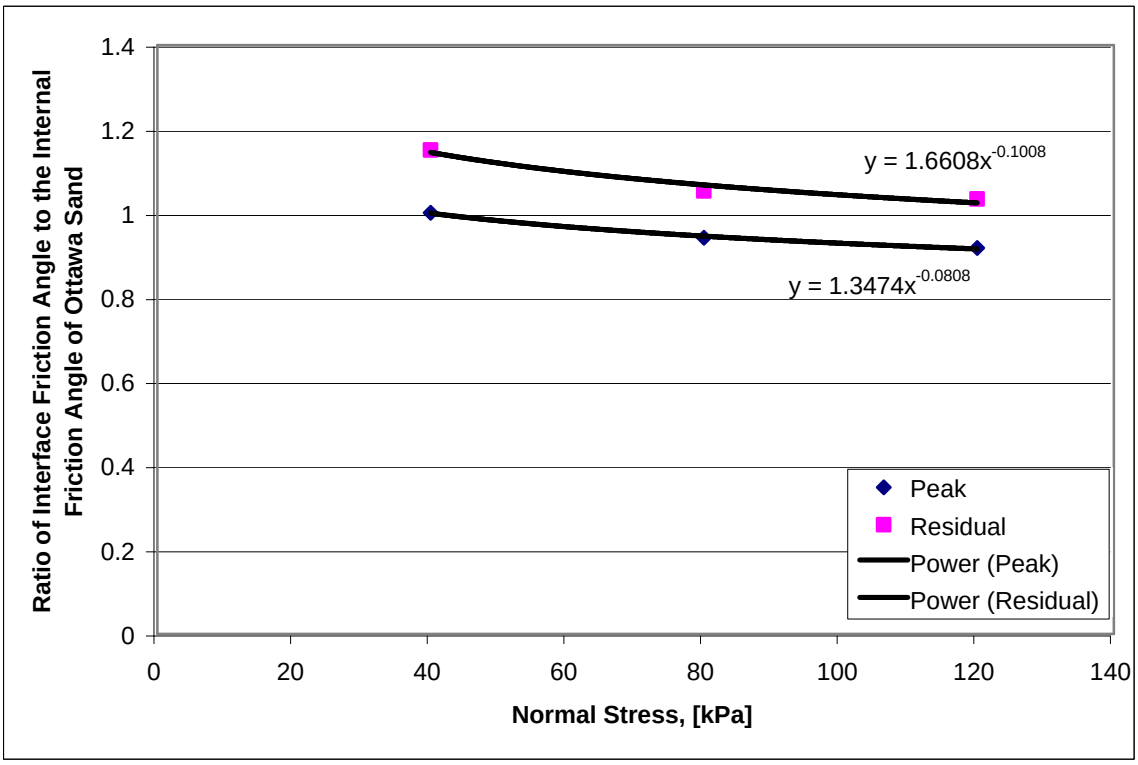


Figure 5.40 Ratio of Interface Friction Angle to the Internal Friction Angle of Ottawa Sand at Various Normal Stresses

# CHAPTER 6

# CONCLUSIONS AND FUTURE RECOMMENDATIONS

## 6.1 Introduction

This study investigated the interface shear behavior of various commercial pipes with two types of sands in relation with the surface topography, normal stress and relative density of the particulate media. The motivation for this study was the interest to predict the factors affecting the pipe-jacking and trenchless technology applications and recommend new approaches to increase the performance of this technique. Tests were performed with a new apparatus specifically designed to measure the interface shear characteristics of the pipes in laboratory under controlled conditions. This chapter summarizes the findings of the experimental study.

## 6.2 Conclusions

### 6.2.1 Equipment Design

Since the conventional interface direct shear tests were performed on planar surfaces and since pipe-jacking is performed in larger scales, a new apparatus was proposed to examine the frictional characteristics in laboratory conditions.

This apparatus consists of a double-wall shear box, of which the inner walls are interchangeable. This design allows testing at different curvatures by attaching the corresponding set of inner walls. The inner walls have their specific design completely compatible with the pipe surface to prevent additional friction forces and leakage of

particulate material. The box was designed as a planar rectangle with a narrow width to approximate the curved surface with the longer edge in the axial direction of the pipe. The validity of this approximation was carefully evaluated in terms of normal stress for different sizes. Also the effects of the boundary conditions were analyzed and used in the determination of the shear box dimensions. In addition, a pipe container was designed and manufactured to restrain the pipe during testing and to serve as a "lubricant pool" for future purposes. Test results showed that this design mounted in a large displacement interface shear device worked successfully.

### 6.2.2 Surface Topography Characterization

Various researchers have shown that the surface roughness has a predominant effect on the interface shear characteristics (Potyondy, 1961, Brumund and Leonards, 1973, Uesugi and Kishida, 1986, Paikowski et al., 1985, Frost et al., 2002). Various parameters were defined to demonstrate different aspects of surface topography among which $R_a$ (average roughness) was used in this study.

Tests performed with Taylor-Hobson Talysurf$^{TM}$ Series-2 stylus profilometer showed that the $R_a$ values of the pipes vary between 6.5 μm (Hobas$^{TM}$ FRP) and 93.9 μm (vitrified clay pipe). The profiles showed different characteristics in terms of asperity size, shape, slope and spacing.

To extend the range of roughness values tested and consequently to force the failure to be in the soil instead of the interface, two artificial pipes were created: Rough sandpapers (No.36 and No.60) were glued to the existing Hobas pipes and consequently

the upper limit of average roughness was increased from 93.9 μm to 143.2 μm (Sandpaper No.36).

A large number of tests were performed to quantify the roughness and to evaluate the repeatability and variation in surface characteristics of the manufactured pipes. The least variation was within the vitrified clay pipe (Std. Dev / Avg. = 13.0%) whereas the highest was within the wet-cast concrete pipe (Std. Dev / Avg = 78.5%). High repeatability was observed.

### 6.2.3 Interface Shear Strength Characteristics

To determine the interface shear characteristics of pipe-soil interfaces, various tests were performed using the new double-wall shear apparatus. In this experimental study, 8 different pipes and 2 types of sand (Ottawa 20/30 and Atlanta blasting sand) were tested at different normal stresses and relative densities. The results were summarized under four different categories studying the effect of surface roughness, particle angularity, normal stress and relative density.

Previous studies have shown that surface roughness is the predominant parameter that determines the interface shear behavior and strength (Potyondy, 1961, Brumund & Leonards, 1973, Uesugi & Kishida, 1986, Paikowski et al., 1985, Frost et al., 2002). Similar findings were observed in this study. The increase in roughness not only increases the interface strength but also changes the shearing mechanism from sliding at the interface to a more complex particle displacement and rearrangement distributed within the whole specimen. When sliding is the predominant mechanism, there is not an obvious post-peak behavior. When the particle displacement and rearrangement is the

predominant mechanism, a clear post-peak softening is observed because particles slipped, rolled, moved vertically, and rearranged at the interface of rougher pipes and reach the stable, residual "minimum-friction" condition. The peak friction occurred after relatively small horizontal displacements varying between 0.8 to 3.3 millimeters depending on the particular roughness.

There is an upper limit for the strength of the pipe-soil system, which is the internal strength of the soil itself. If the roughness is higher than a critical value, the failure moves from the interface into the particulate media. The interface strength varies between a certain minimum value at the theoretically "zero" roughness and the internal strength of the soil. Regardless of the surface topography, the shear strength can not exceed this value. The only pipe whose behavior deviated somewhat from this trend was the vitrified clay pipe. Although its roughness was beyond the critical value, its shear strength was less than the upper limit. This was explained by its different surface profile: The profile does not have sharp corners; the transitions from peak to valleys are smooth and rounded, asperities are considerably less in number.

Also the particle shape strongly influences the interface shear strength. The angular Atlanta blasting sand particles have a stronger interlock with the pipe surface than the sub-rounded Ottawa sand particles and this in turn increases the strength in global scale. The coefficient of friction increased by 16% for smooth Hobas$^{TM}$ FRP and by 18% for rough Packerhead$^{TM}$ concrete pipe when the interface shear tests were performed with Atlanta blasting sand instead of Ottawa 20/30 sand.

In general it is thought that the coefficient of friction is independent of the normal stress. But tests at five different normal stresses showed that the coefficient of friction

decreases with the increase of vertical stress however after a critical normal stress, it remains constant, because the plowing effect creates additional friction forces at the interface. This observation is consistent with Archard's theory (1957) and the findings of Dove and Frost (1999) for the frictional behavior of smooth geomembrane-Ottawa sand interfaces.

The relative density was also shown to affect the interface shear characteristics. Denser specimens had a larger contact area and stronger interlocking at the interface and resulted in higher peak friction values. In contrast, the residual friction coefficient did not change significantly with the change in the relative density since the particle rearrangement is complete; the soil reaches a stable residual condition and void ratio.

## 6.3 Recommendations

This study showed the significance of the surface characteristics of the pipes in determination of the interface shear strength. Smoother pipes have less friction at their surfaces. The peak coefficient of friction of the smooth Hobas$^{TM}$ FRP pipe is 31% less than the one of rough Packerhead$^{TM}$ concrete pipe at N=80 kPa, $D_R$=80%.

The difference is less pronounced in residual coefficient of friction; the coefficient of friction of Hobas$^{TM}$ FRP pipe is 19% less than the one of Packerhead$^{TM}$ concrete pipe. For field application, the majority of the pipes are subjected to residual conditions, while they are jacked. So, a decrease of approximately 19% should be expected in jacking forces in the field, if Hobas$^{TM}$ FRP is used instead of Packerhead$^{TM}$ concrete pipe, assuming that all other parameters are the same. If a certain type of pipe is

preferred due to some other constraints, special treatment may be applied at the pipe surface.

Detailed sub-soil investigation is recommended to predict the jacking forces because the soil type and particle angularity have a significant effect on the shear characteristics. When the jacking is to be performed on an angular soil, a significant increase should be expected in jacking forces.

The peak friction coefficient of friction increased by 8% at Hobas$^{TM}$ FRP, 29% at vitrified clay pipe, and 30% at Packerhead$^{TM}$ concrete pipe when the relative density changed from 48% to 96%. There was no significant change in residual shear strength. It can be concluded that the effect of relative density is more pronounced when the pipe is rougher.

Similarly using the angular Atlanta blasting sand instead of sub-rounded Ottawa 20/30 sand resulted in a 16% increase in friction by Hobas$^{TM}$ FRP, and 18% by Packerhead$^{TM}$ concrete pipe.

The deeper the pipe jacking is performed, the higher jacking forces should be expected, since the friction force increases with the normal load. The rate of the increase is approximately constant after a certain depth because of the effect of the plowing.

For future research in this area, it is recommended to study the effect of lubricants and the lubrication mechanisms on pipe-soil interfaces. In pipe-jacking industry, lubricants such as bentonite are widely used to decrease the jacking forces but the background and efficiency of this application is not clearly understood.

# APPENDIX A

## TECHNICAL DRAWINGS OF THE NEW APPARATUS

SHEAR BOX INNER WALLS

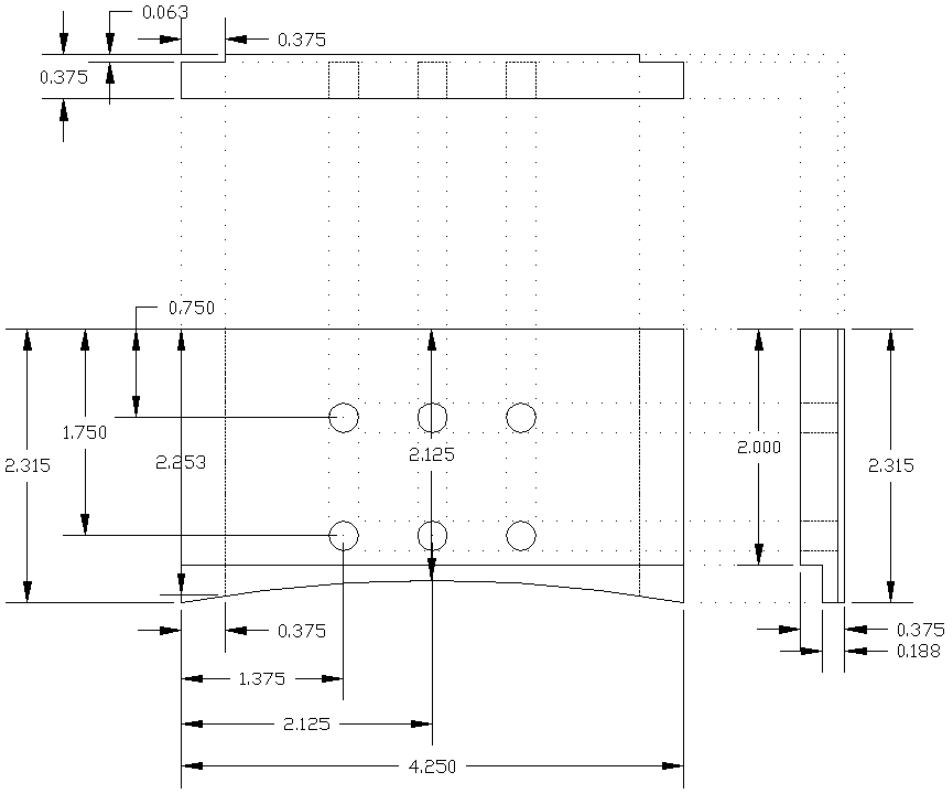


Figure A.1 Inner End Wall of the Box for R=12’’

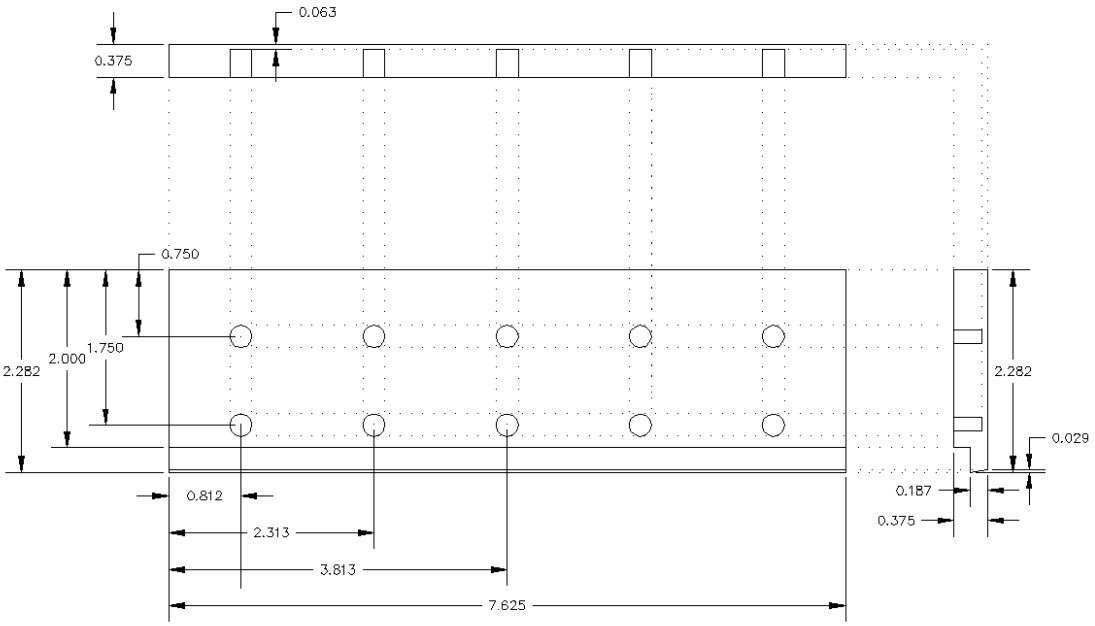


Figure A.2 Inner Sidewall of the Box for R=12’’

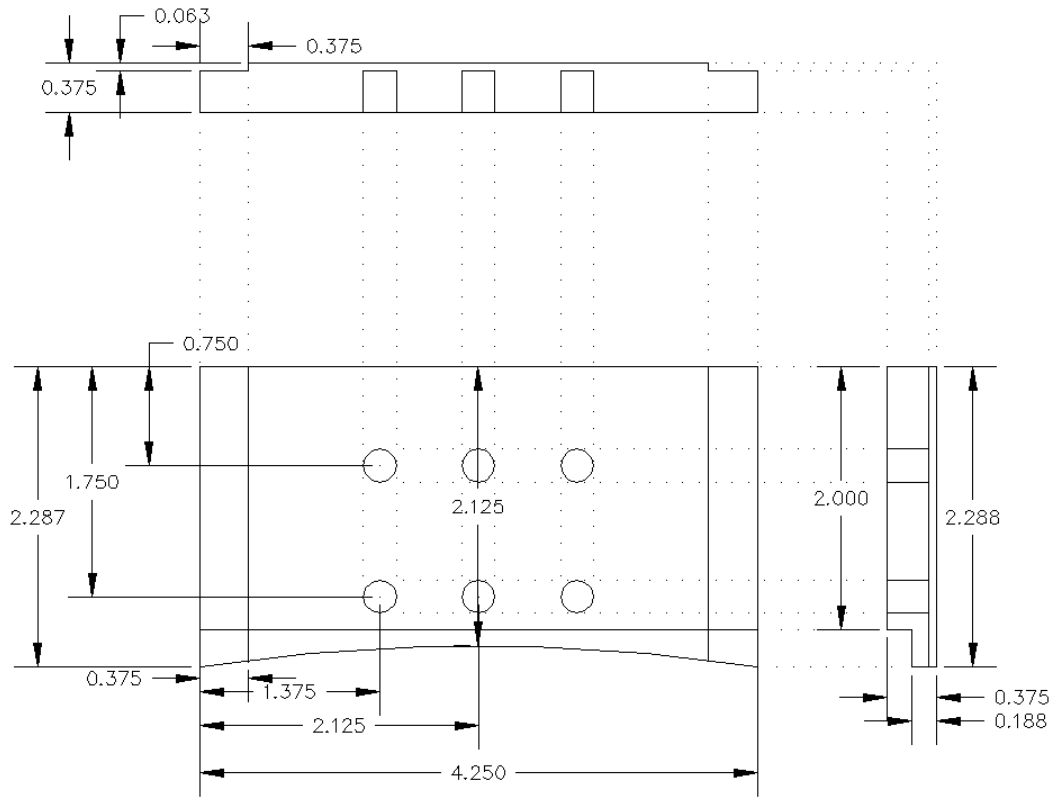


Figure A.3 Inner End Wall of the Box for R=14’’

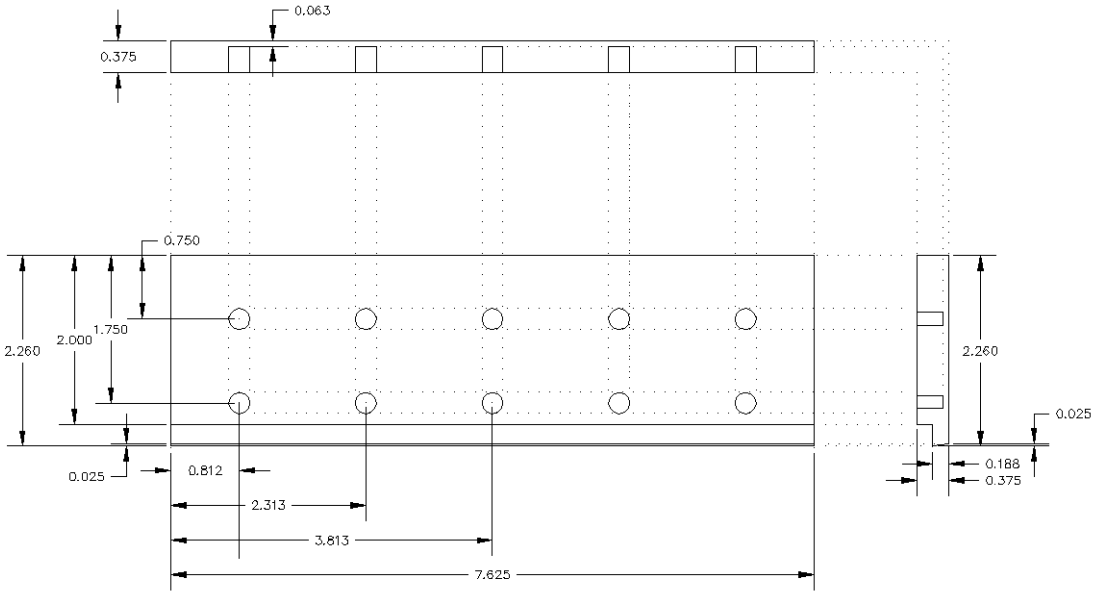


Figure A.4 Inner Sidewall of the Box for R=14’’

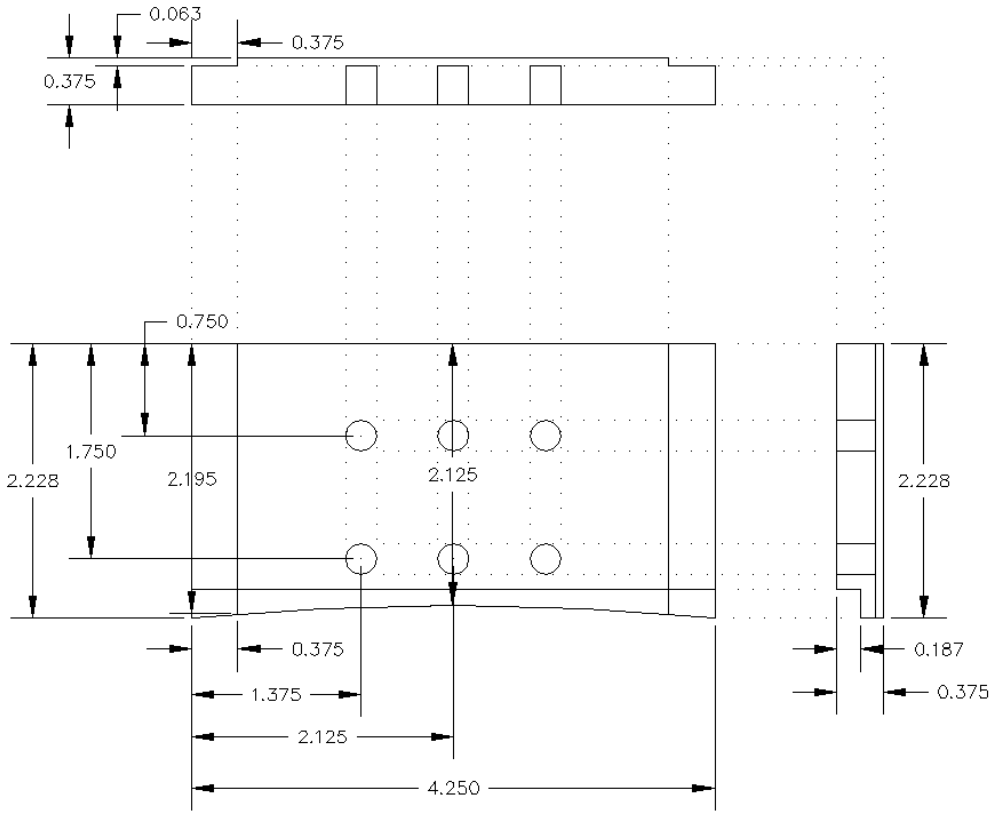


Figure A.5 Inner End Wall of the Box for R=22’’

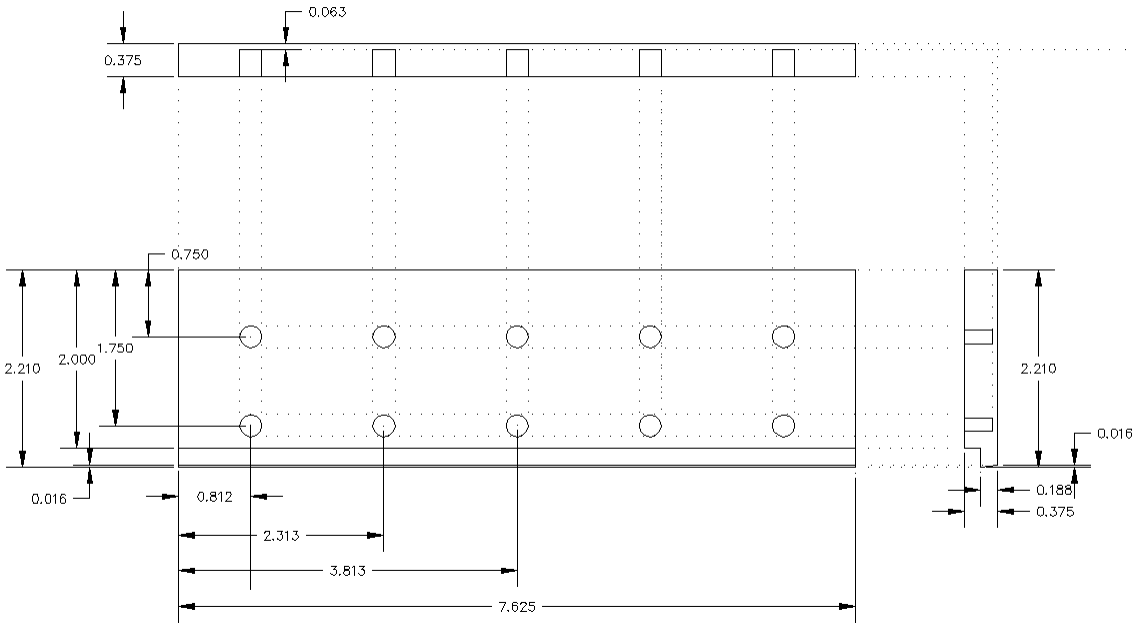


Figure A.6 Inner Sidewall of the Box for R=22’’

SHEAR BOX OUTER FRAME

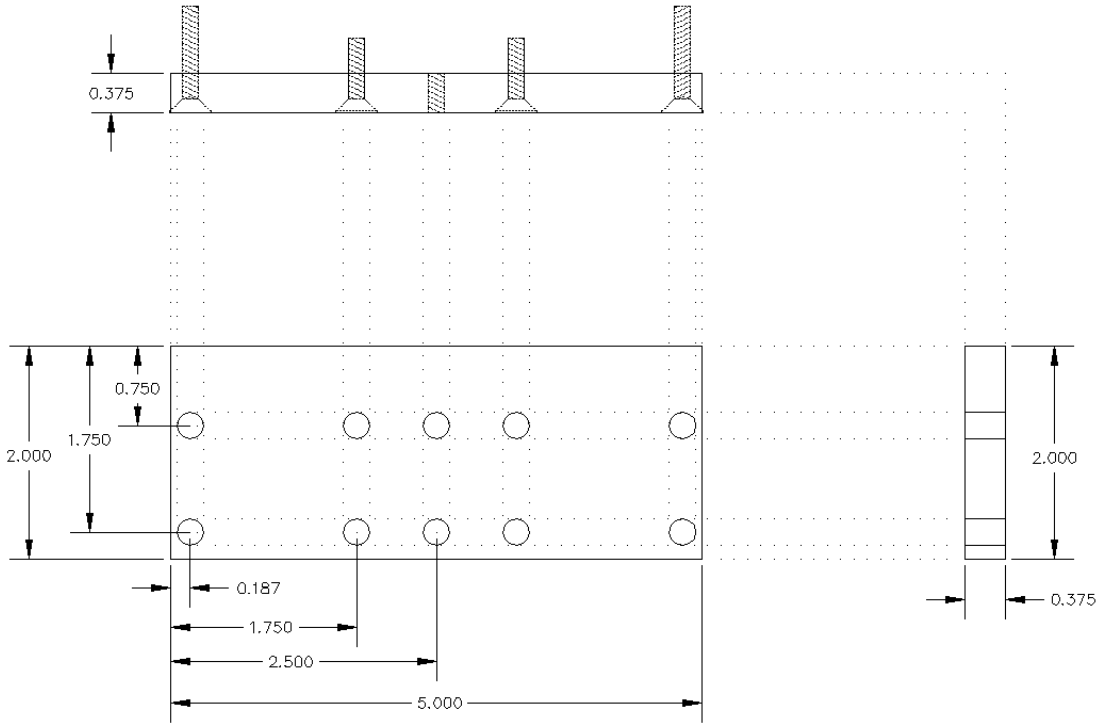


Figure A.7 Outer End Wall of the Box

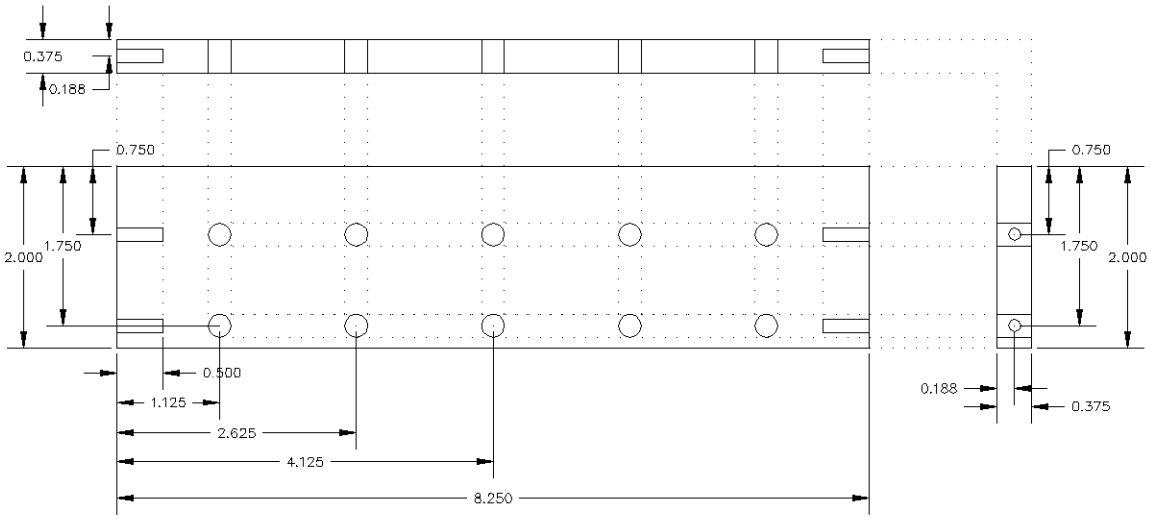


Figure A.8 Outer Sidewall of the Box

LOADING PLATE

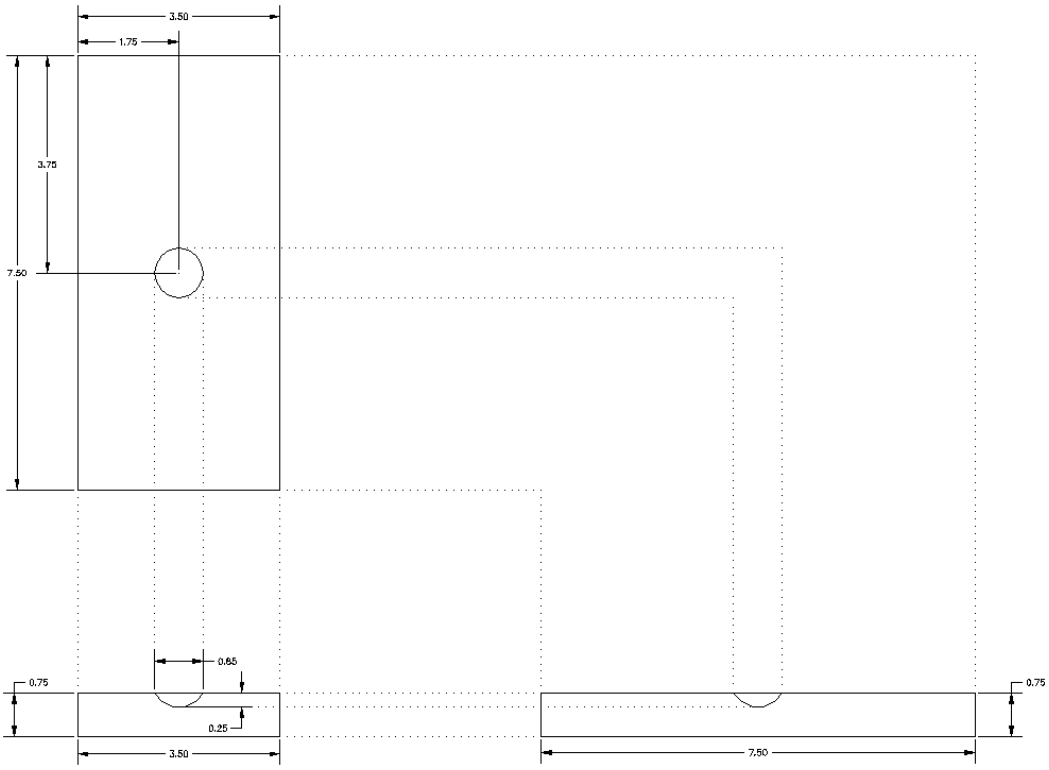


Figure A.9 The Loading Plate

# APPENDIX B

## DIRECT SHEAR TESTS AND DIFFERENT ROUGHNESS PARAMETERS

DIRECT SHEAR TESTS

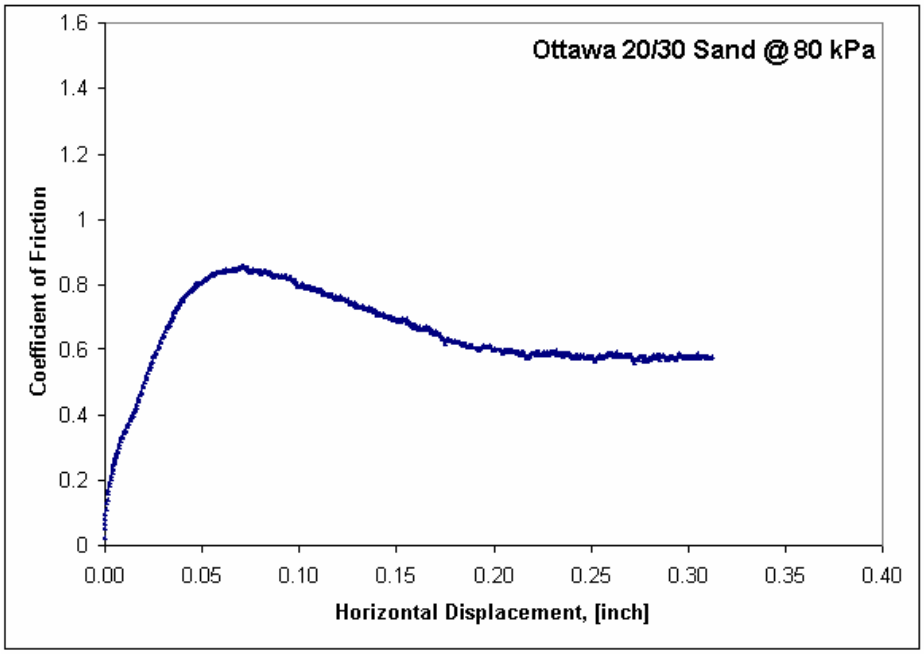


Figure B.1 Direct Shear Test of Ottawa 20/30 Sand at 80 kPa and $D_r$=71%

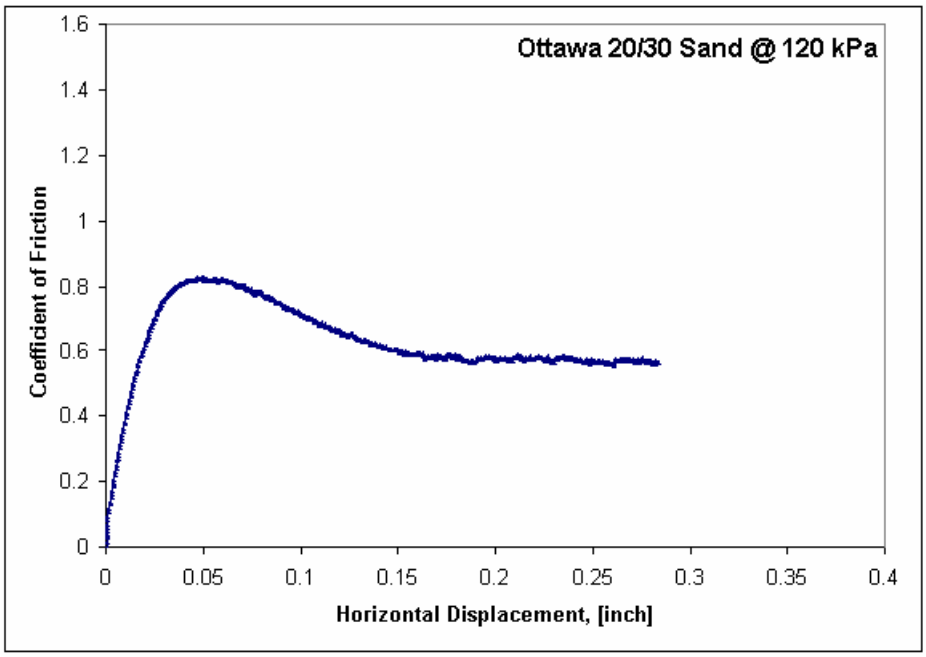


Figure B.2 Direct Shear Test of Ottawa 20/30 Sand at 120 kPa and $D_r$=73%

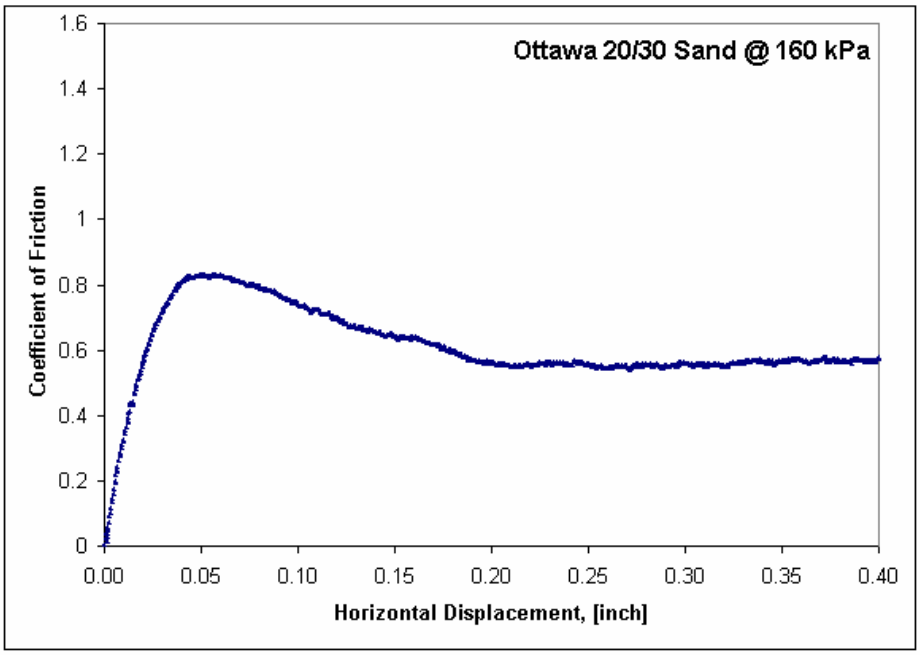


Figure B.3 Direct Shear Test of Ottawa 20/30 Sand at 160 kPa and $D_r$=78%

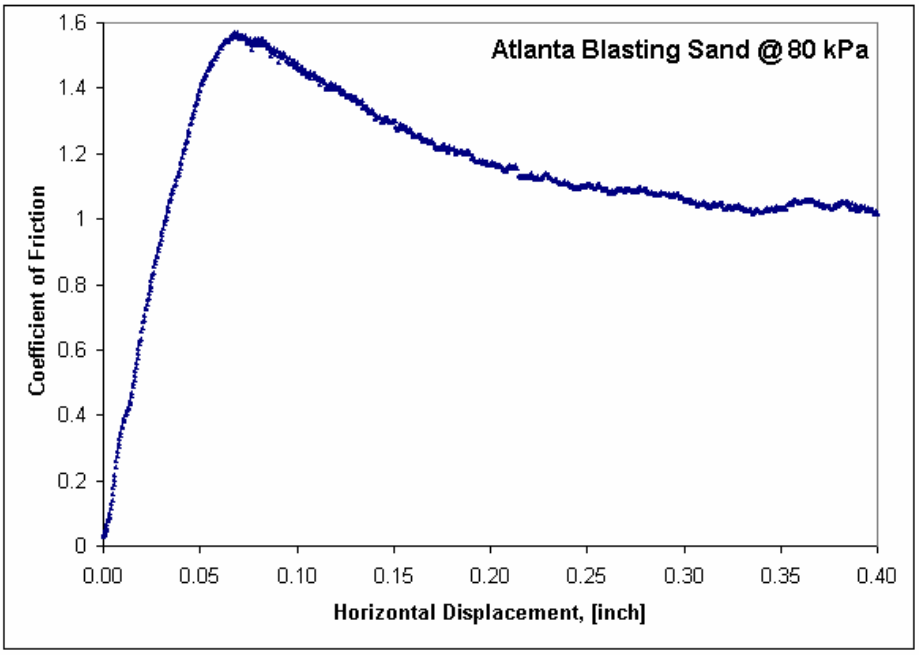


Figure B.4 Direct Shear Test of Atlanta Blasting Sand at 80 kPa and $D_r$=71%

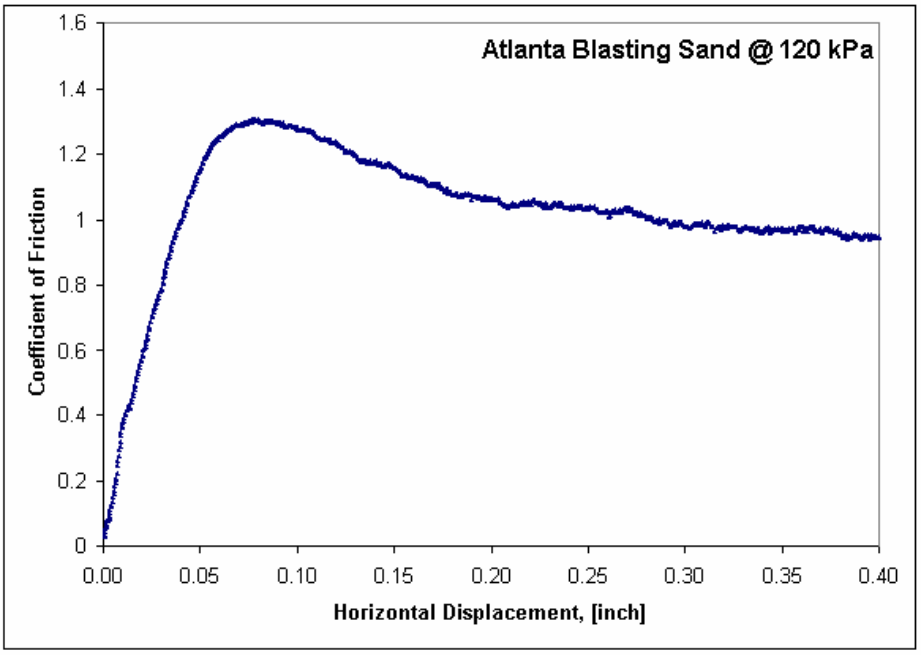


Figure B.5 Direct Shear Test of Atlanta Blasting Sand at 120 kPa and $D_r$=80%

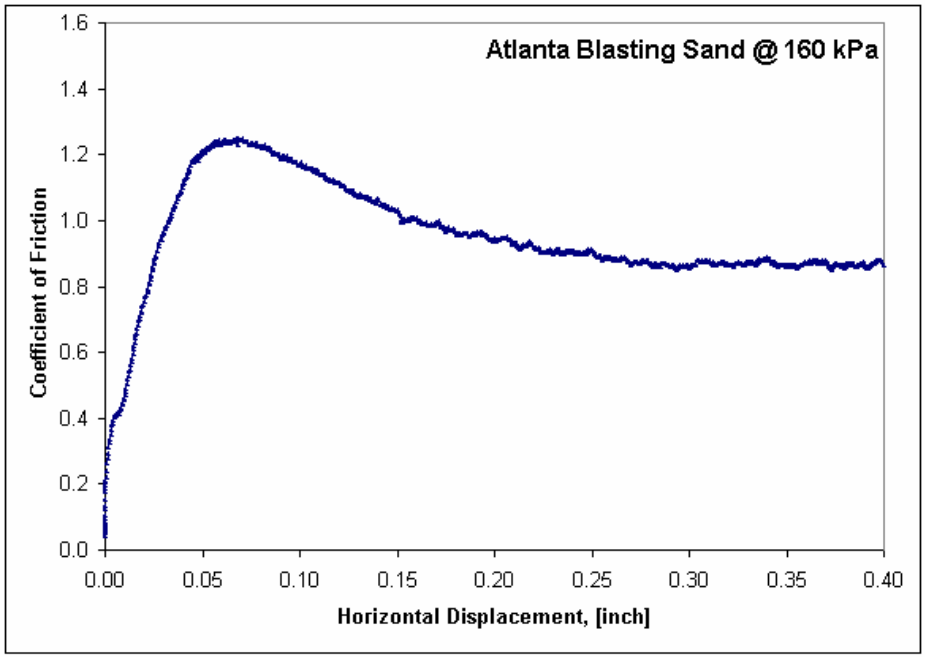


Figure B.6 Direct Shear Test of Atlanta Blasting Sand at 160 kPa and $D_r$=75%

DIFFERENT ROUGHNESS PARAMETERS

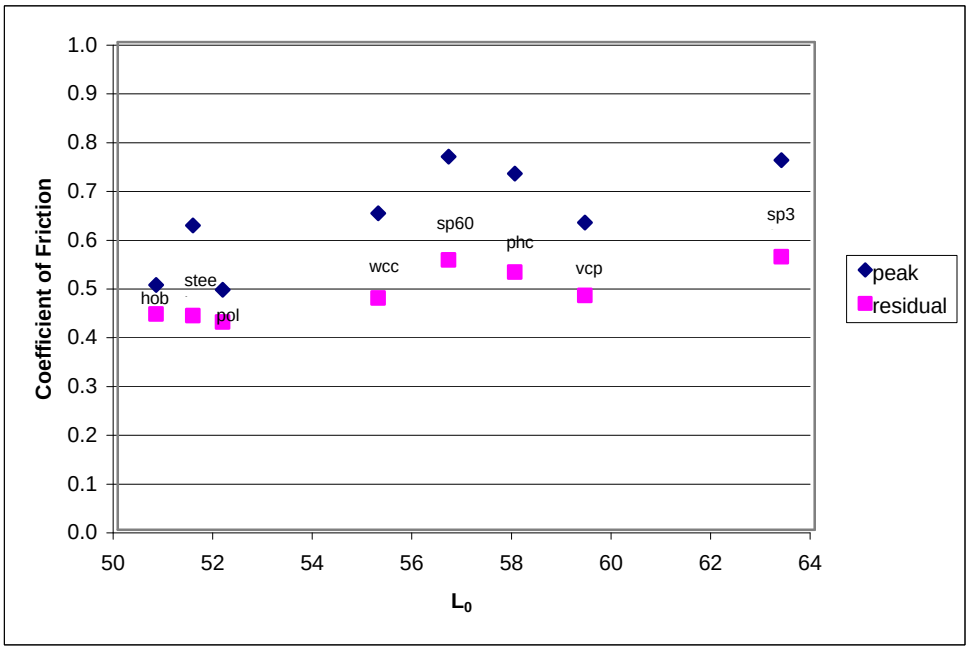


Figure B.7 Coefficient of Friction versus $L_0$ for Peak and Residual Strength of Various Pipe-Ottawa 20/30 Sand Interfaces at 80 kPa

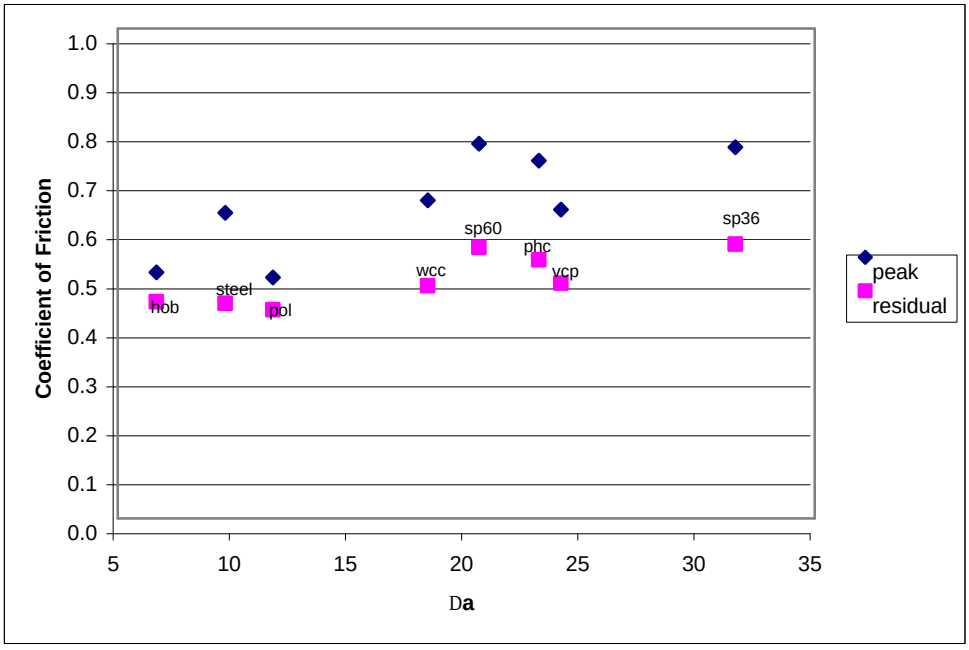


Figure B.8 Coefficient of Friction versus Δa for Peak and Residual Strength of Various Pipe-Ottawa 20/30 Sand Interfaces at 80 kPa

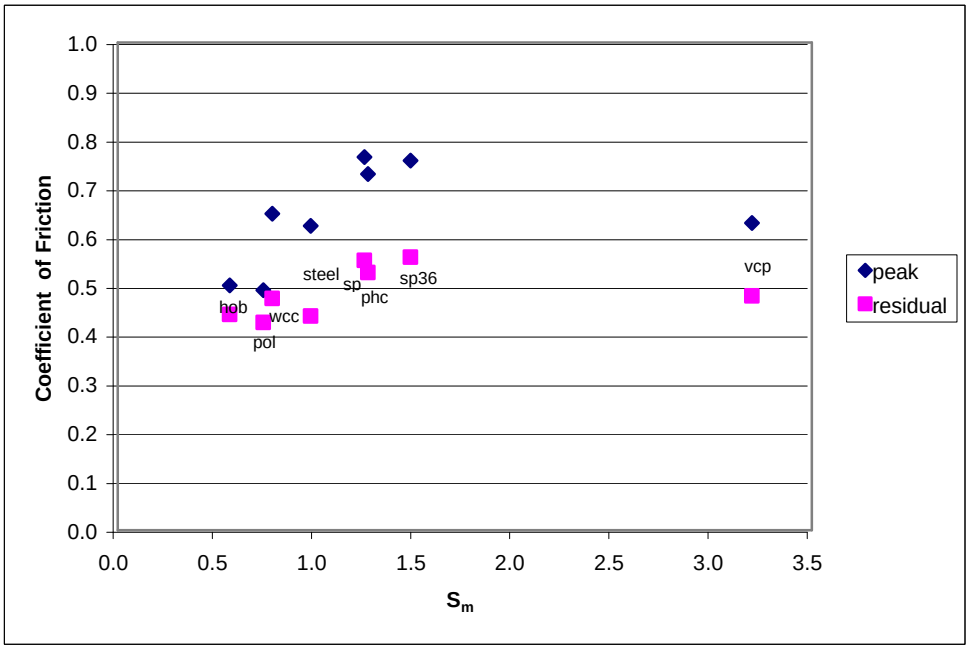


Figure B.9 Coefficient of Friction versus $S_m$ for Peak and Residual Strength of Various Pipe-Ottawa 20/30 Sand Interfaces at 80 kPa

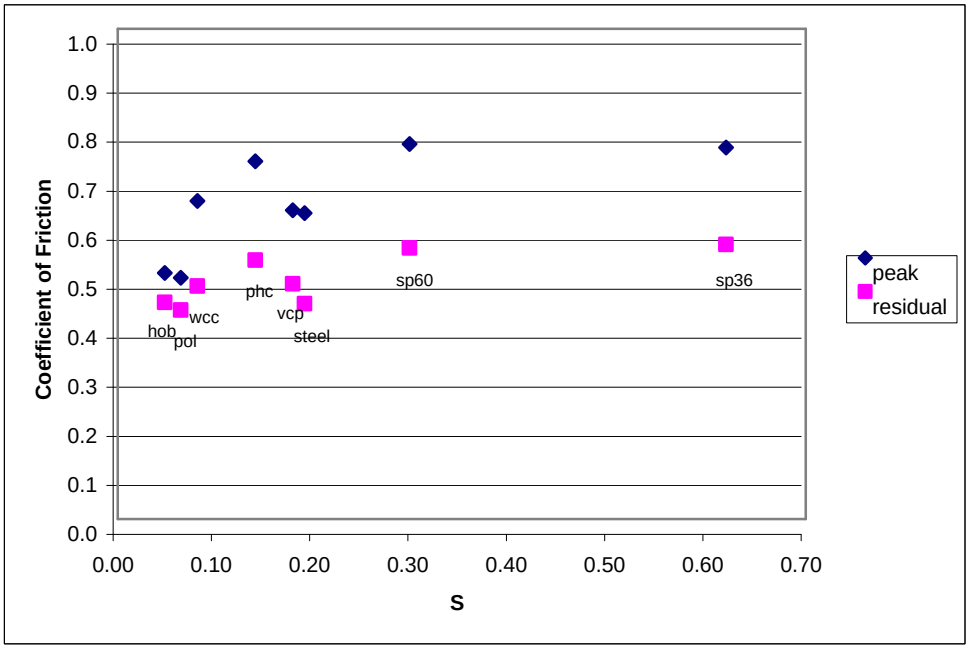


Figure B.10 Coefficient of Friction versus S for Peak and Residual Strength of Various Pipe-Ottawa 20/30 Sand Interfaces at 80 kPa

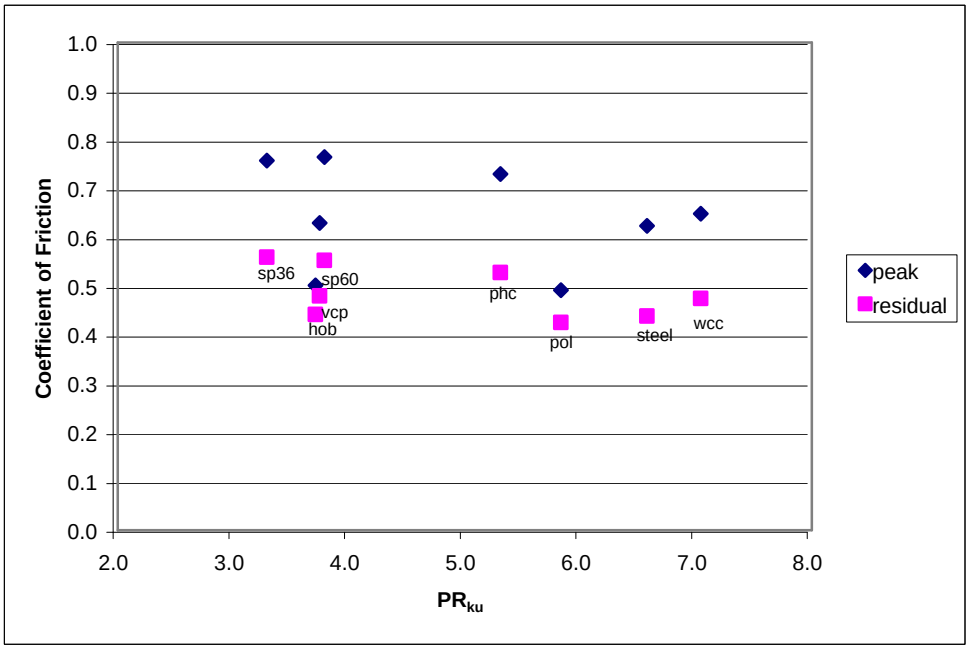


Figure B.11 Coefficient of Friction versus $PR_{ku}$ for Peak and Residual Strength of Various Pipe-Ottawa 20/30 Sand Interfaces at 80 kPa

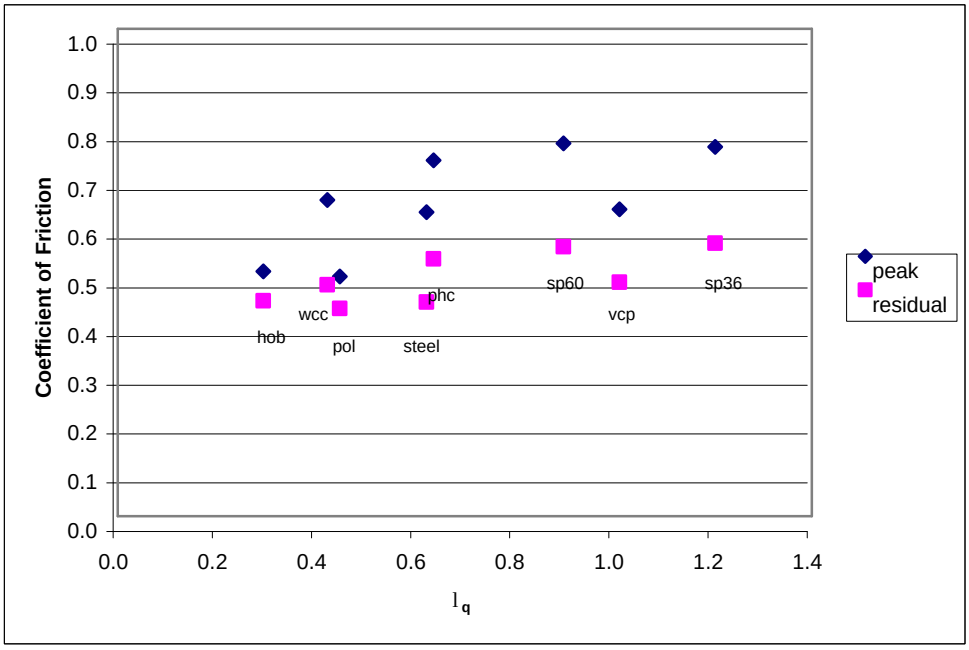


Figure B.12 Coefficient of Friction versus $\lambda_q$ for Peak and Residual Strength of Various Pipe-Ottawa 20/30 Sand Interfaces at 80 kPa

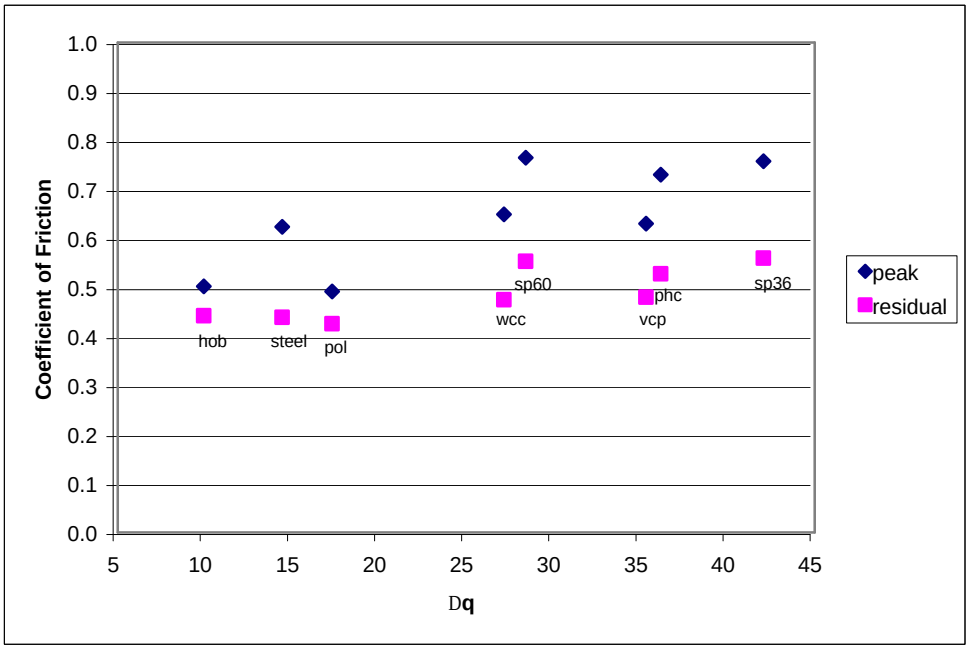


Figure B.13 Coefficient of Friction versus $\Delta_q$ for Peak and Residual Strength of Various Pipe-Ottawa 20/30 Sand Interfaces at 80 kPa

# REFERENCES


Agilent Technologies, Agilent 34970A Data Acquisition/Switch Unit Specifications, Web Page, http://cp.literature.agilent.com/litweb/pdf/5965-5290EN.pdf, (Accessed 27 April, 2004).

Akkol, O**.**, Baykal, G., (1997), "A New Test Device and Method: Geotextile - Soil Interface Cylindrical Test", *Insaat Muhendisliginde Gelismeler III. Teknik Kongre, ODTU, Ankara, Turkey.*

ASCE Standard CI/ASCE 36-01 (2001), "Standard Construction And Guidelines For Microtunneling", 41 pp.

ASTM D422-63 (1990) "Standard Test Method For Particle-Size Analysis Of Soils", 1997 Annual Book Of ASTM Standards, Vol. 04.08, Section 4, pp. 10-16.

ASTM D3080-98 (1999) "Standard Test Method For Direct Shear Test Of Soils Under Consolidated Drained Conditions", 2003 Annual Book Of ASTM Standards, Vol. 04.08, pp. 1-6.

ASTM D4253-93 (1996) "Standard Test Methods For Maximum Index Density And Unit Weight Of Soils Using A Vibratory Table", 1997 Annual Book Of ASTM Standards, Vol. 04.08, Section 4, pp. 501-513.

ASTM D4254-91 (1996) "Standard Test Method For Minimum Index Density And Unit Weight Of Soils And Calculation Of Relative Density", 1997 Annual Book Of ASTM Standards, Vol. 04.08, Section 4, pp. 514-521.

ASTM D5321-02 (2002) "Standard Test Method For Determining The Coefficient Of Soil And Geosynthetic Or Geosynthetic And Geosynthetic Friction By The Direct Shear Method", 2003 Annual Book Of ASTM Standards, Vol. 04.13, pp. 1-7.

Archard, J. F., (1957), "Elastic Deformation And The Laws Of Friction", *Proceedings of the Royal Society of London, Series A, Mathematical and Physical Sciences*, Vol. 243, Issue 1233, pp. 190-205.

Bowden, F. P., Tabor, D., (1939), "The Area Of Contact Between Stationary and Between Moving Surfaces", *Proceedings of the Royal Society of London, Series A, Mathematical and Physical Sciences*, Vol. 169, Issue 938, pp. 391-413.

Bowden, F. P., Tabor, D., (1956), Friction And Lubrication, John Wiley & Sons Inc, New York, 150 pp.

Brumund, W. F., Leonards, G. A., (1973), "Experimental Study Of Static And Dynamic Friction Between Sand And Typical Construction Materials", *Journal Of Testing And Evaluation, JTEVA*, Vol. 1, No. 2, pp. 162-165.

Butterfield, R., Andrawes, K. Z., (1972), "On The Angles Of Friction Between Sand And Plane Surfaces", *Journal Of Terramechanics*, Vol. 8, No. 4. pp. 15-23.

Degregorio, V. B., (1990), "Loading Systems, Sample Preparation, And Liquefaction", *Journal Of Geotechnical Engineering, ASCE*, Vol. 116. No. 5, pp. 805-821.

DeJong, J. T., Frost, J. D., Cargill, P. E., (2001), "Effect Of Surface Texturing On CPT Friction Sleeve Measurements", *Journal Of Geotechnical and Geoenvironmental Engineering, ASCE*, Vol. 127, No. 2, pp. 158-168.

DeJong, J. T., Frost, J. D., (2002), "A Multisleeve Friction Attachment For The Cone Penetrometer", *ASTM, Geotechnical Testing Journal, GTJODJ*, Vol. 25, No. 2, pp. 111-127.

Desai, C. S., Drumm, E. C., Zaman, M. M., (1985), "Cyclic Testing And Modeling Of Interfaces", *Journal Of Geotechnical Engineering, ASCE*, Vol. 111, No. 6, pp. 793-815.

Drainage Services Department, The Government of Hong Kong Special Administrative Region, Web Page, http://www.dsd.gov.hk/sewerage/technology_employed/pipe_jacking (Accessed 04 June, 2004).

Dove, J. E., Frost, J. D., (1999), "Peak Friction Behavior Of Smooth Geomembrane-Particle Interfaces", *Journal of Geotechnical and Geoenvironmental Engineering, ASCE*, Vol. 125, No. 7, pp. 544-555.

Form Talysurf Series 2 Manual, (1997), *Operator's Handbook*, Rank Taylor Hobson Limited.

Frost, J. D., Han, J., (1999), "Behavior of Interfaces Between Fiber-Reinforced Polymers And Sands", *Journal of Geotechnical and Geoenvironmantal Engineering, ASCE*, Vol. 125, No. 8, pp. 633-640.

Frost, J. D., Lee, S., Cargill, P. E., (1999), "The Evolution Of Sand Structure Adjacent To Geomembranes", *Proceedings Geosynthetics '99*; Vol. 1, pp. 559-573.

Frost, J. D., DeJong, J. T., Recalde, M., (2002), "Shear Failure Behavior Of Granular-Continuum Interfaces", *Engineering Fracture Mechanics*, Vol. 69, No. 17, pp. 2029-2048.

Frost, J. D., Park, J. -Y, (2003), "A Critical Assessment Of The Moist Tamping Technique", *ASTM, Geotechnical Testing Journal*, Vol. 26, No. 1, pp. 57-70.

Geocomp ShearTrac II Direct/Residual Shear Device Specifications, Web Page, http://www.geocomp.com/Productmanager/prod_specs/Direct-Residual%20Shear.pdf (Accessed 30 April, 2004).

Hsieh, C., Hsieh, M-W., (2003), "Load Plate Rigidity And Scale Effects On The Frictional Behavior Of Sand/Geomembrane Interfaces", *Geotextiles and Geomembranes Journal*, Vol. 21, Issue 1, pp. 25-47.

Interface Advanced Force Measurements, Series SM-1000 Load Cell Specifications, Web Page, http://www.interfaceforce.com/PDF_files/sm.pdf, (Accessed 27 April, 2004).

Kulhawy, F. H., Peterson, M. S., (1979), "Behavior of Sand-Concrete Interfaces", Proceedings, *Sixth Pan American Conference On Soil Mechanics And Foundation Engineering*, Vol. 2, Lima, Peru, pp. 225-236.

Ladd, R. S., (1974), "Specimen Preparation And Liquefaction of Sands", *Journal Of Geotechnical Engineering Division, ASCE,* Vol. 100, No. GT10, pp. 1180-1184.

Ladd, R. S., (1977), "Specimen Preparation and Cyclic Stability Of Sands", *Journal Of Geotechnical Engineering Division, ASCE,* Vol. 103, No. GT6, pp. 535-547.

Ladd, R. S., (1978), "Preparing Specimens Using Undercompaction", *ASTM, Geotechnical Testing Journal, GTJODJ*, Vol. 1, No. 1, pp. 16-23.

Lanzo, G., Vucetic, M., Doroudian, M., (1997), "Reduction of Shear Modulus At Small Strains In Simple Shear", *Journal Of Geotechnical and Geoenvironmental Engineering, ASCE*, Vol. 123, No. 11, pp. 1035-1042.

Miura, S., Toki, S., (1982), "Sample Preparation Method And Its Effect On Static And Cyclic Deformation-Strength Properties Of Sand", *Soils and Foundations*, Vol. 22, No. 1, pp. 61-77.

Mulilis, P. J., Chan, C. K., Seed, H. B., (1975), "The Effects Of Method Of Sample Preparation On The Cyclic Stress-Strain Behavior Of Sands", EERC Report 75-18.

Mulilis, J. P., Seed, H. B., Chan, C. K., Mitchell, J. K., Arulanandan, K., (1977), "Effects Of Sample Preparation On Sand Liquefaction", *Journal Of Geotechnical Engineering Division, ASCE*, Vol. 103, No. GT2, pp. 91-108.

Ooi, L. H., Carter, J. P., (1987), "A Constant Normal Stiffness Direct Shear Device For Static And Cyclic Loading", *ASTM, Geotechnical Testing Journal, GTJODJ*, Vol. 10, No. 1, pp. 3-12.

Paikowsky, S. G., Player C. M., Connors, P. J., (1995), "A Dual Interface Apparatus For Testing Unrestricted Friction of Soil Along Solid Surfaces", *ASTM, Geotechnical Testing Journal, GTJODJ*, Vol. 18, No. 2, pp. 168-193.

Porcino, D., Fioravante, V., Ghionna, V. N., Pedrono, S., (2003), "Interface Behavior Of Sands From Constant Normal Stiffness Direct Shear Tests", *ASTM, Geotechnical Testing Journal, GTJODJ*, Vol. 26, No. 3, pp. 289-301.

Potyondy, J., G., (1961), "Skin Friction Between Various Soils And Construction Materials", *Geotechnique*, Vol. 11, pp. 339-355.

Purdue University Construction Engineering & Management, Web Page, http://cem.www.ecn.purdue.edu/CEM/Trench/micro.html, (Accessed 4 June, 2004).

Rad, N. S., Tumay, M. T., (1987), "Factors Affecting Sand Specimen Preparation By Raining", *ASTM, Geotechnical Testing Journal, GTJODJ*, Vol. 10, No. 1, pp. 31-37.

Tatsuoka, F., Haibara, O., (1985), "Shear Resistance Between Sand And Smooth Or Lubricated Surfaces", *Soils And Foundations*, Vol. 25, No. 1, pp. 89-98.

The Pipe Jacking Association, Web Page, http://www.pipejacking.org/index2.html (Accessed 19 May, 2004).

Thomson, J., (1993), Pipejacking And Microtunnelling, Blackie Academic & Professional, London, 273 pp.

Trans-Tek, Inc. Series 0244 Linear Variable Differential Transformer Specifications, Web Page, http://www.transtekinc.com/Catalog_PDFs-01/LVDTs/Ser240_01F.pdf (Accessed 27 April, 2004).

Uesugi, M., Kishida, H., (1986), "Frictional Resistance At Yield Between Dry Sand And Mild Steel", *Soils and Foundations*, Vol. 26, No. 4, pp. 139-149.

Uesugi, M., Kishida, H., (1986), "Influential Factors of Friction Between Steel And Dry Sands", *Soils and Foundations*, Vol. 26, No. 2, pp. 33-46.

Ward, H. C., (1982), "Chapter IV: Profile Characterization", Rough Surfaces, Thomas, T.R., ed., London: Longman Group Limited, pp. 72-90.

Zettler, T. E., (1999), "Operational Induced Changes In Geomembrane Surface Topography", MSc Thesis, School of Civil and Environmental Engineering, Georgia Institute of Technology, 264 pp.